Investigation of a Biosensor for DNA Detection

A thesis presented in partial fulfilment of the
requirements for the degree of

Master of Engineering

in

Electronic Engineering

at

Massey University,

School of Engineering and Advanced Technology (SEAT)

Auckland, New Zealand

Massoud Alipour

January 2011

To my wife

Laya

My daughters

Elena & Erica

Acknowledgements

I would like to thank my supervisor: Dr. S.M. Razaul Hasan for his support throughout the duration of the project. Without his guidance and persistent help, this thesis would not have been possible. Thanks for his suggestions, patience and encouragement, which makes me finally brave enough to start this academic journey from a very beginning level.

I would also like to thank my family for their unconditional support.

Abstract

The aim of this project was to design a fully electronic sensor to detect hybridized DNA. In this study an integrated circuit for measuring capacitance of the sensor has been designed, which uses DNA as dielectric between the fingers of the sensor.

Nowadays, bio-sensors are widely used in electrical sensing where, most of these sensors use the conversion of capacitance for sensing. Some of the benefits of capacitive sensors are: high resolution, high sensitivity, low power dissipation, the ability to be integrated with other circuits, good stability and near zero thermal factors in heat exposure. Capacitive sensors are not affected by magnetic disturbances from electrical fields.

The first challenge in this study was bonding Single-strand DNA (ssDNA) to the sensor, which has been explained in chapter 2. After bonding ssDNA, the sample ssDNA will connect to their pairs on the sensor in the process called hybridization and the bonded addition then changes the capacitance of the sensor. To measure the change of the sensor's capacitance it is necessary to use interface circuits called "readout circuits". These circuits convert every change in the capacitive value to electrical changes such as current, voltage, frequency or pulse bandwidth to make the processing easier. Changes in the signal are very small, making factors such as noise and offset very important.

There are different methods available in measuring the changes in capacitance, which are discussed in this thesis and their advantages and disadvantages are described. After considering the best choice in DNA sensor, a suitable circuit for measuring the capacitance changes has been designed and simulated. Considerations for reducing noise and offset is also built in to the design of the circuit, Correlated Double Sampling (CDS) and Chopper Stabilisation (CHS) methods are used. Also, to achieve optimum results, these two methods are combined in this thesis. From the results of simulations, it is concluded that CDS and CDS&CHS methods are best suited for our design.

In chapter four, at first, two methods for detection of the capacitance in the sensors are demonstrated in the form of block diagrams, and then the advantages and disadvantages of these methods are discussed. After choosing the better method, every part of that method was implemented separately, as an integrated circuit. After linking the different parts, an analogue integrated circuit was designed that turned the capacitive variations to time period variations. Then a digital circuit was designed in order to turn the period time variations to a digital output. The analogue part of the circuit was simulated using 0.25µm technology parameters

in Tanner software and the digital part was simulated with VHDL software. The results of these simulations are presented in chapter five. This study succeeded in reaching an accuracy of *0.7fF* (Femto Farad, 10^{-15}) capacitor variations. In the summary some suggestions for further research in this field were given.

Table of Contents

List of Figures

List of Tables

Glossary:

A/D: Analogue to digital
ASV: Anodic Stripping Voltammetry
C/F: Capacitor-to-Frequency
CDS: Correlated Double Sampling
CHS: Chopper Stabilisation
CMOS: Complementary metal–oxide–semiconductor
CSA: Charge Sensitive Amplifier
DNA: Deoxyribonucleic acid
DIAPOPS: Detection of Immobilized Amplified Products in a One Phase System
EDC: Ethyl-dimethylaminopropyl-carbodiimide
GBM: Gain Bandwidth
HPR: Horseradish Peroxidase
LPF: Low Pass Filter
LSI: Large Scale Integration
MEMS: Micro Electromechanical System
MOSFET: Metal–oxide–semiconductor field-effect transistor
OLEDs: Organic light emitting diodes
OpAmp: Operational amplifier
PCR: Polymerase chain reaction
PLL: Phase Locked Loop
PSD: power spectral density
PM: Phase-Margins
QCM: Quartz Crystal Microbalances
RNA: Ribonucleic acid
SAM: Self-Assembled Monolayer
SC: switched capacitors
SNP: Single Nucleotide Polymorphism
SNR: Signal-to-Noise Ratio
SPR: Surface Plasmon Resonance
ssDNA: Single strand of denatured DNA
TIA: Transimpedance Amplifier
TLC: Thin-layer chromatography

Chapter 1: Introduction to DNA Sensing

1.1 DNA construction

Deoxyribonucleic acid (DNA) contains unique genetic information for every human being and living organism present on earth. When obtaining DNA sequencing data, small errors in this information could result in large mistakes in identification. For the medical profession, failure to provide correct DNA data in such areas as identifying pathogenic organisms could result in fatality. Fast and accurate DNA sequencing tools will provide assurance for both professionals and the private individual.

DNA, as shown in Fig. 1-1, is a double stranded helix formation of sugar-phosphates connected together by four base elements, or nucleotides. These four base elements are, Adenine (A), Cytosine (C), Guanine (G) and Thymine (T). The order in which the base pairs (nucleotides) appear on the helix defines the unique DNA signature of a particular organism or person [1].

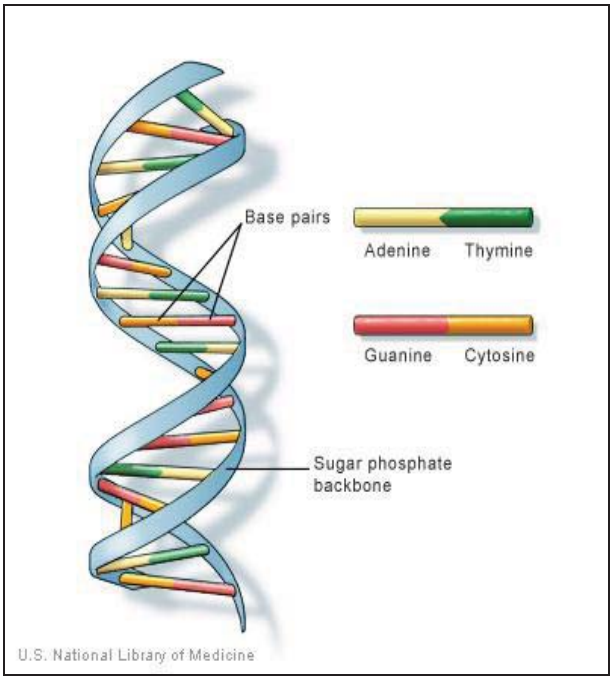

Fig. 1-1: DNA. Image from U.S National Library of Medicine

A unique condition of DNA bonded pairs is that the pairs Adenine and Thymine will only bond with each-other and Guanine and Cytosine will only bond with each-other [1]. This condition is used in identifying DNA sequences by way of the process known as hybridization, where the strands and bonds are unwound and broken by heat. A single strand

is then used to match a sample, which is also hybridized. When the sample and the testing hybrid are exposed to one another a match will cause the strands and pairs to re-attach.

1.2 Vocabulary of genomics

DNA: Deoxyribonucleic acid; strands of double helix nucleotides containing genetic sequence information.

RNA: Ribonucleic acid; a cellular intermediary that converts genetic information to proteins.

Nucleic acid: A macromolecule composed of chains of monomeric nucleotides as shown in Fig. 1-2.

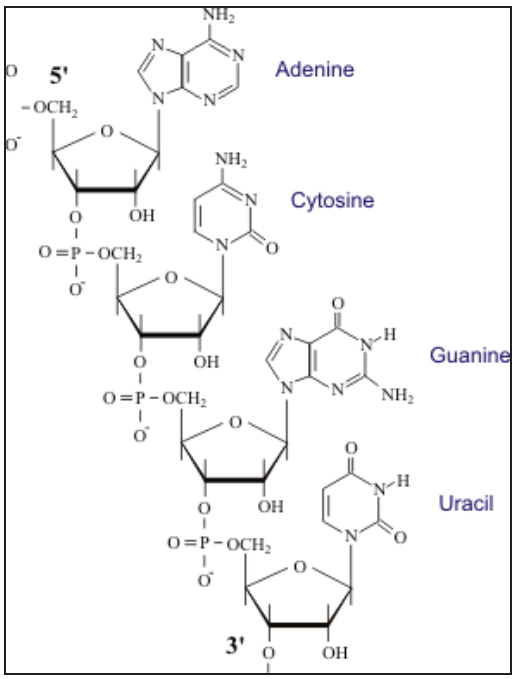

Fig. 1-2: Nucleic acid. Image from the National Human Genome Research Institute (NHGRI)

Nucleotide: Productive sequencing units in DNA; Adenine, Thymine, and Guanine, Cytosine (A, T, C, G), as shown in Fig. 1-3

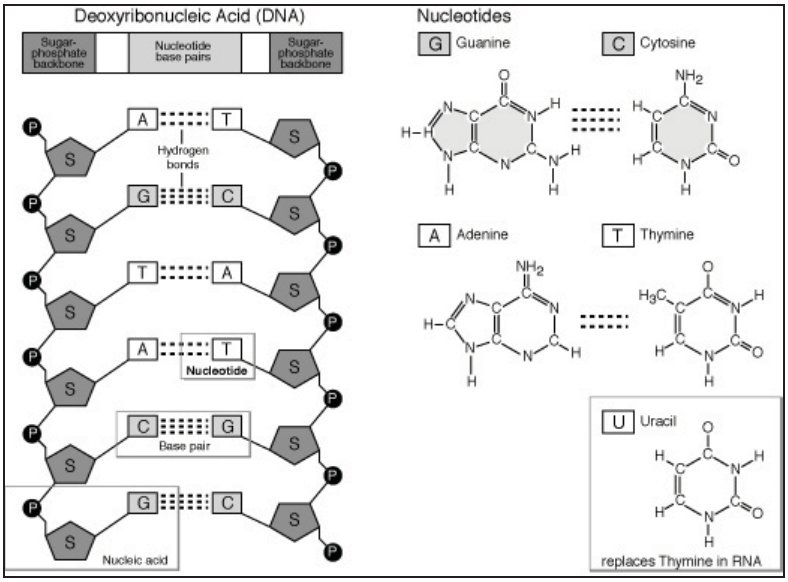

Fig. 1-3: Nucleotide. Image from the National Human Genome Research Institute (NHGRI)

Hybridization: a process where two separate single strings of DNA (or RNA) bind to form a double chain. Hybridization shows in Fig. 1-4.

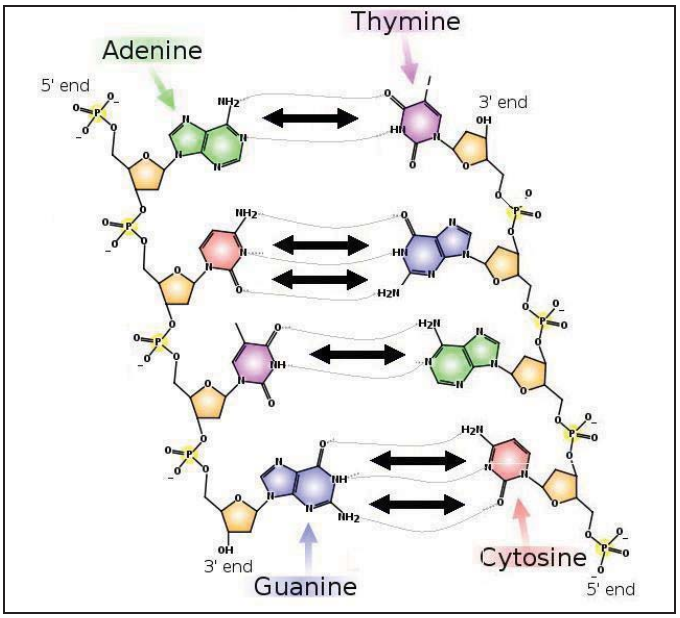

Fig.1-4: Hybridization. The main image from Wikipedia but has been modified.

Complementary DNA: Single stranded DNA synthesized from mDNA.

Denaturing: A method of stripping DNA into two separate strands.

Polymerase chain reaction (PCR): A technique of replicating a small significant DNA sequence.

Phosphodiester bond: DNA polymer carbon link between 5 prime phosphate and 3 prime hydroxyl groups of a deoxiribose group. Fig. 1-5

ssDNA: Single strand of denatured DNA

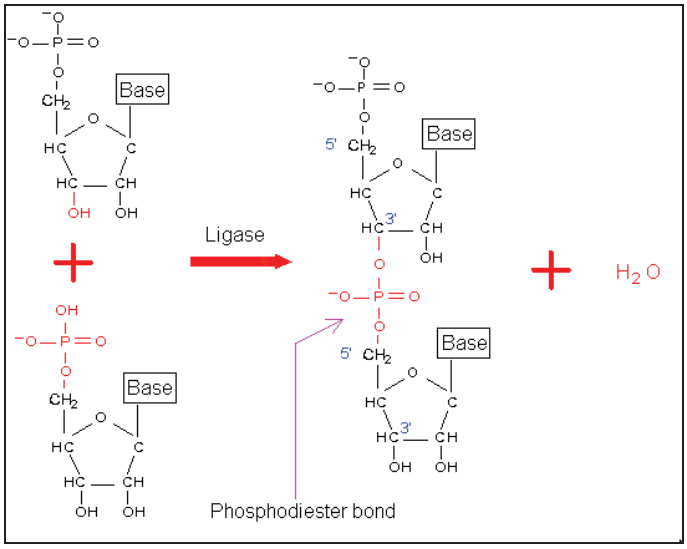

Fig. 1-5: Phosphodiester bond

1.2 Simple and effective: the principle of PCR

Polymerase Chain reaction is the process of copying DNA. The repetitive cycle consists of three stages [75]:

1: Reaction solution containing molecules of DNA (for copying), polymerase (DNA that can copy), primers (as Initiator copy DNA) and nucleotides (which are attached to the primer.) up to 95 degrees Celsius heat, this is because the two chains will separate, this process is known as denaturing. The denatured strand is called ssDNA.

2: Lowering the temperature to 55 degrees, this causes DNA primers to reconnect the single strands of the hybrid and the sample. A hybridization process will stabilize if that piece of DNA and primer are complementary.

3: Extension or expansion: Temperature is increased again to 72 degrees this time. This is the best temperature for the polymerase function to increase nucleotides DNA chain. At the same time any flaccidity link through lack of matching compliments between the primers and DNA will be broken.

Whenever these three steps are repeated the number of copies of DNA molecules is doubled. After 30 cycles, about one million molecules of a single piece of DNA double-chain have been cloned [89, 90].

1.4 The Sensor

The proposed sensor requirement is dependent on measurement of a significant variation in the capacitive value of the sensor due to the introduction of physical phenomena.

Capacitive sensors have numerous advantages, including: high-resolution, high sensitivity and low power consumption, the ability to be integrated with other circuits. Capacitors are thermally stable and have good stability against temperatures near zero. They also protect against scattered electric fields. Capacitive sensors are also widely used in applications such as pressure sensors, acceleration, and humidity [2].

Capacitive changes in a capacitive sensor are dependent on three characteristics, the size of the plates, their distance apart and the coefficient of the dielectric between the plates.

Intermediate circuits are used to convert the very small changes in sensor capacitance into usable values such as current, voltage, frequency or pulse width [3].

The sensor has been designed to work as a parallel-plate capacitor as shown in Fig. 1-6. The gap between the electrodes is denoted by '*r*' where,

$$0.5\mu m < r < 0.6\mu m \tag{1-1}$$

The capacitance of the sensor changes when DNA is attached to the electrodes. In this sensor, first ssDNA is bonded to the electrodes. The ssDNA acts as a primary dielectric and exhibits the dielectric constant denoted by ε_1. After hybridization, the dielectric property of the ssDNA is changed and a new dielectric value is obtained which is denoted as ε_2.

In the sensor "*h*" is the height of the electrodes and "*w*" is the width of the electrodes.

The dimensions of the interdigitated sensor electrode are mostly dependent on the minimum channel length of integrated circuit process technology. For a 0.5 μm CMOS technology the width of the sensor ("*w*") usually is in range of *100 to 200* μm [4].

$$100\mu m < w < 200\mu m \tag{1-2}$$

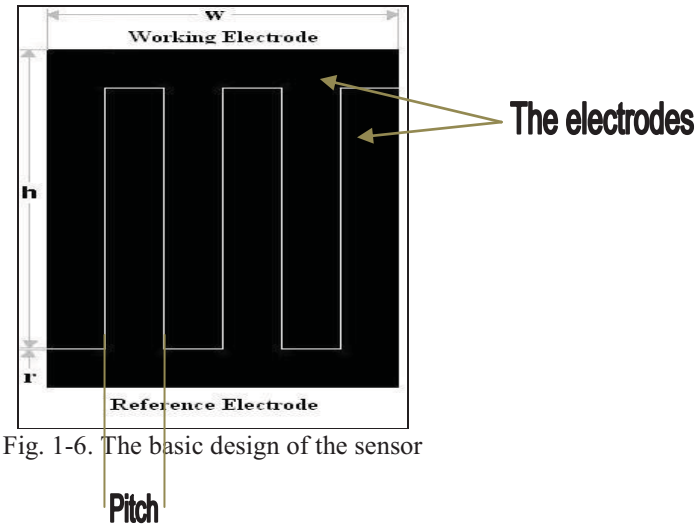

Fig. 1-6. The basic design of the sensor

1.5 Principles in Method of Sensing

This study focuses on the real time detection of the DNA via hybridization using a capacitance sensor technique; where, the magnitude of the sensor's response time is larger than or equal to $0.2\mu s$ and is less than $0.4\mu s$.

The detection sensor is designed using two electrodes on a monolithic CMOS wafer in close proximity to each-other. The electrodes act as the plates of a parallel-plate capacitor. ssDNA is bound to the plates in a covalent bond through oxides on a chemical polymer.

After the sample ssDNA is applied to the sensor and hybrid pairs bind successfully, the addition of bonded DNA changes the dielectric constant in turn changing the capacitance of the sensor array. Fig. 1-7 shows the chart of charge and discharge in capacitive sensors.

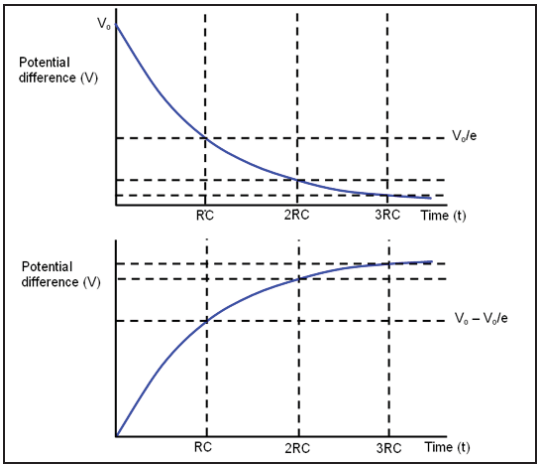

Fig. 1-7: Charge and discharge

The change in the DNA sensor's capacitance (ΔC) is a hyperbolic; however, it must change to linearly. To convert ΔC into linear gradient, a capacitance detection circuit has been used. Generally three methods for detecting changes in capacitance in capacitive sensors are used. These methods are:

1.5.1 Using an RC oscillator. An oscillator, whose output frequency is dependent on the magnitude of the sensor's capacitance, is used to change the non-linear relationship of ΔC into a linear change in frequency; however, this method of detection has low sensitivity. In addition, the oscillator can be used alongside a PLL[1], which converts the oscillator's frequency into a voltage [5]. This circuit can be designed with the sensor using CMOS technology.

1 Phase Locked Loop

1.5.2 Using switched-capacitor: The DNA sensor is used to provide an Op-Amp feedback via a (positive/negative) feedback loop. The Op-Amp's output voltage, alongside dielectric changes, has a linear gradient/rate of change [6].

1.5.3 Using a Microprocessor: In this method using a pre-loaded table of data which is obtained by multiple experiments. By bonding ssDNA to the sensor and hybridizing DNA, creating a voltage in output of switched capacitor circuit or after low-pass PLL filter. This voltage is then converted to a digital signal by an A/D and becomes an address in memory. The data address in the memory is equal to the changes of the sensor capacitance. Interval data shows the sensor accuracy. For increased sensor sensitivity A/D bits or memory size can be increased [7].

In chapter 2, offered two methods of bonding DNA to the sensor and different methods of detecting the changes in the sensor have been explained. Chapter 3 is literature review of biosensors and noise reduction methods and the capacitance detector circuit has been designed in chapter 4. The final chapter is simulation results and some recommendation for future works.

Chapter 2: Methods of bonding DNA to a sensor and detecting DNA

2.1 Bonding ssDNA to the electrode

This study offers two methods to bond DNA to the electrodes. The first method is using Carbodiimide and the second method is using SAM and Organic surfaces.

2.1.1 Option 1: Carbodiimide

In this option, Carbodiimide - Ethyl-3-(3-dimethylaminopropyl)-Carbodiimide can be used to bond ssDNA to the sensor by way of coupling 5 prime phosphate group end [8].

The reaction of the binding is activating an EDC (Ethyl-dimethylaminopropyl-carbodiimide) the 5'-phosphate group on the solid condition of primer (It could be a group of phosphoryl on any single- or double-stranded of DNA).

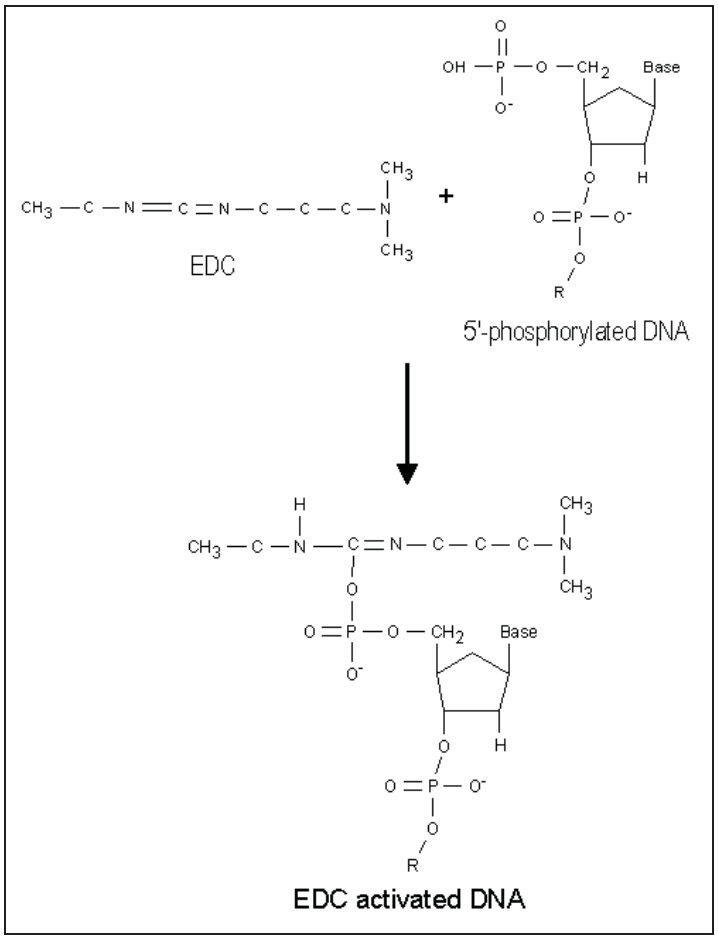

Fig. 2-1. Ethyl-dimethylaminopropyl-carbodiimide

Fig. 2-2 shows the basic response of DNA Carbodiimide activating with one methylimidasole.

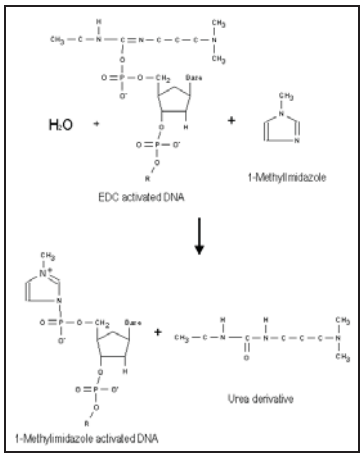

Fig. 2-2. Methylimidasole activated DNA

Because the half-life of EDC activated DNA is too short in H_2O (water), further conversion with 1-methylimidasole is necessary. It is more stable in aqueous solution the reaction of 1-Methylimidasole with the EDC activated DNA and forms another active group.

After attachment to the phosphate group, 1-Methylimidasole is a very capable leaving group on the 5'-end of the DNA and investigation for increase of the joint reaction have produced good results by this reagent [9].

On the NucleoLink surface, a reactive group with the 1-methylimidasole activated DNA to form a covalent bond between the electrode fingers and the ssDNA.

This bond is thermostable and is not affected by high temperatures in the thermal cycling during the DNA amplification of DIAPOPS[1].

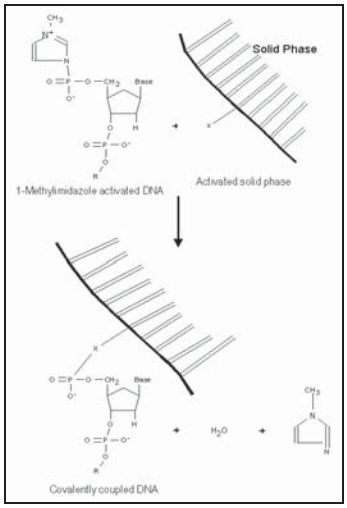

Fig. 2-3 Covalently coupled DNA

[1] Detection of Immobilized Amplified Products in a One Phase System

2.1.2 Secondary Option: Bonding DNA molecules to a thin gold layer

In this method, SAM[1] and Organic surfaces can be used to bond DNA to the sensor. To explain this method, first the SAM is explained.

2.1.2.1 Nano Sciences

The size of work piece in nano technology is from 1 to 100nm. The components used in Micro technology (e.g. Micro Electronics, Photonics, MEMS[2] and Micro Fluids) are built by way of photolithography. Nano systems have interesting and useful behaviours in Quantum phenomena (e.g. Quantum entanglement, near field optical effects, Limited electron, Tunnelling electron and Ballistic transport) based on subdomain phenomena (e.g. overlapping double layers in fluids) [10]

Chemistry is one of the main base tools in nano sciences, creating or breaking bonds between atoms or a group of atoms is a major part of chemistry and the result of these kinds of reactions are molecules with size of 0.1-100nm. Development of new synthesis methods can produce nano-structures on homogeneous bases 1-100 nano-meters in new and different shapes (spherical, ropes, wire-shaped, semi-spherical and cubic) and has created various compounds (organic, metal oxide semiconductor). Examples of these are nano-crystals, nano-wires [11], nano-tubes [12] and block copolymers [13]. In the field of medicine, drug delivery, in electronic and optical applications, magnetic fields are utilized for digital or analogue manipulation. In Biology, cells (the basic units of life) at a glance, are a complex set of biological nano-machines. Some cell components are in the nano meter-scale dimensions. For example, Catalytic and other active systems such as enzymes, ribosomal, proteins and complex protein-RNA, cell membrane bi-lipid layers, ion channels, cell structure components (Actin and small pipes), DNA, RNA, protein engines and mitochondria [14]. New tools to aid viewing and modification of molecular and atomic particles, such as electronic microscopes are an important part in the science of nanotechnology. The ability to view, modify and create shapes of nano meters in size, has presented some very attractive ideas resulting in new behaviours, such as, the nano-robots, “gray goo” has attracted much attention [15].

[1] Self-Assembled Monolayer (SAM)
[2] Micro Electromechanical System (MEMS)

Examples of this category include: composite materials of modified hardness and strength, electrical conductivity, super-compressed material, organic electronics (e.g. organic light emitting diodes (OLEDs)), new biosensors, and electron tools.

2.1.2.2 Surfaces and the common denominator in nano science

One of the distinctive features of nano scale structures is that unlike the microscopic materials, surface to volume ratio is very high. The volume of an object ($V \alpha L^3$ where L is characteristic length of the object) reduces much faster than its surface area ($S \alpha L^2$) then: $\frac{S}{V} \alpha L^{-1}$ which L is dimensional of the molecular or atomic. This behaviour creates an effect that causes virtually every atom to share a surface or in other words nanostructures composed completely of surfaces. Surfaces are a solid state of material, moreover, a surface is the place that has a maximum characteristic gradient (in Phase mass material, gas, liquid and solid, gradient is almost zero). Atoms or molecules in nano scale structures have different states of surface when compared to molecules in normal mass materials, offering free energies of different modes of electrical reactivity, movement and structure. [16, 17].

Structure and chemical composition on the inside of macroscopic objects determines many physical properties of the material such as electrical and thermal conductivity, hardness and resilience, the physical properties of nano-structures strongly depends on surface and common environment and not the mass of the material.

2.1.2.3 SAM and Organic surfaces

Bare metal surfaces, with a coating of metal or metal oxide, will allow bonding of organic materials very quickly because the adsorption reduces free energy between the metal oxides and metal [18]. This adsorption (Adsorption - attraction of atoms or molecules (generically known as "monomers") from an adjacent gas or liquid to an exposed solid surface) will change their common properties and change stability between nanostructures and metal oxides.

This process uses organic materials as an electro-static blocker or physical action against the accumulation, aggregation and reactivity of surface atoms, reducing or electrically insulating the layer on a metal surface. Self-Assembled Monolayer (SAM) is a simple system, flexible and appropriate for changing the underside surface properties of metals, metal oxides and semiconductors. Table 2-1 shows the numbers of “headgroups”, which bond to metals, metal oxides or semiconductors. The group of SAMs that have been studied most are SAMs that

resulted from adsorption of alkanethiols and DNA on surface of *gold* [19], *silver* [15], *copper* [20], *palladium* [18, 21], *platinum* [22] and *mercury* (*Hg*) [23].

		Morphology of Substrate	
Ligand	**Substrates**	**Thin Films or Bulk Material**	**Nanoparticles or Other Nanostructures**
ROH	Fe_xO_y		35
	Si-H	36	
	Si	37	
RCOO-/RCOOH	α-Al_2O_3	38,39	
	Fe_xO_y		40
	Ni		41,42
	Ti/TiO_2	43	
Rcoo-OOCR	Si(111):H	44	
	Si(100):H		
Ene-diol	Fe_2O_3		45
RNH_2	FeS_2	46	
	Mica	47	
	Stainless steel 316L	48	
	$YBa_2Cu_3O_7$-δ	49	
	CdSe		50
RC≡N	Ag	51	
R-N≡N^+(BF_4^-)	GaAs(100)	52	
	Pd	52	
	Si(111):H	52	
RSSR'	Ag	89	90
	Au	20	90-92
	Au	93	
RCSSH	Au	94	
	CdSe		95
$RS_2O_3Na^+$	Au	96	98
	Cu	97	
RSeH	Ag	99	
	Au	100,101	
	DcSe		102
RSeSeR'	Au	101	

Table 2-1: Numbers of headgroups [24]

2.2 Methods of reading capacitance changes in capacitive sensors

Various methods for detection of capacitive sensors capacitor are presented. Usually readout circuits of capacitance sensors convert the capacitance changes to three values: voltage,

current or frequency. The voltage or current converter circuits can be divided into two groups [25].

A) Circuits in continuous-time: Such circuits convert capacitance changes to continuous-time voltage-mode or continuous-time current-mode. Charge Sensitive Amplifier (CSA) and Transimpedance Amplifier (TIA) convert capacitance changes to continuous-time voltage and current.

B) Discrete-time circuits: In such circuits switched capacitors (SC) are used and capacitance changes are converted to voltage.

In some methods, changes in capacitance sensor are converted to frequency (Capacitor-to-Frequency). A C/F Converter can be implemented by using an oscillator whose output frequency depends on the capacitance sensors. This method is called the Relaxation oscillator method. The performances of the above methods are described in next sections.

2.2.1 Methods of Circuits in continuous-time

2.2.1.1 Transducer impedance amplifiers

In capacitive sensors, transmission load produces ac current which can be detected by an impedance converter amplifier. The figure below shows a schematic of the readout circuit of the impedance converter amplifier. In this circuit a variable capacitor Sense C_s is used and a fixed reference capacitor C_r in half bridge configuration provides two ac signals, which drive with 180 degree differences. C_p is parasitic capacitance in the input amplifier [26]. These amplifiers are widely used in light receptors for sensing the current of the photo diodes [25].

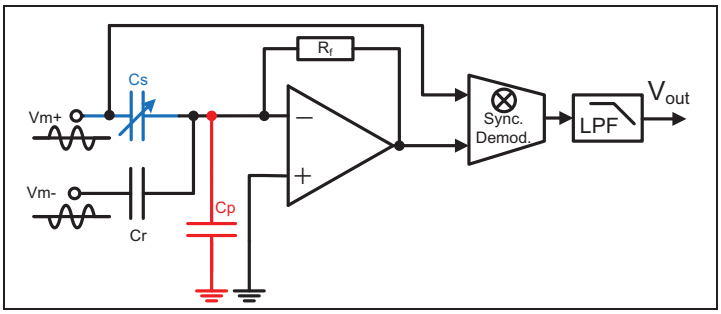

Fig. 2-4 Simplified block diagram of amplifier circuit impedance converter [26]

The bridge output by an operational amplifier with feedback resistance R_f is kept at virtual ground and the output current of the bridge through R_f goes to the output. Virtual ground input reduces the effect of parasitic capacitance. The circuit output voltage can be calculated as follows:

$$|V_{out}| = 2\pi f_{drive} V_m R_f \Delta C \qquad (2\text{-}1)$$

Where, R_f is the feedback resistance, ΔC is the sensor capacitance changes, V_m is the drive voltage amplitude and f_{drive} is the frequency of the drive voltage. This impedance converter circuit's governing equation acts as a differentiator, which in turn acts as a high-pass filter.

In such circuits, noise is determined by two factors: noise-induced amplifier and thermal noise due to feedback resistance. Also, the poles related to R_f limits the bandwidth to $f_{p1} = \frac{1}{\left(2\pi R_f \left(2C_s + C_p\right)\right)}$. If noise in the amplifier is kept to a minimum, noise performance is determined by thermal noise created by the feedback resistance. In this case, minimum detection of capacitance is as follows [26]:

$$\Delta C_{\min-rmsp1} = \frac{\sqrt{BW}}{V_m}\sqrt{\frac{2k_B T\left(2C_{s0} + C_p\right)}{\pi GBW_{amp}}} \tag{2-2}$$

Where GBW_{amp} is gain bandwidth of the amplifier. It is observed that the minimum capacitance variation with drive voltage is inverse relationship. It means that at lower drive voltages, the resolution of circuit decreases.

Most circuits of continuous-time in capacitive sensors use conversion of capacitance to voltage as opposed to converting capacitive units sensed into current.

2.2.1.2 Charge sense amplifiers

The following schematic shows the charge sense amplifier [3].

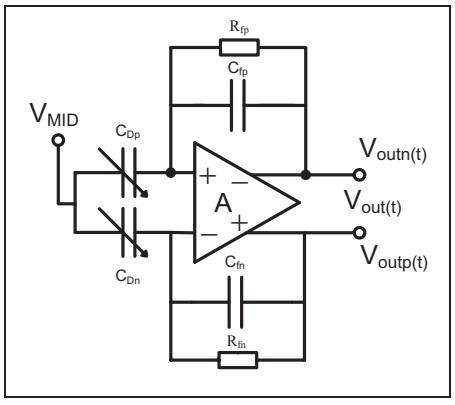

Fig. 2-5 Schematic of charge sense amplifier circuit [3]

In the above circuit, C_{Dp} and C_{Dn} represent sensor capacitance, and R_{fp} , R_{fn} , C_{fp}, and C_{fn} are the resistors and capacitive feedback. A sense charge amplifier is used to convert changes in the capacitor sensor to voltage. This method uses an Integrator charge obtained from the charge current into or out of the capacitive sensors with fixed bias voltage when the capacitor

varies. If the sensor capacitors have almost linear changes, we can write them as $C_{Dp}=C_D+\Delta C_D/2$ and $C_{Dn}=C_D-\Delta C_D/2$, in this case the convert function will be as follows:

$$H(s)=\frac{V_{out}(s)}{\Delta C_d(s)}=\frac{s.V_B/C_f}{s+1/(R_fC_f)} \quad (2\text{-}3)$$

According to this equation which is single-polar of high-pass type, two-point observed for design. *-3dB* frequency is equal to $1/(2\pi R_fC_f)$, which means that if there is a decrease in frequency signals, the amount of passive feedback component is dominant. Secondly, if accurate gain is required, the voltage V_B needs to be accurate across the sensor because it is directly related to the gain. Resolution of the capacitive sensor readout circuit is usually limited by noise. Noise caused by the sense amplifier circuit charge arises from two factors: operational amplifier and feedback resistance. Also the leakage of currents at the input is limiting the noise reduction performance. Monolithic construction of a converter is an expensive technology and not common, circuits can be overcome with parasitic capacitance, which may be several times larger than the capacitance being detected. However, charge sense amplifiers are not sensitive to parasitic capacitance and this is one advantage to this method, but they are not suitable in controlling low frequency noise [23].

2.2.2 Discrete-time methods

2.2.2.1 Capacitive switching technique

Circuits mentioned in the above section are known as circuits in continuous-time, meaning that the signal in time domain is not discrete or sampled and has value at all times. However, a discrete time signal is discontinuous, i.e. it only has a value at specified intervals, with not value during the “in-between” time. An intermediate circuit for capacitive sensors in discrete-time can be constructed with capacitive switching circuits. A switched capacitor circuit takes the capacitor’s signal’s sample and converts it to a voltage. Readout switched capacitor circuits are widely used in capacitive sensors. In such circuits, the sample signal is related to charge-voltage. Because the virtual ground of the switch capacitor circuits and dc bias establish valid nodes, the sense signal is not sensitive to parasitic capacitance input and undesirable charges. Fig. 2-6 shows switched capacitor amplifier circuit schematic. [31].

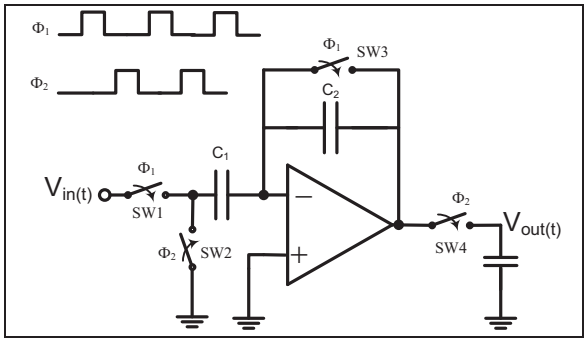

Fig. 2-6 Switched capacitor amplifier circuit schematic [26]

Signals ϕ_1 and ϕ_2 are two non overlapping clock signals. When any of these signals are high or low, the switch related to them is either opened or closed. During the phase of ϕ_1, a sample is taken from the input signal $V_{in}(t)$ (could be continuous or discrete time) in the capacitor C_1 . If the capacitor C_2 is reset during the phase of ϕ_2 , The charge sampled from C_1 transferring to C_2 and output signal $V_{out}(t)$ after transferring will be $(C_1/C_2).V_{in}((n_s\text{-}1/2).T_s)$ which $(n_s\text{-}1/2).T_s$ is the sampling interval (The sample that ϕ_1 is going down) and n_s is index sample. Now, the voltage is stored on the capacitor charge C_L and can be transferred to next subsequent processing blocks.

In capacitive sensors, the capacitor C_1 in Fig. 2-6 is replaced with the variable capacitor C_s sensor as shows in Fig. 2-7 [26].

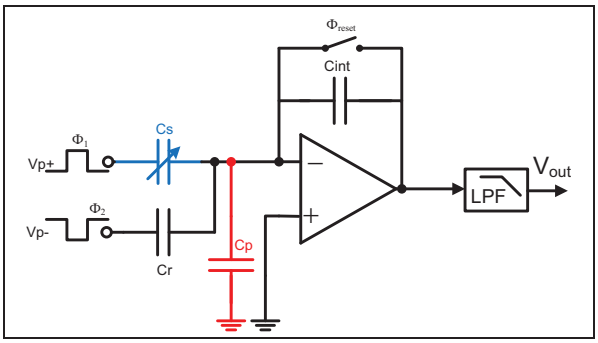

Fig. 2-7 Capacitive switching circuit schematic used in capacitive sensors [26]

In this circuit, sense capacitor C_s and reference capacitor C_r with opposite polarity voltages are charged and then a load package, dependent on the capacitance changes of the capacitor through the feedback capacitor is going to the output. Eq. 2-4 is the output voltage equation.

$$V_{out} = V_p \frac{\Delta C}{C_{\text{int}}} \tag{2-4}$$

In capacitors switches, flicker noise (*1/f* noise) and amplifier offset can be removed by the CDS[1] method. This method is explained in the next chapter.

[1] Correlated Double Sampling

Noise switch sampling (called *kT/C*) with double sampling and subtracting it from the output signal can be eliminated as shown in Fig. 2-8 by using C_0 eliminated *kT/C* [26].

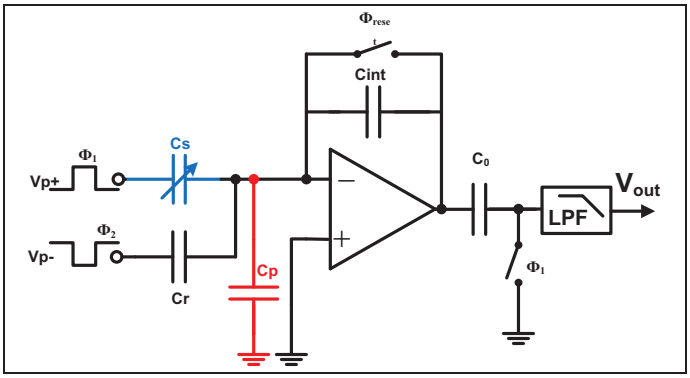

Fig. 2-8 Switched capacitor circuit with noise reduction *kT/C* [26]

Switch ϕ_1 will turn off after ϕ_{reset} goes to zero (Turn off). In this case, the noise sample of the reset switch is at the end of the reset phase stored in C_0. In ϕ_2 the voltage stored in C_0 is subtracted from the output of the amplifier which eliminates kT/C_{int}.

The resolution of the readout capacitive circuit is calculated as follows [26].

$$(\Delta C_{\min-rms})^2 = \frac{1}{f_s}\left(\frac{16k_BT(2C_{s0}+C_p)C_{\text{int}}}{C_{out}} + 2k_BTC_{\text{int}}\right)(BW) \tag{2-5}$$

Where C_{out} is the total output capacitance of the amplifier and f_s is the sampled frequency.

As mentioned before, offset and *1/f* noise of the amplifier will be eliminated by a correlated double sampling method. Therefore minimum capacitance is calculated using equation 2-4 [26].

$$\Delta C_{\min-rms} = \sqrt{\frac{1}{f_s}}\left(\sqrt{\frac{16k_BT(2C_{s0}+C_p)C_{\text{int}}}{C_{out}}}\right)(\sqrt{BW}) \tag{2-6}$$

According to the above equation it is demonstrated that circuit resolution will be improved by increasing the sampling frequency.

2.2.3 Relaxation oscillator method

Principle of this method is that the sensor capacitance changes are converted to frequency or time period. A relaxation oscillator is an oscillator in which a capacitor is charged gradually and then discharged. This oscillator is usually made with a resistance or current source, a capacitor and comparator.

Fig. 2-9 shows work based on a resistance relaxation oscillator [34].

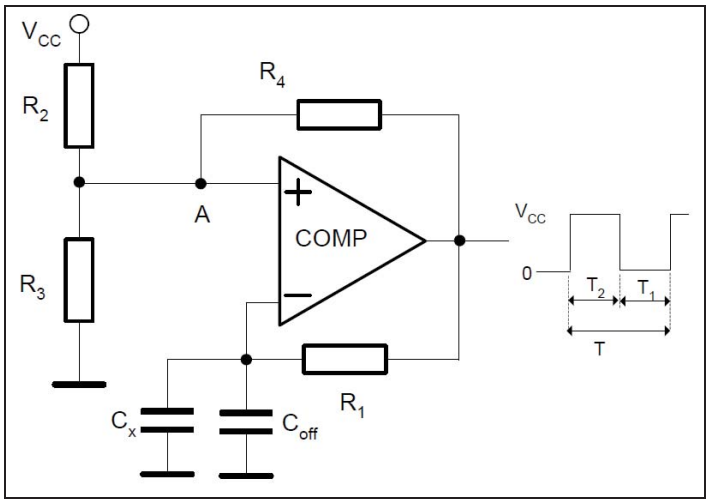

Fig. 2-9 Work based of a resistance relaxation oscillator [34]

In this circuit, C_x is unknown capacitor and C_{off} is offset capacitor. Capacitors are charged through the resistance which in this case the voltage passing through them will have exponential curve. Equations related to this circuit are as follows [34].

$$T = R_1\left(C_x + C_{off}\right)\ln\left(\frac{V_{TH}}{V_{TL}}.\frac{V_{TL}-V_{cc}}{V_{TH}-V_{cc}}\right) \tag{2-7}$$

$$V_{TH} = \frac{(R_2+R_4)R_3V_{cc}}{R_2R_3+R_2R_4+R_3R_4} \tag{2-8}$$

$$V_{TL} = \frac{R_3R_4V_{cc}}{R_2R_3+R_2R_4+R_3R_4} \tag{2-9}$$

Where, V_{TH} and V_{TL} are threshold voltages in node A. By using a multiplexer, such as in the following figure, capacitor C_x can be calculated according to the time period output [34].

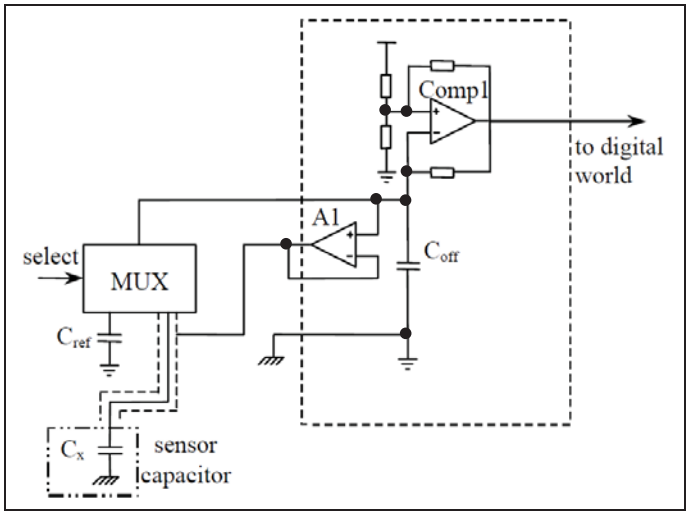

Fig. 2-10 Using a multiplexer to calculate an unknown capacitance according to the time period [34]

$$T_x = R_1\left(C_x + C_{off}\right)\ln\left(\frac{V_{TH}}{V_{TL}}.\frac{V_{TL}-V_{cc}}{V_{TH}-V_{cc}}\right) \tag{2-10}$$

$$T_{ref} = R_1\left(C_{ref} + C_{off}\right)\ln\left(\frac{V_{TH}}{V_{TL}}.\frac{V_{TL}-V_{cc}}{V_{TH}-V_{cc}}\right) \tag{2-11}$$

$$T_{off} = R_1 C_{off}\ln\left(\frac{V_{TH}}{V_{TL}}.\frac{V_{TL}-V_{cc}}{V_{TH}-V_{cc}}\right) \tag{2-12}$$

$$C_x = \frac{T_x - T_{off}}{T_{ref} - T_{off}} C_{ref} \tag{2-13}$$

C_{ref} is a capacitor with known value. The electrical output of a relaxation oscillator usually is a sawtooth wave, triangle wave or square wave. If only a small part of exponential ramp had been used, we will get an approximate linear ramp. However, if a full sawtooth wave is required as in Fig. 2-11, charging resistance is replaced with a constant current source. This figure is an example circuit of reference [32] to convert capacitance changes to a time period, uses a constant current source for charging the capacitor.

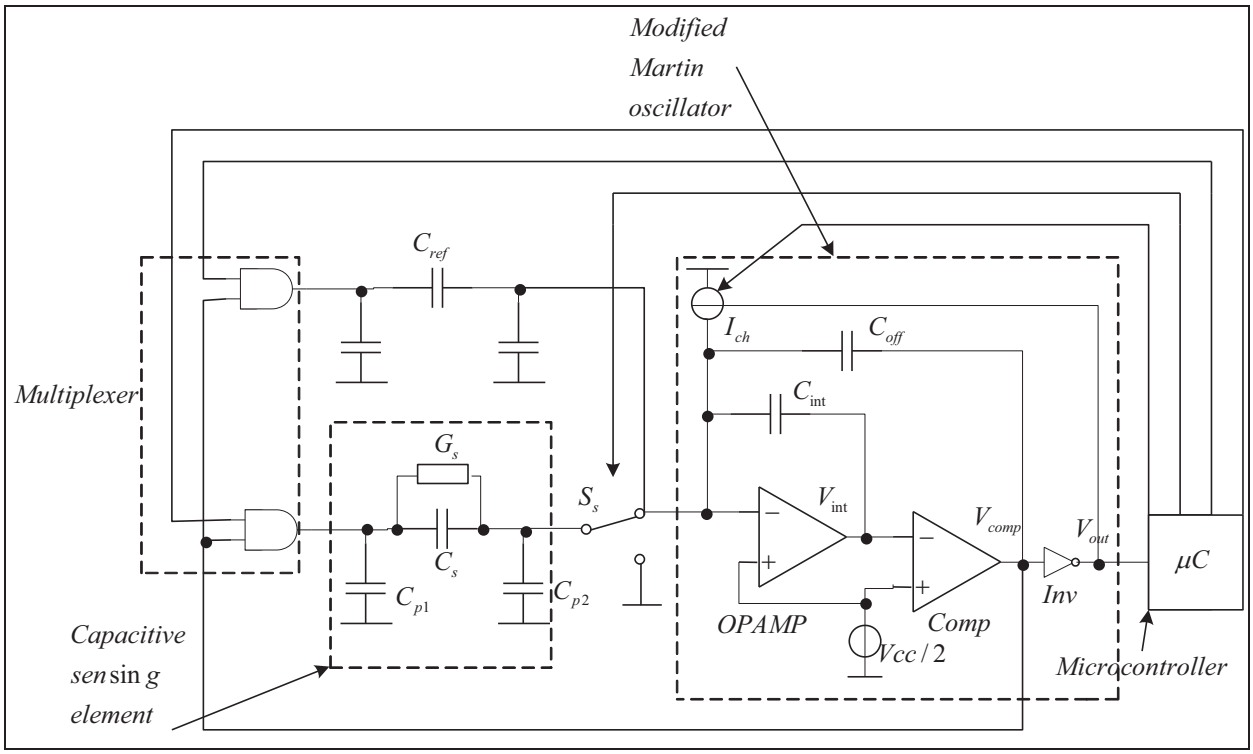

Fig. 2-11 Circuit presented in reference [32] to a relaxation oscillator in which capacitors are charged with a constant current source

The mediator in Fig. 2-11 includes a relaxation oscillator (modified Martin oscillator), a multiplexer and a microcontroller. In this circuit, C_s is a capacitive sensor and G_s a

conductivity parallel shunt. In all capacitive sensors, pollution, congestion and non-precision assembly of matter can create a conductivity shunt, G_s, in parallel with the capacitor sensor. Capacitor C_{ref} is a specific reference capacitor with valueless shunt conductivity. Modified Martin oscillator linearly converts the capacitance values to modulated period signal. The switch S_s is used to connect sense elements to the oscillator. The multiplexer is controlled by a microcontroller, selecting the capacitor to be measured. The multiplexer must also have low output impedance to drive the capacitor. The microcontroller measures the period and calculations are based on a measurement algorithm.

In this method, the time measurements are high (400 ms) [32] and suitable for measuring large capacitances. Therefore, this circuit does not have high accuracy and is not considered an appropriate method to use in this study.

2.3 Comparison between methods listed

In this chapter, various circuits for capacitive sensor reading DNA sensor capacitance are presented. This study presents the advantages and disadvantages of the various methods in order to select the best circuit suited for detecting capacitive changes in a DNA sensor.

As mentioned before, these circuits can be applied in continuous or discrete-time. Circuits sensing voltage in continuous-time need a bias circuit to provide DC bias in nodes of sensing. The figure below, shows a sample circuit in continuous-time, where the resistance R_b has been used to provide bias [25].

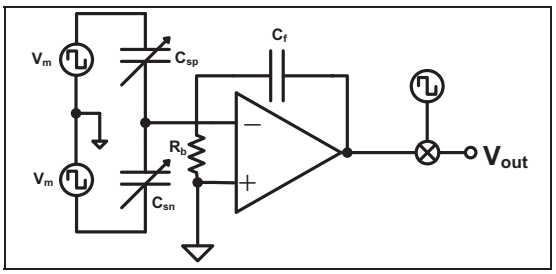

Fig. 2-12. Capacitor detector with the continuous-time voltage with the capacitor feedback structure

To prevent signal attenuation, the resistance should be much larger than the sensor ac impedance, in the range of 10^6 – 10^8 Ω. In practice, the real resistances are barely usable because large resistance not only occupy large silicon areas but also have large parasitic capacitances. In such cases, some components with high ac impedance are used as a bias circuit, such as reverse bias diodes, sub-threshold MOSFETs and MOS switches [35]. However, providing reliable dc bias in sensor nodes is a major challenge for circuitry with

continuous-time voltage. The other disadvantage of the continuous-time circuits is that referred input noise from resistances that provide the bias at low frequencies are high.
In the switch capacitor circuits, larger resistances to provide dc bias are not necessary. Since the switching operation itself creates a proper bias that resolves the requirement for use of large resistances in the circuits. Also, the capacitive switching circuits which create a virtual ground are less sensitive to parasitic capacitance. In such circuits, flicker noise of the amplifier can be eliminated with CDS[1] or CHS[2] methods.

These methods are explained in greater depth in the next chapter. The main disadvantage of a switch capacitor circuit is noise interference (due to sampling procedures). To improve SNR[3] in circuits, increasing the sampling frequency or designing structure in the circuit that limits the bandwidth of noise interference can be used. A major advantage of discrete circuitry in time is that it uses less surface area on the silicon, because as mentioned, it does not require large resistors. Also switched capacitor circuits can convert capacitance to digital values directly [31].

Mediator electronic circuits where the output signals are modulated can be connected directly to a microcontroller. Moreover, such interfaces could easily be implemented with a relaxation oscillator and applied to capacitive sensors. The capacitance to frequency converters, in terms of power consumption and space occupied on the chip surface, are very efficient, but the application according to their high sensitivity to temperature, is limited [36]. Such circuits also require a conductivity shunt to remove parasitic capacitance. Fig. 2-13 shows the results comparing methods which are in reference [26]. In the figure indicated, capacitor resolution for the various designs with $V_p=3V$ and $V_m=1V$ (Vm and V_p are drive signals).

[1] Correlated Double Sampling
[2] Chopper Stabilisation
[3] Signal-to-Noise Ratio

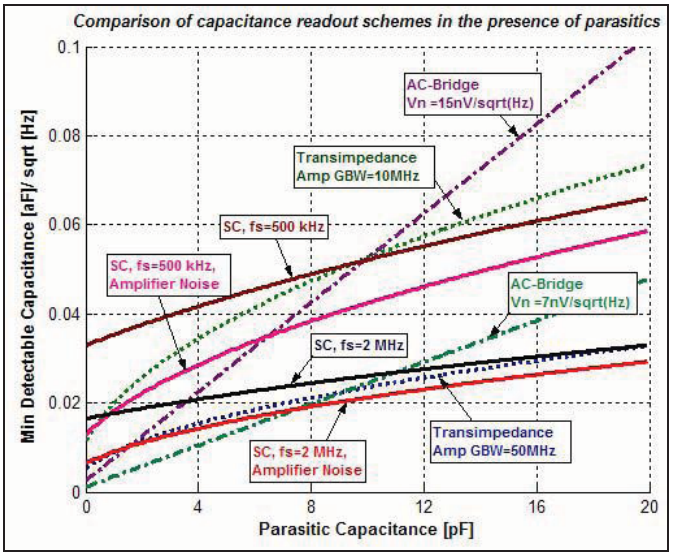

Fig. 2-13 Resolution of readout circuit capacitance compare to parasitic input capacitors [26]

For impedance converter amplifiers, a minimal capacitance can be detected by increasing amplifier gain bandwidth. Resolution of capacitive switches for C_{int}=0.5pF and C_{out}=15pF (capacitors as shown in Fig. 2-8) and two sampling frequencies of 500 KHz and 2 MHz are plotted. Resolution is better when frequency of sampling is increased and noticeably improved when noise of *kT/C* is removed. Virtual ground on the amplifier input of impedance converters and switch capacitor circuits readout reduces the effect of parasitic capacitance input. The figure below shows the capacitive resolution against C_p (parasitic capacitance) for two C_{s0}=1pF and C_{s0}=100fF as input parasitic capacitance changes. Minimum available capacitance increases when the capacitor sensor is larger.

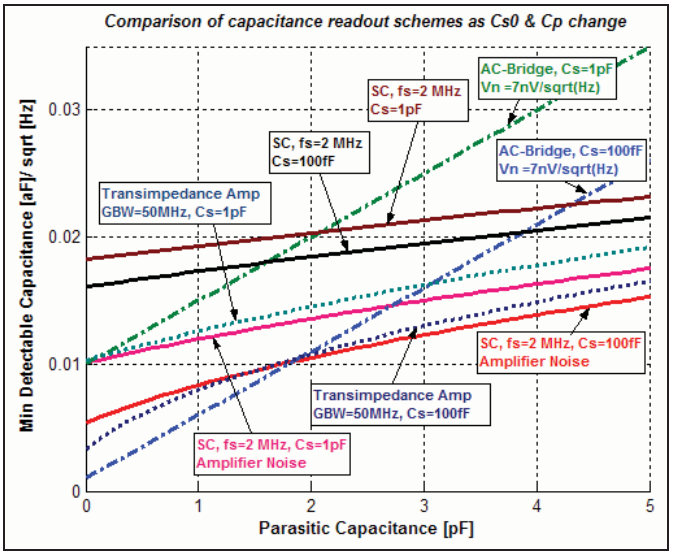

Fig. 2-14 Minimum capacitance can reveal changes in the parasitic capacitance and sensor capacitance bias [26]

Chapter 3: Literature review

3.1 Biosensors

Since 1993, the concept of biosensors, as discussed by Millan and Mikkelson [37], were introduced and numerous groups have done extensive studies in this area. Most molecular biosensors have very specific processes to identify analytes. The role of the sensor is to create a suitable method for a complex target probe in order to identify the electrical signal. Minimum required element to form a biosensor is: a suitable molecular identification transducer connected to the obvious physical mechanism. DNA molecules have a strong and specific interaction between complementary base pairs of target and probe fields; hence, they provide a very good indicator for detection and diagnosis. In short, the probe molecules bonded to a surface allow optimal interaction between pairs of bases. The signal of this hybridization can then be detected by a transducer, which might be an electrochemical transducer [38], optical transducer [39], Gravimetric transducer [40], Surface Plasmon Resonance (SRP) [41] or electric transducer [42]. Electrochemical methods incorporate such features as being fast, ease of use, and lower construction costs compared to other methods. An outline of target molecule detection by the sensor is shown in Fig. 3-1. Hybridisation methods to generate proper electrical signals are briefly described.

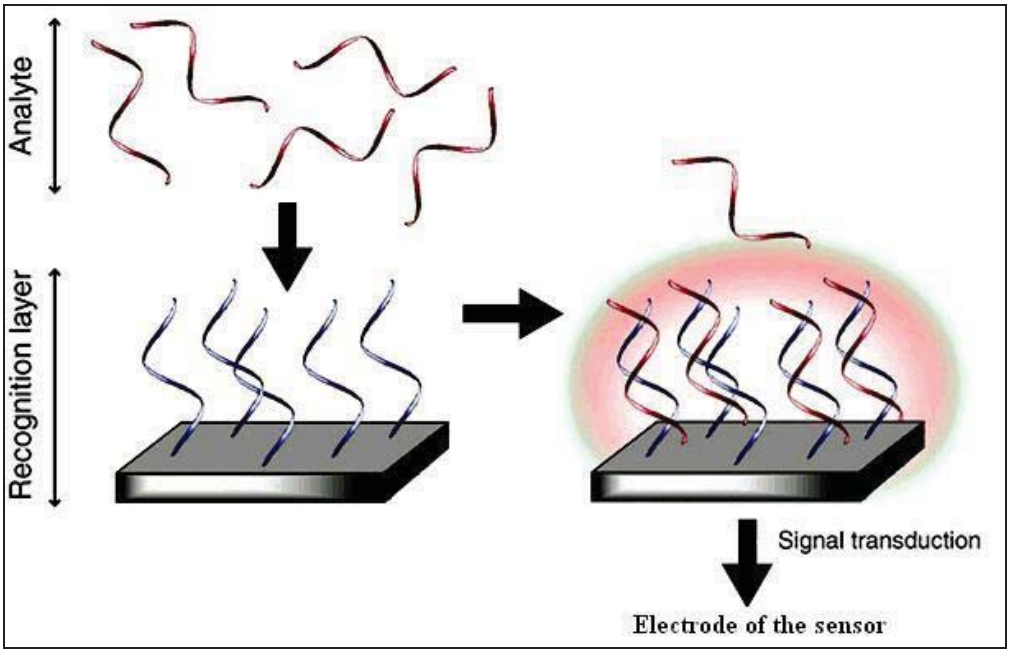

Fig. 3-1: Outline target molecule detection by sensors [62]

3.1.1 Optical transducer

3.1.1.1 Fluorescence

Optical fluorescence biosensors have high sensitivity and it can detect molecules up to 10^7 molecules/cm^2. With this type of biosensors arrays contain thousands of sequence specific probes [43-44] that are known as Gene chips [45-46] and simultaneously many samples are analysed.

Further to nucleotide sequence and gene probes, reliability is required for molecular recognition. In addition to cost and complexity of tools used in this method, low manufacturing efficiency, synthesis and stigmatization of target molecules and non-uniform radiation intensity fluorophore, are the main causes in lower accuracy of this method in clinical diagnosis of diseases.

3.1.1.2 Surface Plasmon Resonance (SPR)

SRP is an optical technique which changes reporting from reflection of thin metal that has an analyte absorbed on it (Fig. 3-2). This method is suitable for identifying target molecules in an array structure [47]. This method, also like the florescence method, is expensive and complicated so mostly used in well established labs for research purposes.

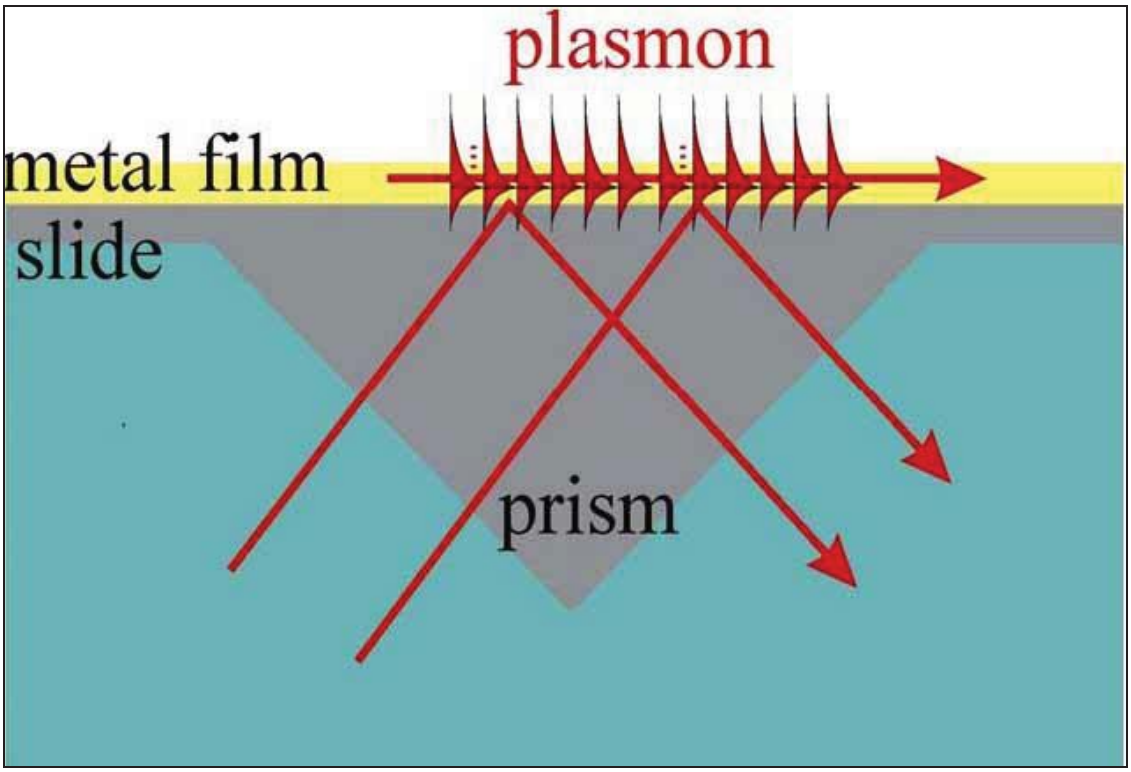

Fig. 3-2. Scheme of SRP techniques to identify target molecules absorbed on the surface [62]

3.1.1.3 Direct optical method

The most direct method of optical identification, the use of single DNA target strings attached to gold nanoparticles, which is easily detected after hybridization of the modified target sequences with the probe molecules, the solution changes colour [48]. Using silver solutions related to photography and scanning techniques of colour changes, the sensitivity level 100PM can be obtained [49]. This simple and sensitive method provides a good perspective to develop the methods of the optical transducer.

3.1.2 Mass transducer

Measurement of frequency changes in an established mass layer, on which the target molecule is connected. QCM[1] technology [50] is shown in Fig. 3-3. This tool is very sensitive and provides good possibilities in detecting hybridisation in real time. However, using QCM in liquid solution requires more research with new techniques to amplify the signals have been the focus of further research [51]. In addition to this method, changes in mass can also be assessed as radiation reflected from the surface of a very thin moving needle[2] revealed by laser fields [52]. In this method, the mass increase following hybridization is detected by laser light that is reflected from the surface of the needle as it deviates. This technique is useful for the development of linear arrays. Limitations of this method are expensive tools and technical difficulties in construction of the needle.

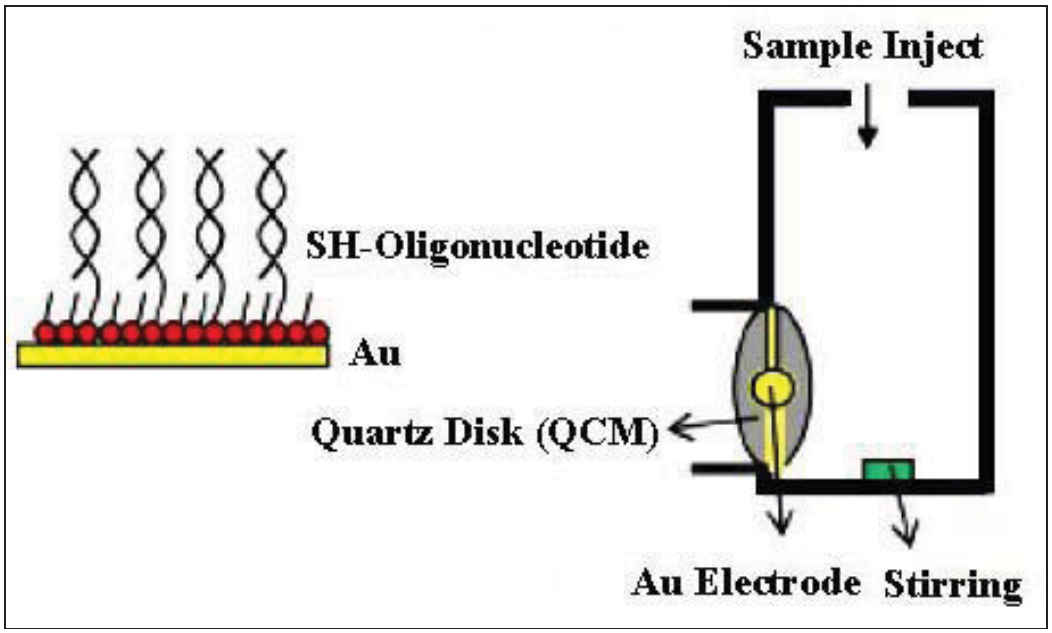

Fig. 3-3 Scheme the process of target molecule detection technique using QCM

[1] Quartz Crystal Microbalances
[2] Microfabricated Cantilever

3.1.3 Electrochemical identification

DNA detection and genetic tests require the following factors:

1. Sensitivity
2. Speed of operation
3. Low-cost
4. Equipment that is simple to operate.

Electro-chemical biosensors for DNA detection work on the basis of converting hybridisation activity into an electric signal. The Electro-chemical conversion process uses enzymes, Intercalated substances, or electro-active polymers in operation. Since the electrochemical reactions directly produce signals, this means there is less need for expensive converters. In addition, DNA probe sequences can be bonded on electrode surfaces by very a variety of methods. Creating electro chemically signals has two basic formats, direct methods and indirect methods [53-54].

3.1.3.1 Direct electrochemical of DNA detection methods

A: DNA detection based on passing electric current in DNA

In one of these methods, DNA molecules are bonded between two ends of a micro gap, and then silver is applied to enable attachment to the DNA molecules. A flow of electric current from these silver wires represents a state that hybridisation has occurred [55]. Another method is a surface between two electrodes of Ti (Titanium) and Au (Gold) bonding the probes, the target Sequence will be hybridised and additional growth of silver on the reporter DNA molecules allows a flow of electric current from the silver growth wire [56].

B: Using internal signals of DNA to detect hybridisation

Direct methods usually concentrate on the inherent electrochemical activity of nucleobases. Adenine and Guanine are active bases of electrochemical activity because they are easily adsorbed with an oxide [57-58]. Nucleobases will adhere to the surface of a mercury electrode by way of redox (reduction-oxidation reaction) on the surface of a carbon electrode. A basic technique to detect and identify DNA via electrochemical method is redox and restored DNA on a mercury electrode. Measurement techniques such as constant current chronopotentiometry or voltammetry square wave are used to differentiate between ssDNA and Target bound dsDNA [59-60].

Adsorption properties have provided suitable techniques in working with micro-litre volumes in electrochemical methods, so it is possible to measure very small quantities of DNA with

this method [61]. Another process involved with redox DNA is ASV (anodic stripping voltammetry). A highly sensitive method made by electrostatic charge assists in gradual accumulation of DNA on the electrode surface before being measuring by electrochemical means.

Purine bases in DNA are oxidised by electro-chemical action. In this method different kinds of electrode can be used, such as Carbon, Gold, Tin oxide-indium (ITO) and electrodes coated with the polymer discussed in [62]. Although this method has high sensitivity, the need for very high potential for direct oxidation of DNA, the electrochemical process also has very high background current fields.

Palecek and colleagues [63], and Wang [64], had developed a two-stage technique for capturing target sequences of DNA using DNA probe fields immobilised on magnetic beads. After the target DNA hybridization process, magnetic beads are separated from the solution analyte. The accumulated DNA is depurinated in an acidic solution (to remove purine groups) and free Guanine adenine used for analysis by ASV[1] methods. The smallest detection limit of this assay is 40 Femtomoles[2] which is $2x10^{10}$ molecules.

C: Using electrochemical impedance to detect DNA hybridisation

Hybridisation of two DNA strings on the electrode surface changes the band of semiconductor potential, this shift is a curve along a potential axis. These properties can be used to detect direct DNA hybridisation without using molecular labelling.

D: Field effect sensors in DNA hybridisation detection

The basic operation of this sensor is in the changes of properties of surface electrodes when hybridisation occurs on the surface. Concentration levels in nanomolar DNA binding occur within a few seconds and are identified as single base mutation in a 12-mer sequence [65].

Two commercial microarray chips designed for DNA detection, the Genelyzer and Motorola esensor^{TM} have been released to the public market [66-67]. Genelyzer has ability to detect most kinds of SNP[2]. A very appealing technique created with a new idea polypyridyl complexes of Ru^{+2} and Os^{+2} ions as mediated electrochemical oxidation level Guanine in DNA or RNA structures due to $Ru(bpy)^{+3}3$ increase limitation of nucleic acid detection. However, researchers still haven't solved the problems of high potential as yet [68].Fig. 3-4.

[1] Anodic Stripping Voltammetry
[2] Single Nucleotide Polymorphism

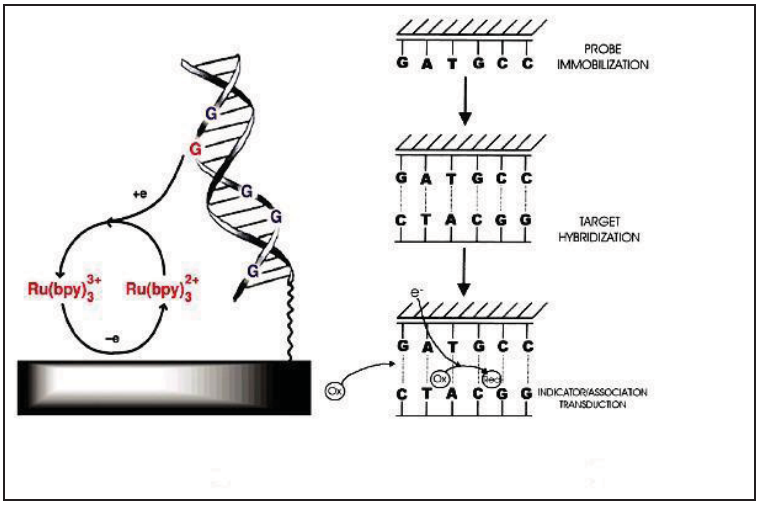

Fig. 3-4. Poly pyridyl complexes of Ru^{+2} and Os^{+2} ions as mediated electrochemical oxidation of Guanine in DNA or RNA structures due to $Ru(bpy)^{+3}3$ increase limitation of nucleic acid detection [69]

3.1.3.2 Indirect electrochemical of DNA detection methods

A: DNA as an intermediate transfer of charge in electrochemistry

Redox-active molecules that normally have interactions with the structure of two spiral strings of DNA are used for electrochemical DNA detection. In this form of analysis, DNA has both a reactive role and the role of intermediaries in the electrochemical process. This method is very simple and highly accurate.

B: Electro-static probe molecules

In this method of electrochemical detection, DNA probes are adsorbed on a carbon electrode surface, then after hybridization process of target DNA, greater amounts of $Co(phen)3^{3+}$ ions are connected to the surface of the electrode due to the negatively charged electrode surface.

In Steel et al.'s work [70], they offer an effective method to identify DNA hybridization, which utilises $Ru(NH_3)_6{}^{+3}$ to mediate bonding of DNA to the electrode's surface.

Application of these cations, (positively charged atom) has provided the exact method, robust and reliable for measuring the amount of DNA on the electrode surface.

C: Intercalative Molecules

Detection and measurement of electro-active sensors that enters the gaps of DNA bases or the electro-static interaction with single-stranded DNA are base indirect methods [71]. In this method the probe is bonded to the electrode by way of hybrid target sequences placed in a solution containing the active molecules. After a specified time, the electrode is washed and measurement carried out by way of an electrochemical method for diagnosis or detection. Several metal complexes (coordination complex) such as Phenanthro [72-73], ruthenium

bipyridine [74] and anti-cancer substances, such as epirubicin chinomycine [75-76] are used in electrochemical detection. [77]. A new approach, intercalative molecules have been used to report the amount of target DNA or single, double string DNA. Here, the inherent ability of double-stranded DNA to mediate transfer of electric current is considered.

When DNA bases are normally matched, transfer of electric current is possible; however, if there's a mismatch in the structure of DNA, the natural electric flow at the length of DNA is reduced. Transmission of electric current along the DNA molecules determines the structural changes, e.g. Devastation, which is the structural error between the base couples and even proteins binding DNA, which has been discussed in literature [78]

To increase the sensitivity of this method, coulometric measurement of redox ferrocyanide-mediated methylene blue is used [79]. During the electro-static process, electrons from the electrode surface mediated by DNA, binds to the intercalative molecule of methylene blue the addition of methylene blue, causes redox of ferrocyanide in the solution and thus more electrons become transferred to methylene blue and DNA bases. When the structure DNA's bases is not coupled properly, methylene attached to the DNA (in terms of catalytic activity) will be inactive so that signal intensity will be reduced, as shown in Fig. 3-5 [42].

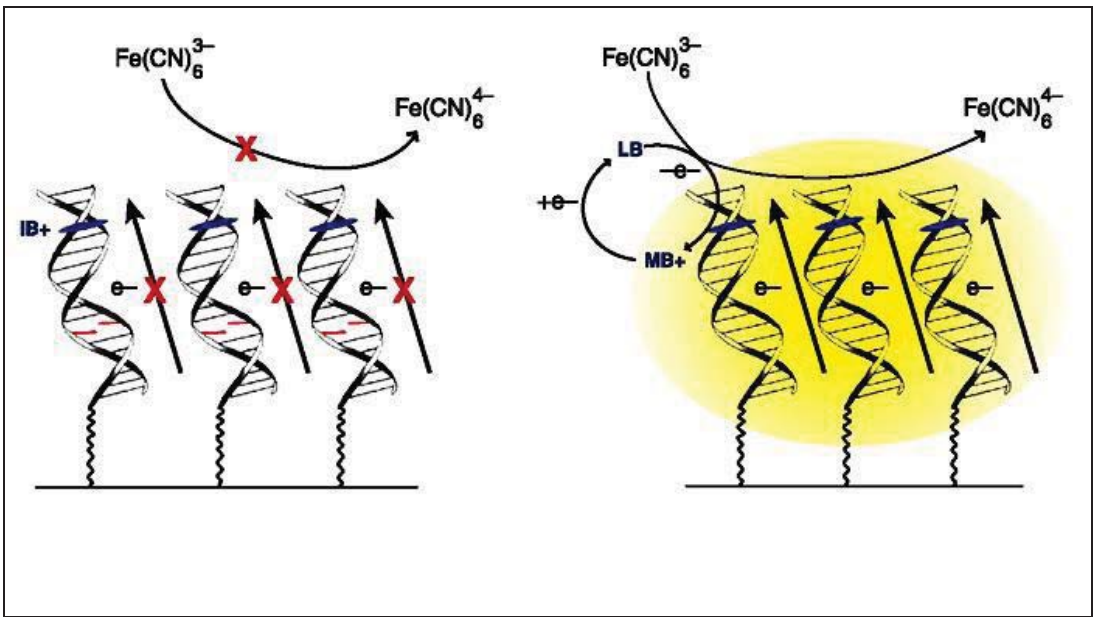

Fig. 3-5. Using label molecules for detecting of mutations in the target sequence [69]

By using this method with an electrode diameter of 30μm to about 10^{18} molecules in a double string can be detected. Hence property transfer of electric current on DNA plays an effective role in determining the SNP, the sensitivity electrocatalyst, to achieve simple structure array and also identify the exact target DNA.

3.1.4 Identifying proteins and small molecules attached to DNA

DNA molecules have a uniform structure, regardless of the length and type of nucleotide sequence, establishing structures of a self assembling monolayer on the electrode surface. Many laboratories around the world use this simple design of biosensor, which provides a method for identifying and tracking proteins and other small molecules. One such chemical protein, which has recently been studied as part of an electrochemical DNA sensor for detection, is arsenic trioxide [74]. In this example, voltammetric signals from Guanine oxidation upon exposure to AS2O2 decreases; where, when time and concentration of arsenic trioxide is greater there is a decrease of voltammetric signal. Reaction between Guanine and arsenic trioxide will cause destruction of purine bases. Therefore, this method can be used for detecting the molecules that are irreversibly bonded to DNA; thus, providing a method for tracking the environment of many molecules. Currently with PCR, using this method, a biosensor for diagnosis of anthrax has been developed [75]. In other studies, the behaviour of the transfer of DNA's electric current for identification of electrical proteins has been used [76]. In this study, two DNA strings that have the ability to bond covalently to protein and daunomycin, which is an active intercalative molecule on the gold electrode surface, form a non-compact SAM layer.

To prevent the interaction between daunomycin and the electrode surface, the electrode surface is completely covered with mercaptohexanol. Then the DNA-modified electrode is exposed to a solution with M.HhaI protein (base-flipping enzyme). The signal related to daunomycin is strongly reduced, which indicates that binding of proteins has taken place. If M.HhaI mutated enzyme is used, a base tryptophan inserted into the creates a vacancy (due to enzyme activity) and a daunomycin signal is returned. Thus, the DNA-modified electrode provides a powerful tool for diagnosis in a variety of proteins.

3.1.5 Detection of DNA by bonding the probe to an enzyme

Using such probes, which have an enzyme, would have much use in the electrochemical DNA detection [80-81]. Using enzymes, a detection limit 20pmol L^{-1} with about 13-35μL of 38-base DNA, has been reported. In another experiment using horseradish peroxidise

enzyme, detection limit 0.5 fm has been reported [82]. In later work to reduce non-specific effect connection, magnetic beads with the enzymes were used [83-84]. Heller and colleagues [85] attempted to identify and detect DNA in the electropolymerisation of polymer with few cationic molecules in order to create a layer of polymer gel on the electrode surface. Target DNA with probe DNA hybrid and the other end of target DNA bound to a reporter oligonucleotide single strand with HRP[1]. This technique, using carbon electrodes with a layer of polyester, which is very cheap, has been used. In a new method, Willner and colleagues [80] have been able to detect a DNA hybrid by using the process of using a biocatalyst at the probe-modified electrode surface. Fig. 3-6 shows this method.

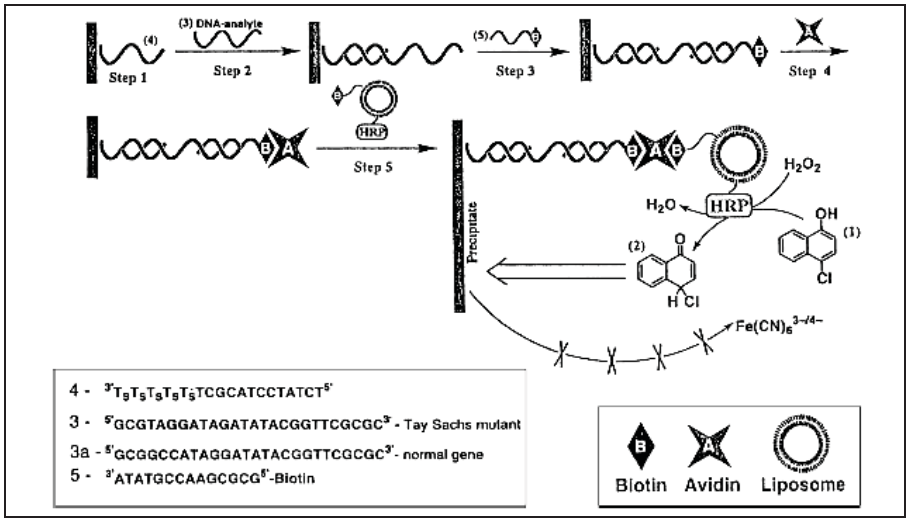

Fig. 3-6. Detection by way of a biocatalyst

3.1.6 Detecting electrochemistry of DNA by using metal nanoparticles

3.1.6.1 Nanoparticles

Over the past decade many advances in the use of nanotechnology methods for molecular diagnosis have been made and still more effort is being made to design Biosensors for accurate, sensitive, and selective diagnosis [81]; furthermore, the use of nanoparticles to detect nucleic acids and proteins has been investigated. Due to the size of the nanoparticles and physical adjustability coupled with chemical behaviour (including electrical, electrochemical, optical and magnetic properties), these sensors are a good candidate to replace the current popular colour phosphorescence molecules for molecular labelling [81, 82, 83]. Nanoparticles as labels increase, sensitivity, speed and flexibility to test the presence of biological material or measure activity. Nanoparticles can be used for efficient identification of microorganisms, cancerous tissues, etc in vivo and in vitro. [81, 82, 83]

In this study the use of four types of nanoparticles will be discussed. These particles are classified based on the readout mechanism provide.

[1] Horseradish Peroxidase (HRP)

3.1.6.2 Gold Nanoparticles

The particle sizes are three to one hundred nanometers and because several measurement methods, such as optical density, fluorescence, Raman scattering, electric current and magnetic force can be used to identify DNA nanoparticles, this is a good method with which to design biosensors. DNA detection using gold nanoparticles, compared to common genomic detection systems, have ten-fold sensitivity and have a hundred thousand times more features [81, 82, 84].

3.1.6.3 Optical readout

Using optical and thermal properties of gold nanoparticles probes aggregated as a detection method, the interaction between bonded oligonucleotide (DNA Probe) on the gold nanoparticles and DNA target causes assembly of nanoparticles joined together into a network that will change colour. This feature of changing colour is provided by interaction between the surface Plasmon of the particles and change in the distance between the gold nanoparticles. This colour change indicates the presence of a target molecule in the sample and it is visible without any equipment. Target molecules at different temperatures also causes a sharp colour change [90, 91], which is shown in Fig. 3-7.

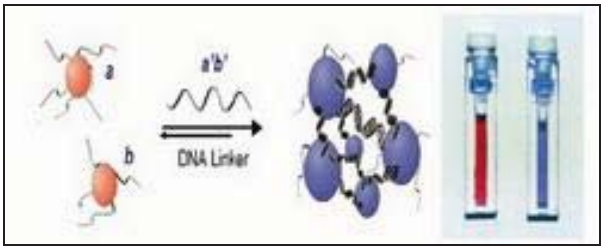

Fig. 3-7 Optical characteristics of gold nanoparticles, separate and aggregated

By transference of the mixture of aggregate created between bonded DNA to its complementary chain, and strings with varying degrees of sequence (to supplement the chain) on TLC[1] at different temperatures, it is possible to evaluate the standard hybrid model at different temperatures.

By using these properties of colour and temperature, this design can be used to detect mutations in the target DNA samples. In other words, this method can identify SNP mismatches [88, 91]. Fig. 3-8 demonstrates how to use this method to detect mutations in target DNA.

[1] thin-layer chromatography (TLC)

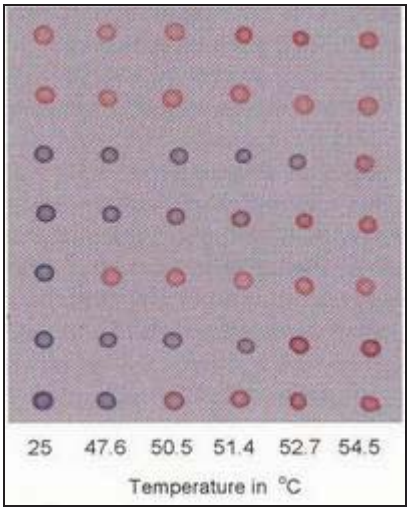

Fig. 3-8 SNPs detection using nano-gold-DNA probes

Sensitivity colorimetric detection methods with silver redox (Ag) by the gold nanoparticles will increase sensitivity. The Scanometric Method is a sandwich measurement method, which includes a string attached to the substrate DNA (or DNA Chip), a target sequence, and a gold nano-probe. Bonding target molecules and probe sequences attached to a gold nano-platform creates a series of gray spots showing the concentration of the sample specific of target molecule. Intensity of these gray spots can be viewed by a scanner or even the naked eye. By using silver and redox on gold nanoparticles, as shown in Fig. 3-9, detection sensitivity can be raised [86, 87].

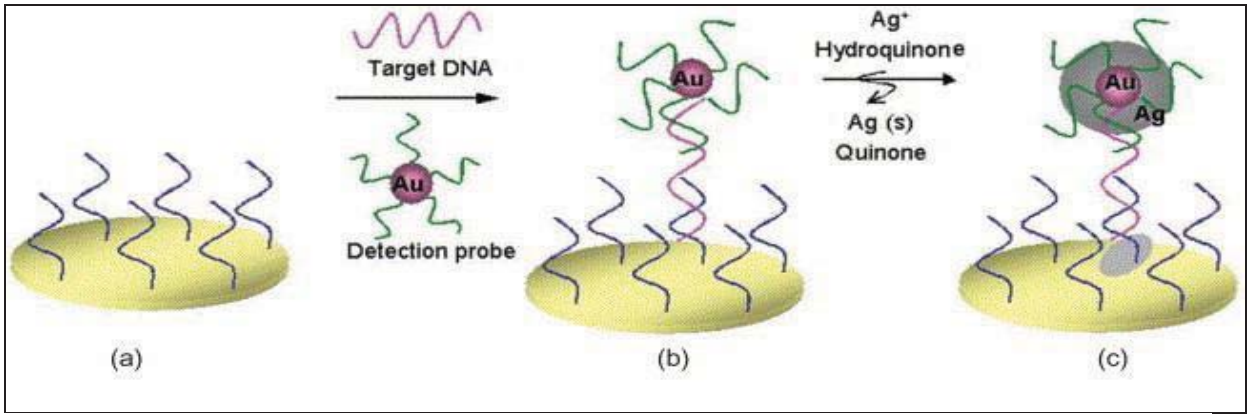

Fig. 3-9 Detecting DNA by Scanometric method [82]

By using different gold nanoparticles (and thus different colours) simultaneously, detection of multiple target molecules is possible. These molecular detection methods have four times as many features and hundred times more sensitivity compared to current methods of fluorometry [87].

One example of this method is bio-barcode. Bio-barcode is a synthetic DNA selective sequence for a target DNA, which is used for diagnosis of DNA in Fig. 3-11 or protein, as pictured, in Fig. 3-10 in biological samples.

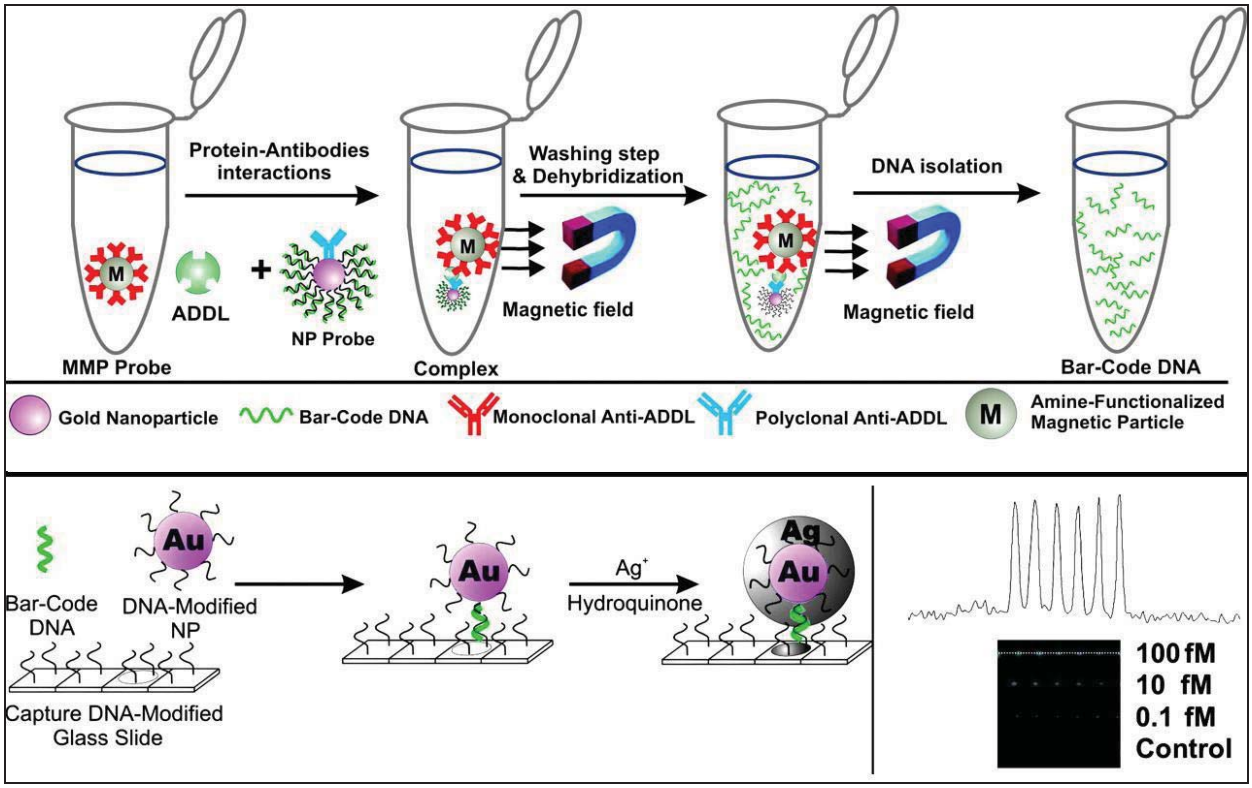

Fig. 3-10 Protein detection in cerebrospinal fluid (CSF), based on the Bio-Barcode [88]

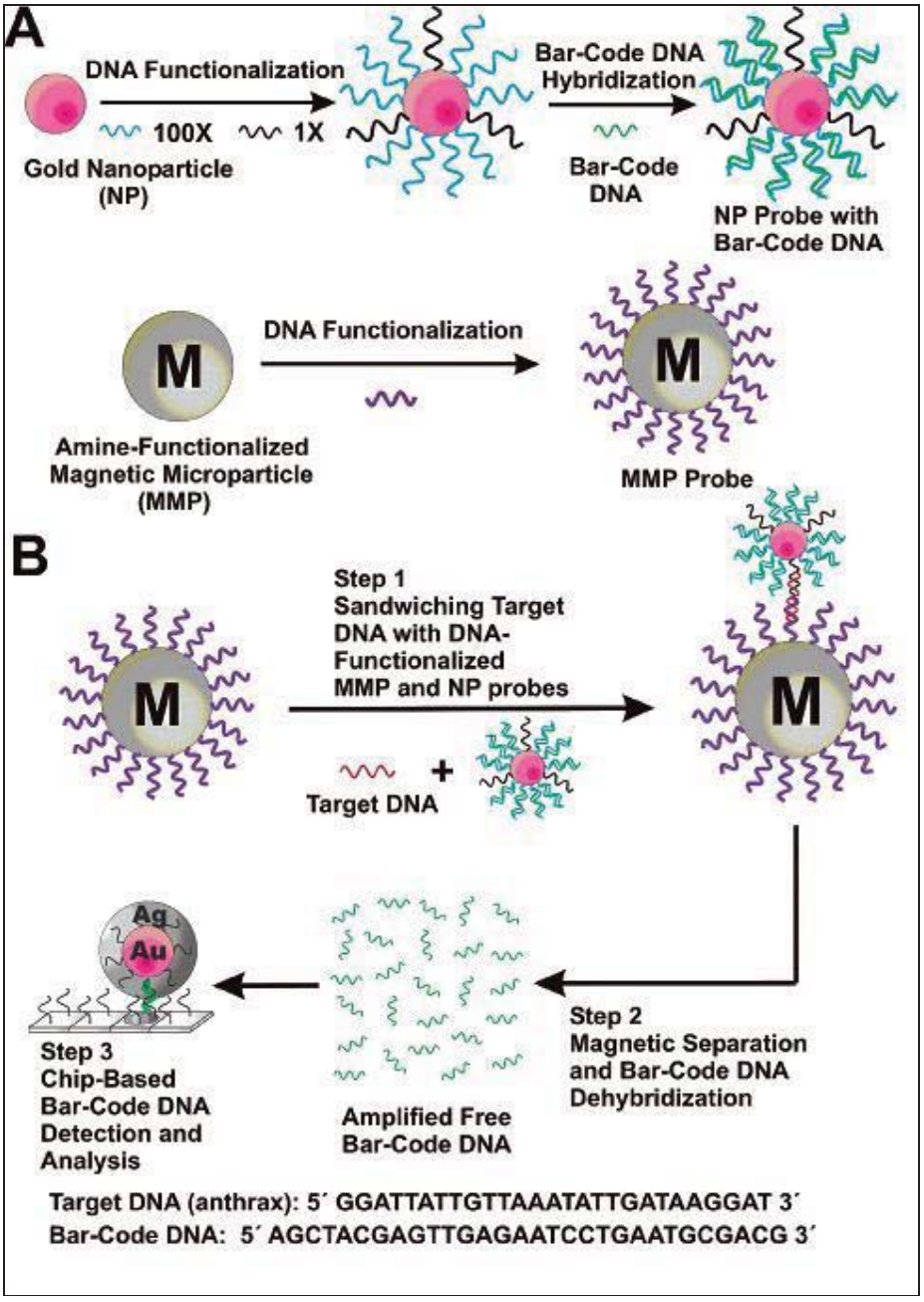

Fig. 3-11. DNA detection based on Bio-Barcode [89]

A: DNA detection

This method uses a chain of desired DNA sequence (Bar-Code DNA) design and also makes a complementary string after activation on the gold nanoparticles. A third string of DNA that is complementary to the first part of the DNA target, after activation, is bonded on magnetic particles. When placed over the two particles in the solution, if there is a target DNA, even in small quantities, this causes a connection between the two particles. In the next step, the second particle can be separated from the solution by their magnetic behaviour and then using factors (such as Denaturation compounds) that separate the two strands of DNA, separating

and identifying DNA bar-code from the complementary. This method can also use compounds such as silver, which raises detection sensitivity. Thus, small quantities of a DNA sequence can be detected and measured without the need for PCR [90].

B) Detection or measurement of protein by using Bar-Code DNA

In this method, like the previous method, a complementary sequence of choice has been used with gold nanoparticles. Also, polyclonal antibodies are bonded on the gold particles in order to measure the protein. Antibodies are also bonded on magnetic particles. By entering the two sets of particles in the solution containing the desired protein the protein bonds to the antibody and both the particle surfaces connect to each-other. After washing and removal of other materials by way of the magnetic field properties of the second particle, it can be separated from the solution as the previous method, after separating the string DNA barcode from its supplement by Denaturation, it is possible to identify and measure DNA barcode for the presence of the desired protein in the sample [89].

3.1.6.4 Electrical detection of biological molecules using gold nanoparticles

Another method to identify a DNA target is by electrical detection. In this method, DNA probes are bonded on micron-sized pages (chip) between two electrodes. The probes are designed with complementary halves of the DNA target. The gold nano-probes design is such that it is a complementary oligonucleotide DNA target to the other half. The gold nanoparticles are placed in the median between the two electrodes. By adding silver, between two electrodes the silver is drawn into the cavity creating a bridge between two electrodes. The presence of target DNA is indicated by the changing electric current. The level of accuracy of this method is 500fm and it is also used in immune assays [86, 91].

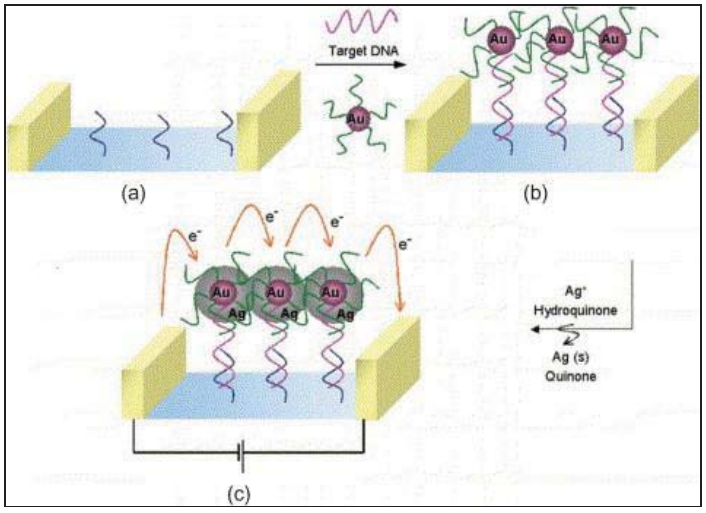

Fig. 3-12. DNA hybridisation detection [88]

3.2 Methods for noise reduction and offset in readout circuit of capacitive sensors

3.2.1 Noise sources in sensor circuits

The resolution in readout of a capacitive sensor circuit is limited by the noise. Noise is caused by two different sources. The sensor itself always generates noise, for example mechanical wastes. The main source of mechanical noise in the sensor is due to Brownian's motion of gas molecules around the mass resistance. The total noise equivalent acceleration is as follows:

$$TNEA = \frac{\sqrt{4k_B TD}}{M} = \sqrt{\frac{4k_B T\omega_r}{QM}} \tag{3-1}$$

The above equation shows that to minimise mechanical noise, quality and resistant mass should be increased.

The electronic circuits that are used to read the capacitance changes are another source of noise. Noise is a major limitation parameter for analogue designers. For this reason, there will be a compromise between the other parameters, such as power, gain, etc. In addition, because noise affects the minimum detectable signal in amplifiers, especially in low voltages supplies, noise is a very important factor for analogue designers. In active linear circuits, most active elements are in the operational amplifier. In OpAmps with input MOS transistors at low frequencies, the input current is extremely small, but the actual input voltage of the OpAmp is usually comparatively large (1-10mV). Basically, OpAMPs are influenced by several nonlinear effects, including: noise (mostly *1/f* and thermal), the offset voltage to the input and also the signal voltage, which is required in order to produce the output voltage of OpAmp. Usually thermal noise has frequency bandwidth, *1/f* noise, offset and input signal, low frequency signals and narrow band [92]. The following section introduces noise consideration with respect to MOSFETs.

3.2.1.1 Noise sources in MOSFET transistors

Two important sources of noise in MOSFET transistors are: thermal noise related to the conduction channel resistance and flicker noise or *1/f* noise. For lower frequency applications, calculating and analysis in noise performance with regard to the above mentioned noises sources alone are enough. In this study only two types of noise are discussed. Also at the end of this chapter, the DC offset is also explained.

3.2.1.1.1 Thermal noise in MOS transistors

When a MOS transistor is in the on mode, the current flowing between the source and drain creates a channel based on reverse resistance between them. The channel substrate by

minority carriers, under an appropriate gate control voltage is formed. Same as resistance, random motion of free carriers in the channel, produces thermal noise in the terminals of the fragment. If there is no voltage between source and drain ($V_{ds}=0V$), the reverse channel can act as a homogeneous resistance. According to the theory of Nyquist, thermal noise current spectral density of a short circuit is given as follows [93]:

$$i_d^2 = 4kTg_0 \tag{3-2}$$

Where k is the Boltzmann constant[1], T is the absolute temperature, and g_0 is the conductivity in channels with a zero voltage change between drain and source.

In analogue applications, most MOS transistors work in the saturation area where the channels can't be considered as homogeneous resistance. In this case, drain current noise of a short circuit could be calculated by making dividing the channel into significant amounts of small sections of Δx as shown in Fig. 3-13.

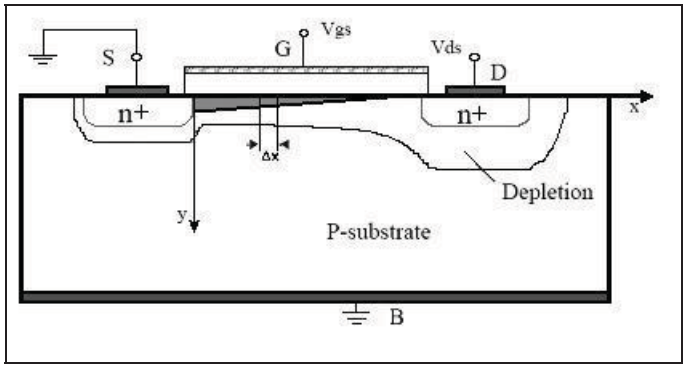

Fig. 3-13 structure of NMOS transistor in saturation mode

Thus, noise spectral density of current drain in the transistors is obtained as follows [93].

$$i_d^2 = 4kT\gamma g_m \tag{3-3}$$

Coefficient γ for long-channel transistors is equal to 2/3 and for MOSFETs under microns it is necessary to replace it with larger amounts [94].

Equation 3-3 shows thermal noise behaviour of MOSFET channel with negligible substrate effect.

[1] Boltzmann constant = $1.3806503 \times 10^{-23}$ m^2 kg s^{-2} K^{-1}

3.2.1.1.2 Noise *1/f* (Flicker) in MOS transistors

In the MOSFET boundary between gate oxide and silicon infrastructure there are interesting properties. Because silicon crystal is ends in this area, many dangling bonds are produced that caused the additional energy states (Fig. 3-14).

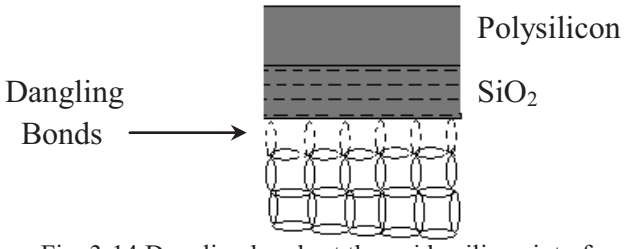

Fig. 3-14 Dangling bonds at the oxide-silicon interface [94]

When carriers are moving at the border, some of them are randomly trapped and again they are released, which produces flicker noise in current drain. Unlike thermal noise, the average power of flicker noise cannot be easily predicted. Since flicker is dependent on the Borders' cleanliness of the oxide - silicon border there will be different amounts of noise flicker from one CMOS chip technology[1] to another [94].

Flicker noise is easily modelled with a voltage source that is series to the gate and its value will be obtained approximately from the following equation [94]:

$$\overline{V_n^2} = \frac{k}{C_{ox}WL} \cdot \frac{1}{f} \tag{3-4}$$

Where, k is a constant value and dependent on manufacturing process and technology, its value is decreased by reducing the technology (Size of L) through the use of advanced processes. According to equation 3-4, the noise spectral density is inversely proportional to frequency.

Because the phenomena of trap set up and release related to dangling bonds mostly occurs in the lower frequencies, the flicker noise also called as *1/f*. Note that the amount of noise is not dependent on the temperature and bias current; reversed dependence of *W* value indicates that to reduce this noise, a simple method is by increasing the surface of the transistors. It is believed that PMOS devices have less *1/f* noise than NMOS because PMOS transistors transfer the holes, which are heavier than electrons within a buried channel, which has distance from the oxide - silicon boundaries. To obtain the equivalent of this noise in drain, the equation 3-4 multiplying to square of transistor transconductance is used. To calculate the flicker noise it is also necessary to pay attention to corner frequency.

[1] The size of L

Corner frequency is the frequency where the thermal noise and the flicker noise level is equal and sets a criterion of how much of that band noise is confused with flicker noise. For transistors below microns, this number has been reported between 500 KHz to 1MHz [94].

3.2.1.2 DC offset in MOSFET transistors

The differential pair in Fig. 3-15(A), if $V_{in}=0$ and the circuit is completely symmetrical, then $V_{out}=0$, however, if there is dissonance in the circuit, V_{out} will not be zero. In this case it can be said that the circuit has a DC offset of the same amount as the output voltage, while the input is zero [94]. In practice, if the offset voltage is returned to the input this means that the voltage applied to the input will make the output zero (Fig. 3-15 (B)). Note that as $|V_{os.in}| = |V_{os.out}| / A_v$ same as random noise, in the random offset also mark (+ or -) is no significance.

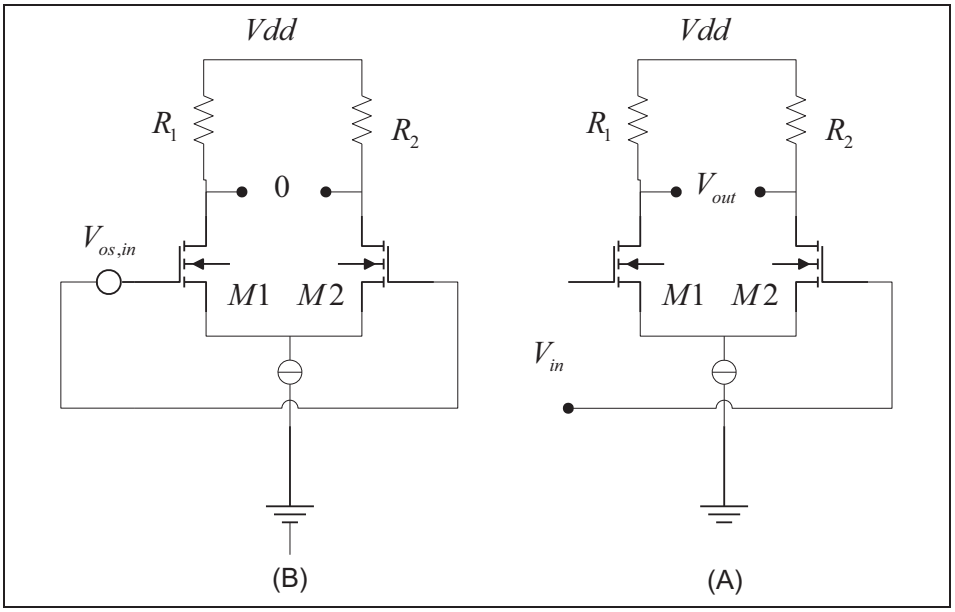

Fig. 3-15 One simple differential pair to show offset; A) differential pair with output offset b) circuit (a) that the offset has been transferred to the input

In the circuits with consecutive amplifiers, offset could amplify so much so that the offset level moves in the non-linear region. The most important effect of offset: reducing accurately measured of the signal. In reference [94], the input offset voltage, is obtained as follows:

$$V_{os.in} = \frac{V_{GS} - V_{TH}}{2} \cdot \left[\frac{\Delta R_D}{R_D} + \frac{\Delta(W/L)}{(W/L)} \right] - \Delta V_{TH} \tag{3-5}$$

Where, according to Fig. 3-16, the following assumptions are considered:

$$V_{TH1} = V_{TH}, V_{TH2} = V_{TH} + \Delta V_{TH} \tag{3-6}$$

$$R_1 = R_D, R_2 = R_D + \Delta R_D \tag{3-7}$$

$$\left(\frac{W}{L}\right)_1 = \left(\frac{W}{L}\right), \left(\frac{W}{L}\right)_2 = \left(\frac{W}{L}\right) + \Delta\left(\frac{W}{L}\right) \tag{3-8}$$

Equation 3-5 is an important result. Because shows the dependence of $V_{os.in}$ to dissonance and bias conditions. Note that:

1. Dissonance effect increases through resistance and the transistor size effectively increases voltage.
2. Dissonance of threshold voltage is fed directly back to the input.

Therefore, it is better to reduce V_{GS}-V_{TH} by decreasing bias current of the differential pair or increasing the transistor's width (W). If two input differential pairs were a short circuit, they create some noise in the output, which is a voltage that is changing with time changes. Offset can be considered as a low frequency noise that when measured appears to be stable.

3.3 Noise reduction methods

Because signal frequency of the DNA sensor relatively is low, the most dominant noise source is components of *1/f* noise in incremental input levels. As mentioned before, this component is inversely proportional to gate size. *1/f* noise can be reduced by a few of the methods below [93]:

- The first method is to use large size components in input to reduce *1/f* noise is related to these components. The disadvantage of this method is that the input capacitance is increased, which in capacitance sensor detection increase parasitic capacitance and reduces sensitivity.
- The second method is to use the buried channel components in order to overcome the effects of channel surface states. This method requires processing steps that are not usually used in standard LSI[1] technologies in mass production circuits.
- The third method is operating input transistors in the lateral bipolar mode, which is compatible with CMOS process. *1/f* Noise will be extremely reduced because the minority carriers' current is taken out of the oxide -Silicon surface. However, this method is not suitable due to base current of the bipolar transistor producing high impedance.
- The fourth method is using special circuit techniques to reduce *1/f* noise and offset, such as CDS and CHS methods.

[1] Large Scale Integration

Several articles are used from CDS and CHS methods for noise reduction and elimination of offset. These methods will be discussed.

3.3.1 CDS method (Correlated Double Sampling)

In micro-machine applications, the size of sensor capacitors ranges between several hundred femto farads up to a maximum of Pico farads. Furthermore, capacitor switching applications create noise sampling of the order of: kT/C [99]. Therefore, in order to achieve high resolution, a low-noise design of capacitance sensing with low offset is needed. CDS is an effective method to reduce low frequency noise (*1/f*), remove offset noise, the effects of injected load, and *kT/C* noise in switched capacitor circuits and amplifiers. References 94 to 98 have used these methods.

Fig. 3-16 shows a capacitance measurement circuit using capacitive switches [99]. The output voltage of this circuit is equal to:

$$|V_o| = \left| -V_S \cdot \frac{C_{S+}}{C_I} + V_S \cdot \frac{C_{S-}}{C_I} \right| = \left| \frac{V_S}{C_I} \cdot \left[C_S - \frac{\Delta C}{2} - C_S - \frac{\Delta C}{2} \right] \right| = \frac{\Delta C}{C_I} . V_S \qquad (3\text{-}9)$$

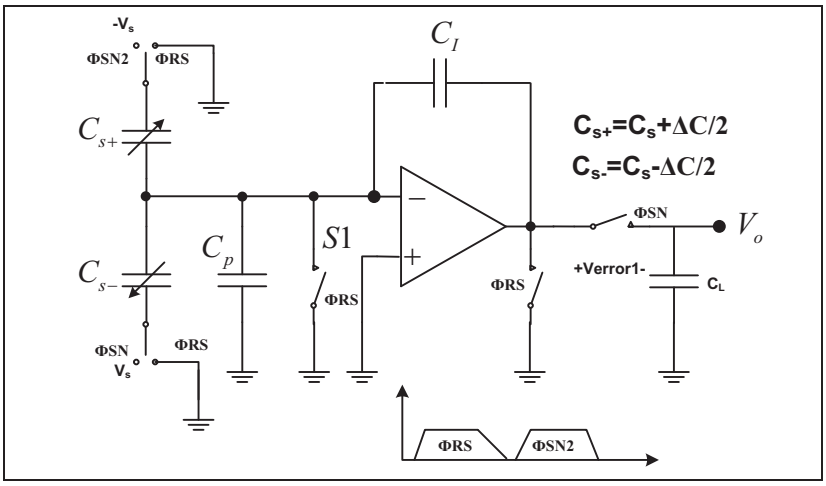

Fig. 3-16 A capacitance detector circuit using switches capacitor method

This section describes the CDS method to remove flicker noise, amplifier offset, and also *kT/c* noise due to injection load of switches.

3.3.1.1 Elimination of noise by using the CDS technique

CDS is expressed simply by adding a holder capacitor C_H and a phase clock, which is shown in Fig. 3-17 in next page [95].

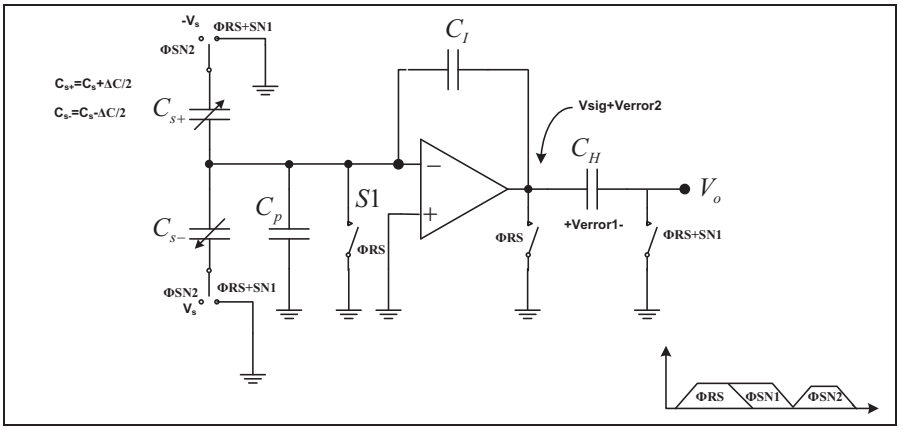

Fig. 3-17 The circuit shows how performance CDS

In the circuit, in Fig. 3-18, the end of the reset phase, S1 which is a sampling switch, will open, causing injection load and *kT/C* noise to the amplifier input node.

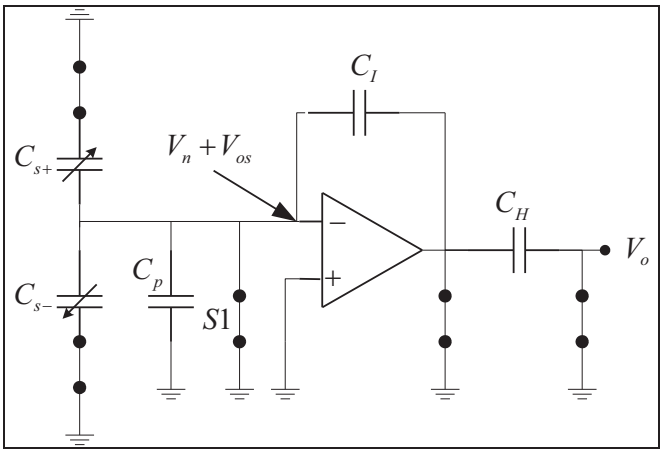

Fig. 3-18 Performance of circuit in Fig. 3-17 in reset phase

During the error detection phase Φ_{SN1}, which includes offset errors, *1/f* noise and thermal noise, injection load and *kT/C* noise, the error is amplified and then stored in capacitor C_H, Fig. 3-19.

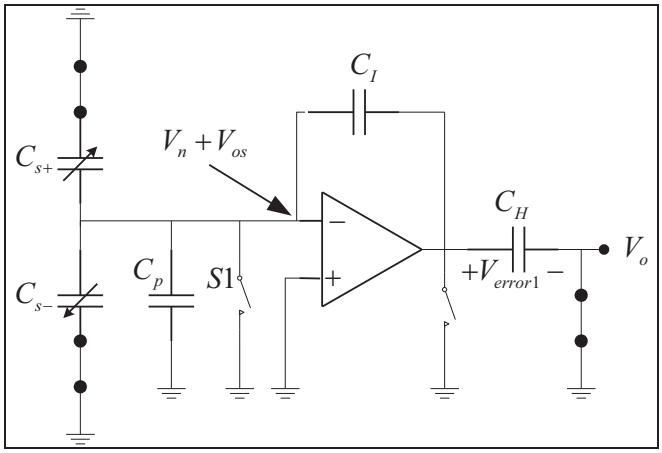

Fig. 3-19 Performance of circuit in Fig. 3-17 in error detection phase

This error value is:

$$V_{out}(n1) = V_{error1}(n1) = \left(1 + \frac{C_P + 2C_S}{C_I}\right).(V_{OS}(n1) + V_n(n1)) \tag{3-10}$$

Where, n1 is the time that Φ_{SN1} is turned off (goes to zero) and $V_n(n1)$ is the noise components (such as *1/f*, thermal and *kT/C*) in the OpAmp input and at the moment of *n1*. Then in detection phase Φ_{SN2} signal, voltages of $\pm V_S$ are applied to sense capacitors. In this phase, amplifier output which includes signal and error will decrease from the previous value stored in the capacitor. Equations in this phase are as follows:

$$\begin{cases} V_{sig} = \dfrac{\Delta C}{C_I}.V_S \\ \\ V_{error}(n2) = \left(1 + \dfrac{C_P + 2C_S}{C_I}\right).(V_{OS}(n2) + V_n(n2)) \end{cases} \Rightarrow V_{Out}(n2) = V_{sig} + V_{error2}(n2) \tag{3-11}$$

$$V_{out}(n2) - V_{out}(n1) = \frac{\Delta C}{C_I}.V_S + \left(1 + \frac{C_P + 2C_S}{C_I}\right).[V_{OS}(n2) - V_{OS}(n1) + V_n(n2) - V_n(n1)] \tag{3-12}$$

According to equation 3-12, since the offset voltage is considered a constant voltage, it has been removed. However, as mentioned before, V_n in the above equations represents noises in the input of the OpAmp such as *1/f*, thermal and *kT/C*. In addition, it is clear that the noise will change with time. White thermal noise has width band and *1/f* noise is narrowband. It means that the time correlation between samples at *1/f* noise is higher than the white noise. So in equation 3-12, *1/f* noise is greatly reduced but not white noise. Therefore V_o output includes the desired signal and little noise, according to Fig. 3-20.

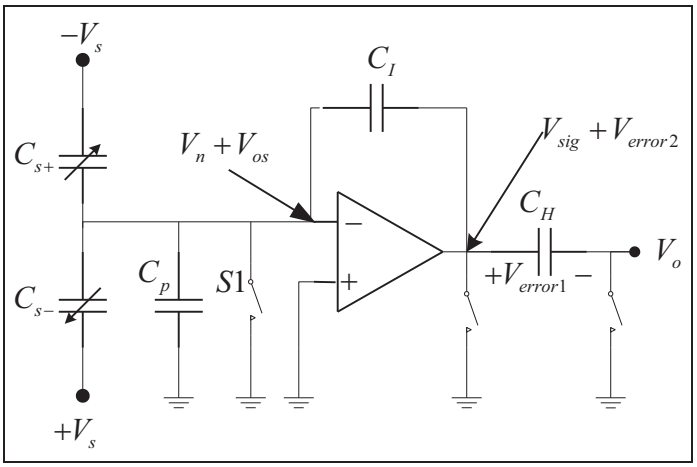

Fig. 3-20 Performance of the circuit 3-17 in sense phase signal of Φ_{SN2}

We can say that this method is operation as a high pass filter and filter noises, because the low frequency noise or dc noise is reduced greatly in this method. Moreover, according to the filtering process, since the CDS is a sampling technique, broadband noise interferes with base band noise, which increases the noise power spectral density in the base band [92].

3.3.2 CHS method

CHS is a modulation technique that can reduce the effects of OpAmp defects applied to the input, such as noise (mainly *1/f* noise and thermal) and dc offset voltage. References 97 to 99 have used this method. The technique uses a transmission signal to high frequency and after it is amplified the signal is returned to the fundamental frequency.

3.3.2.1 Noise removal by using CHS technique

The CHS technique uses a dc carrier to modulate signal amplitude. The chopper amplification principle is shown in Fig. 3-21 [92].

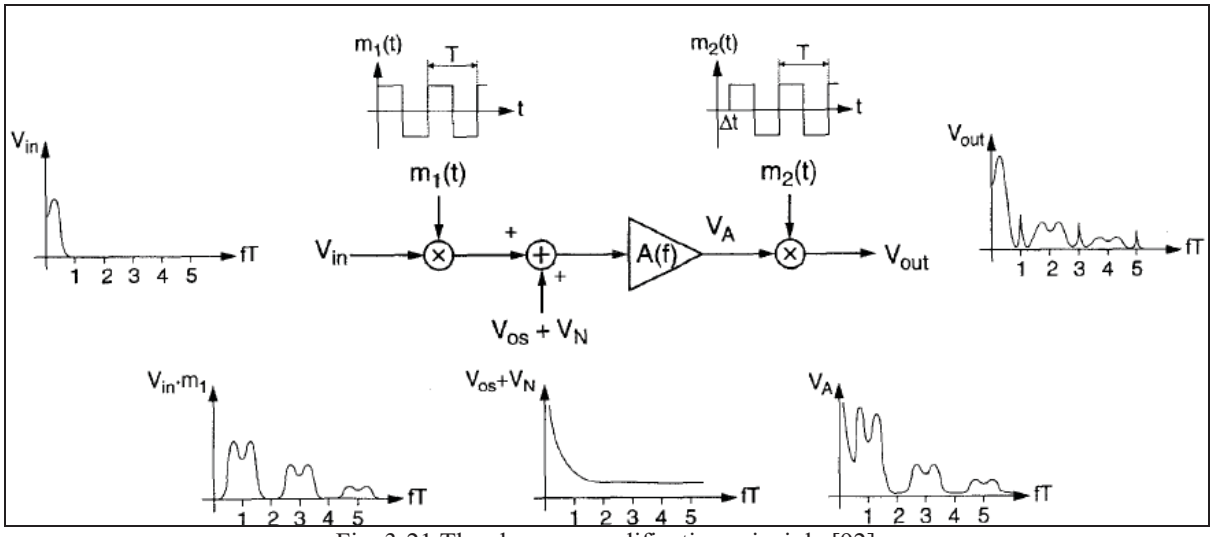

Fig. 3-21 The chopper amplification principle [92]

In this figure, signals of $m_1(t)$ and $m_2(t)$ are carriers of modulation, which demodulates with periods of $T=1/f_{chop}$; where f_{chop} is the chopper frequency. Also V_{OS} and V_n are indicative of dc offset and noise. To prevent interference, the input signal must have less than, or be equal to, half the chopper frequency's band.

Essentially amplitude modulated by using the carrier square wave, transmitted signal to the high frequencies, where, there is no *1/f* noise existing, then after amplification of the modulated signal, then returning it to the base-band (it will be demodulated).

For the carrier periodic with period *T* and duty cycle 50%, Fourier's formula is the following:

$$m(t) = 2\sum_{k=1}^{\infty} \frac{\sin\left(\frac{k\pi}{2}\right)}{\left(\frac{k\pi}{2}\right)} \cos(2\pi f_{chop} kt) \tag{3-13}$$

Where, the Fourier coefficients *k* have the following properties:

$$M_0 = M_{\pm 2} = M_{\pm 4} .... = M_{2k} = 0 \tag{3-14}$$

$k = 0,1,2,3,...$

The modulated signal equal is to the multiplication of the original signal and equation 3-13. Spectrum multiplied by $V_{in}.m_1(t)$ in Fig. 3-21 shows that the signal is transmitted to modulated odd harmonic frequency signal. After amplifying, the modulated signal will be demodulated by multiplying it with $m_2(t)$,which that produces the following equation:

$$V_{out}(t) = 4AV_{in}(t)\sum_{k=1}^{\infty} \frac{\sin\left(\frac{k\pi}{2}\right)}{\left(\frac{k\pi}{2}\right)} \cos(2\pi f_{chop} kt) \sum_{l=1}^{\infty} \frac{\sin\left(\frac{l\pi}{2}\right)}{\left(\frac{l\pi}{2}\right)} \cos(2\pi f_{chop} lt) \tag{3-15}$$

Where, *A* is the amplifier gain in the Fig. 3-21. Fig. 3-22 shows Fourier conversion of this low noise demodulated output signal.

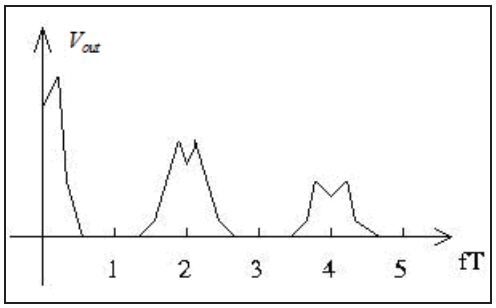

Fig. 3-22 conversion of Fourier ideal low-noise output signal

For extracting the main signal in the amplified form, the demodulated signal is applied to an LPF[1] with cut a off frequency slightly higher than the input signal bandwidth (in this case, half the chopper frequency).

Note that the noise and offset are modulated only once. If $S_N(f)$ represents the power spectral density (PSD) of noise and offset, then PSD of $(V_{OS}+V_N)m_2(t)$, is as follows [92]:

$$S_{CS}(f) = \sum_{k=-\infty}^{\infty} |M_{2k+1}|^2 S_N\left(f - \frac{2k+1}{T}\right) = \left(\frac{2}{\pi}\right)^2 \sum_{k=-\infty}^{\infty} \frac{1}{(2k+1)^2} S_N(f - \frac{2k+1}{T}) \tag{3-16}$$

[1] Low Pass Filter

Therefore, noise and offset are transposed to the odd harmonic frequencies of the modulation signal.

Assuming the input signal V_{in} is a dc signal. If the amplifier has an infinite bandwidth and without any delay, the signal in the output ($V.A$) is the square wave signal with amplitude $A.V_{in}$ and after demodulation it will be a dc signal with value of $A.V_{in}$. In fact, amplifier bandwidth is limited. It means twice the chopper frequency with constant gain A which is zero in other places. In this case as shown in Fig. 3-23, the output signal of the amplifier means $VA(t)$ is a sine wave from chopper signal dc of the main component signal with amplitude $(4/\pi)(A.V_{in})$. Then in the second modulator output V_{out}, has unidirectional sine wave includes harmonic even frequency components (because in regards to Fig. 3-23 the output signal is produced from a even signal, so according to the Fourier series formula, the odd components are zero). The output should be LPF to the desired amplified signal obtained. After been LPF, value of dc is $(8/\pi^2)(A.V_{in})$, it means about 20% decreases in dc gain. Thus, larger bandwidth of the main amplifier leads to greater dc gain.

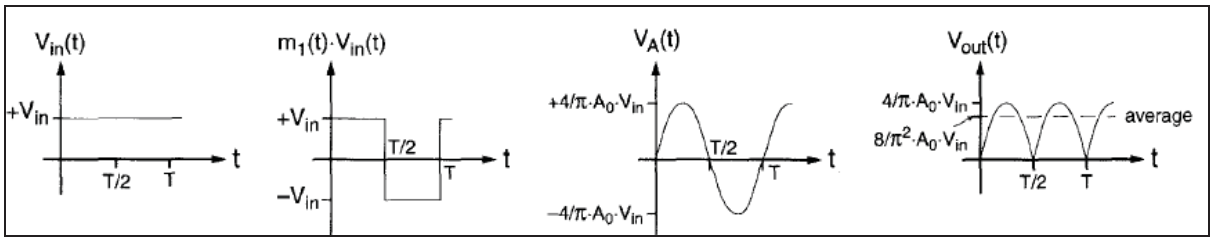

Fig. 3-23 Effect of limited bandwidth of amplifier on the dc input signal

Delay caused by the main amplifier can also reduce the overall dc gain. For example, if the amplifier has infinite bandwidth but produces a constant delay $T/4$ while demodulation of input and output are both the same phases, the output signal is almost a cosine wave (meaning, an odd wave) without a dc component. It means that total dc gain of the CHS amplifier is zero. If the same constant delay between the modulator input and output exists, this means Δt in the Fig. 3-21 is equal to $T/4$, the output signal is a unidirectional sine wave.

For the above results that have maximum chopper amplifier gain, the two modulators' phase shifts must be exactly consistent with the phase shift defined by the main amplifier.

3.3.2.2 CHS effects on noise amplifier

CHS effects is analysed on both white thermal noise and Flicker in this section. First assume that f_C is a cut-off frequency in the main amplifier in Fig. 3-21. Note that, cut-off frequency is a frequency which the amplitude transfer function decreases from its maximum value by

$1/\sqrt{2}$ factor [92]. First the effect of CHS method on white noise has been reviewed. In base-band ($|f| \le o.5 f_{chop}$), S_{CS} in equation 3-16 by PSD the white noise is approximated:

$$S_{CS-white}(f) = S_{CS-white}(f=0) = S_0 \left[1 - \frac{\tanh\left(\frac{\pi}{2} f_C T\right)}{\frac{\pi}{2} f_C T} \right] \tag{3-17}$$

Where S_0 is the white noise of PSD, since the PSD of white noise in the chopper modulator output is less than the original white noise of PSD. If it is assumed $f_{chop} >> f_C$, then $S_{CS\text{-white}}$ can approximated by:

$$S_{CS-white}(f) \cong S_0 \qquad \text{for} \quad |f| \le 0.5 f_{chop} \quad \text{and} \quad f_c >> f_{chop} \tag{3-18}$$

Thus, PSD of base-band noise for high f_C of the main amplifier is almost constant and equal to the original white noise of PSD. This material shows that f_C should not be much larger than the chopper frequency. With respect to *1/f* noise, the input of PSD can be calculated by:

$$S_{C-1/f}(f) = S_0 \frac{f_k}{|f|} \tag{3-19}$$

Where, f_k is the corner frequency of the amplifier. If this input PSD is replaced in equation 3-16, this means that when low frequency noise is transferred to high frequencies the *1/f* noise pole will disappear from base-band because the noise in chopper operation is transmitted to odd harmonics of chopper frequency. Reference [92] shows that PSD chopper *1/f* noise in the base-band can be approximately calculated as follows:

$$S_{C-1/f}(f) = 0.8525 S_0 f_k T \tag{3-20}$$

Residual noise referred to the input in base-band for a normal amplifier is total of equations of 3-18 and 3-20.

Then:

$$S_{CS}(f) = S_0(1 + 0.8525 f_k T) \qquad \text{for} \quad |f| \le 0.5 f_{chop} \quad \text{and} \quad f_c >> f_{chop} \tag{3-21}$$

According to equation 3-21, it is better to select a chopper frequency (f_{chop}) equal to the corner frequency (f_k). Also this equation shows that the resultant increase in white noise PSD base-band is less than *6dB*.

3.4 Comparison CDS and CHS methods

In comparison with the CDS method which is used to improve the gain effective in OpAmps, the CHS technique causes an OpAmp to amplify at a higher frequency signal, so the effective gain is usually decreased. Also dc offset of the CHS amplifier does not remove, but only modulates at the higher frequencies. When high dc gain and maximum signal swing is desired, CDS is the first choice method. In contrast, CHS is preferred for time continuous systems and when the base-band low noise is a critical needed.

In summary, comparison of CDS and CHS methods following results are obtained [101], [103]:

1. Inherently CDS is a sampling of the data method. But the base operation of CHS is modulation, so this can be used for continuous time signals.
2. CDS reduces the noise with low frequency by high pass filter, but the CHS will move the signal in frequency of outside of the band.
3. In one stage CHS continuous time, interference noise does not occur, so the *1/f* noise remains before the second modulation in the base-band. After demodulated, white noise returns to base-band and substitute to *1/f* noise.
4. CDS can be used to improve the effective gain of an OpAmp used in signal processing. In contrast, a CHS system in continuous time causes that OpAmp to amplify a higher frequency, which in this case the effective gain is usually decreased.

As a result, CHS nature of applications that use data sampling circuitry (such as capacitor switching classes) is preferred. Also eliminating the dc offset not that only is modulated to higher frequency in this case by authorised swing signal may be improved. Ability to improve gain in the CDS is an important advantage in some applications. On the other hand, if the system is a continuous time system and low frequency noise is an important issue, CHS can be chosen.

Chapter 4: Design of capacitance detector circuit

This chapter discusses the circuit designed for detecting the changes of capacitance of an integrated CMOS DNA sensor. The circuits in this project use the performance characteristics of relaxation oscillators which are, using very accurate voltage and current sources. In this study, two sensor capacitance dependant detection methods are investigated, describing advantages and disadvantages of each method. Each system block has been designed using CMOS technology.

Having linked all designed circuits together, an analogue integrated circuit, which converts the sensor's capacitance to frequency, has been designed. A digital circuit, which converts the analogue circuit's output frequency into a digital number, has also been designed.

Simulation of the designed circuits has demonstrated their ability to measure capacitance changes in the order to femto Farads (fF). Furthermore, the proposed design delivers an improvement of approximately one hundred times more accuracy compared to previously published work (26, 96, 105, 106).

4.1 Methods of designing the capacitance detection circuit

In relaxation oscillators, proportional current is inversely related to the amount of voltage and capacitance of the DNA sensor. So the frequency of these oscillators can change linearly with a wide range of external components. In addition to the above features these oscillators can also be integrated. Because the frequency or the period of this oscillator is controlled by current, voltage and capacitance values, this type of oscillator can be used in a capacitance meter.

Changes in capacitance of the sensor occur by adding ssDNA or hybrid DNA, which in turn changes the oscillator's frequency.

In the first method demonstrated, one side of the sensor is connected to ground and in the second method the sensor uses a floating value connection as further explained below.

4.1.1 Method 1 for a capacitance detector

In Fig. 4-1, the capacitor C_S represents the sensor. If the DNA sensor is charged and discharged with a constant current, a triangular wave is generated. To measure the time period of the triangular wave, it is converted to a square wave by a Schmitt trigger. Measurement of the period of the square wave is achieved by comparison of a counter with a known clock speed. The frequency of clock counter must be greater than the maximum frequency created by the sensor - oscillator. Maximum frequency of the sensor - oscillator

occurs when the input load is zero. The meaning of the input load is the DNA applied to the sensor.

To charge and discharge the sensor with a constant current and to keep the amplitude of the sensor's voltage change constant, the switch S_1 must to be opened and closed periodically. To control the switch S_1, need a square wave which is provided by the output signal from the Schmitt trigger. This signal causes automatic frequency control fluctuations and stabilized voltage amplitude changes in the capacitance sensor.

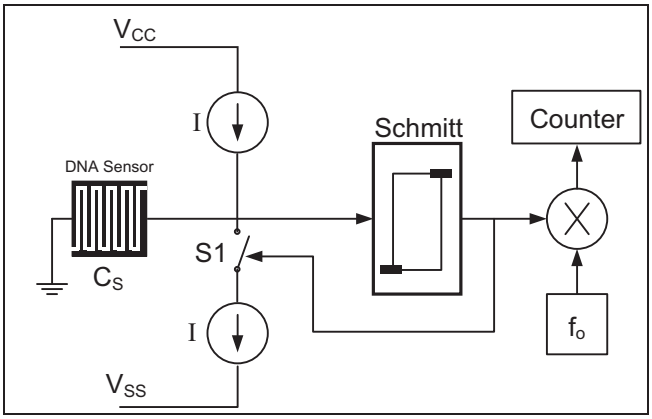

Fig. 4-1 The first method of DNA detector

4.1.2 Method 2 for a capacitance detector

Fig. 4-2 is the block diagram for the second method of measuring the sensor's capacitance. The difference between these methods is the method of sensor connection to the circuit, floating or differential.

In this case, the switches S_1 and S_2 must act in symmetry with each other as a constant current pass through the sensor. In "on" position of the switch S_1, current "*I*" in the capacitor travels right to left and in "on" position of the switch S_2, current "*I*" direction is from left to right through the capacitor.

To control voltage amplitude changes in the sensor and frequency fluctuations, a sample is taken from the differential voltage provided by the sensor; the sample controls the pulses of opening and closing of the switches S_1 and S_2. Control of opening and closing these switches requires two symmetrical square waves that don't have any overlap; for example, the two symmetrical square waves using the Schmitt trigger with differential input - output. The purpose of Schmitt trigger input/output differential is to provide a linear comparative value to pass to the counter. Greater explanation is provided in the section on designing a Schmitt trigger.

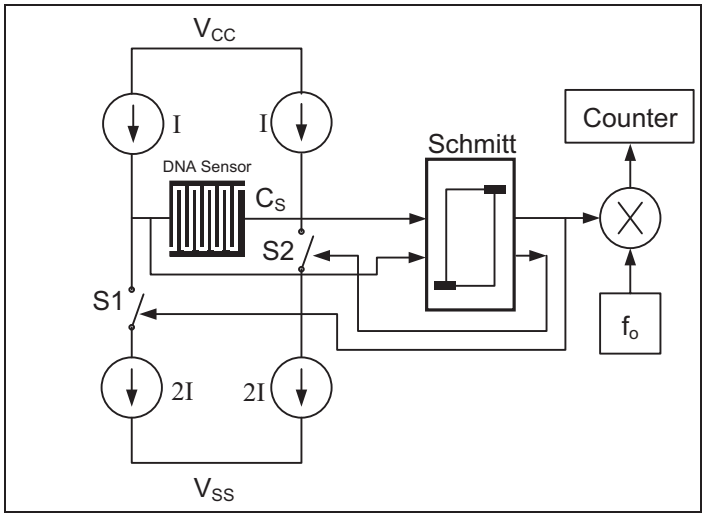

Fig. 4-2 The second method of DNA detector

4.2 Triangular and square wave period

As mentioned, the period of relaxation oscillators with a constant current are proportional to the value of the capacitance in the circuit. The diagrams designed in both methods act as a relaxation oscillator with constant current, so the period of their fluctuations (the output of Schmitt trigger) is proportional to the amount of sensor capacitance and inversely related to the amount of current flow. Because in both methods the DNA sensor is charging and discharging by a constant current, the equations necessary to obtain the period is the same in both methods.

By selecting the source current as $I_2=2I_1=2I$ in the first method (Fig. 4-1) when switch S_1 is open, the DNA sensor is charging with constant current (I), and when S_1 is closed the sensor, it is discharging with the constant current. In the second approach (Fig. 4-2) when the switch S_1 closed and S_2 is open, the DNA sensor is charging with the constant current (I) and when S_1 is open and S_2 is closed, the sensor is discharging with the constant current. If the maximum voltage in charge mode is V_H and minimum voltage for discharge mode is V_L (these values are given by Schmitt trigger) and charge and discharge time t_{ch} and t_{ds} , charge and discharge of the capacitor can be expressed by the following equations:

Equation charge: $$I \times t_{ch} = C\left(V_H - V_L\right) \quad (4\text{-}1)$$

Equation discharge: $$I \times t_{ds} = C\left(V_H - V_L\right) \quad (4\text{-}2)$$

Total times of t_{ch} and t_{ds} are equal to the triangle or square wave period so, the sum result of the above two equations results in the following time period.

$$T = t_{ch} + t_{ds} = 2\frac{V_H - V_L}{I} C \Rightarrow T \propto C \quad (4\text{-}3)$$

If the current charge and discharge are different to each other then:

$$T = (V_H - V_L)\left|\frac{1}{I_1} + \frac{1}{I_2}\right| C \Rightarrow T \propto C \qquad (4\text{-}4)$$

According to the two above equations, the period of square or triangular wave is dependent on the amount of capacitance provided by the sensor; the period has a proportional linear relationship with it. So by measuring the period, the presence of DNA on the sensor can be confirmed.

4.3 Disclosure period changes with changes in capacitance

As mentioned in both the above methods, the time period is proportional to the amount of capacitance provided by the sensor. The sensor in normal mode has a capacitance of C_0 .The input load changes with the application of DNA resulting in $C = C_0 + \Delta C$. The goal in this study is to determine the sensor capacitor changes, namely ΔC.

There are many methods to extract ΔC from T. Among of these methods which have been used in this study, is use of a mirror circuit. The purpose of designing a mirror circuit is to use two parallel circuits acting in tandem to provide a differential comparative reference as shown in Fig. 4-3 and Fig. 4-4. Usually when constructing capacitor sensors to eliminate the environmental impact (e.g. temperature, humidity), a reference capacitor C_R=C_0 and a capacitance sensor C_S is used. Thus, using two parallel circuits, one of the counters, measures the period of the reference sensor C_0 and other counter to measures the period provided by the DNA sensor of $C_S = C_0 + \Delta C$ If $K = 2\frac{V_H - V_L}{I}$ is assumed, then:

$$T_1 = KC_0 \qquad \text{And} \qquad T_2 = K(C_0 + \Delta C) \qquad (4\text{-}5)$$

Where, T_1 and T_2 are the periods measured by the counters. When the outputs from the two counters is taken, then the time difference ΔT is calculated as a linear function proportional to the sensor capacitance changes (ΔC) obtained. Equation 4-6 shows this theory. The advantage of using the two different time periods is to minimise real-time losses due to environmental conditions. Environmental factors such as temperature, humidity, etc., on both C_0 and C_S will be equal in both circuits. In this design the output result is displayed as digital number.

$$\Delta T = T_2 - T_1 = K\Delta C \qquad (4\text{-}6)$$

Thus, by measuring the two differences time period, the changes in capacitance are evident ΔC. Also instead of using the mirror circuit and the reference capacitor C_0, it is

possible to use a single counter, where this counter is able to count the periods that are created by the DNA sensor with a processor that will calculate the difference. A constant value is subtracted from the output (equal to the period established in the oscillator with the capacitor C_0). The disadvantage of this method is accuracy may suffer due to the environmental impacts not being accounted for. To resolve this problem, it is possible to modify the processor so that the sensor's period is measured before DNA is held as a value in a memory register. After applying DNA, the time period in the register is subtracted to give the result as ΔT in the output.

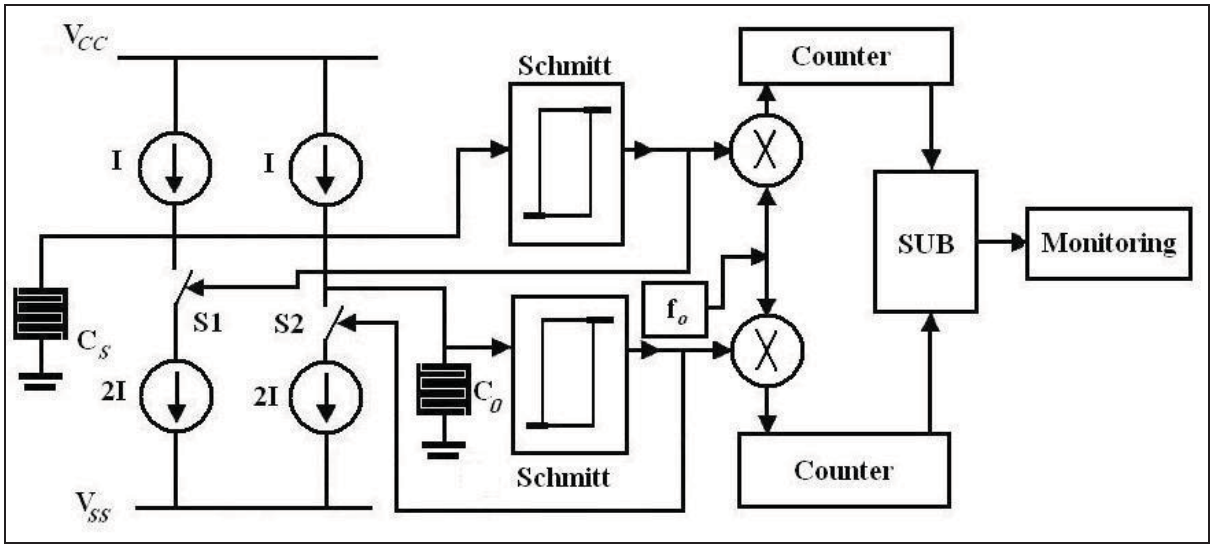

Fig. 4-3 Mirror circuit diagram block of DNA detector for capacitors one side ground

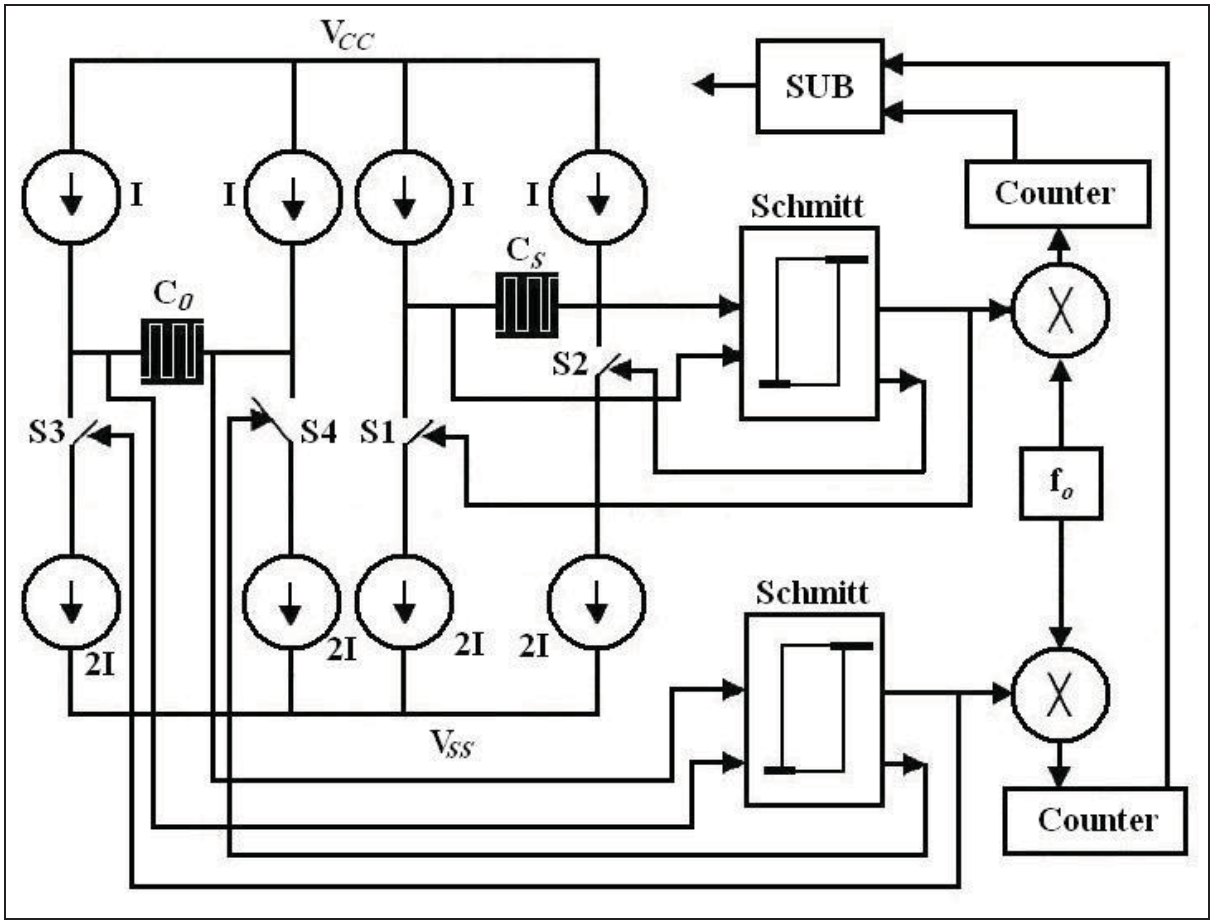

Fig. 4-4 Mirror circuit block diagram of DNA detector for floating capacitors

4.4 Design of current sources

A point that should be noted in this section is the amount of current and its determinants. The main determining component of a suitable current source is the minimum capacitance changes of the sensor, which is also related to the speed of counter, the speed of the comparator and off - on timing of the switches. Other factors determining current are noise and leakage currents. Noise current and leakage currents are very small (less than hundredth nano amps). Maximum capacitance change in the sensor is 0.6 of initial value (The DNA sensor with no load) for example if an accuracy of 50fF is required to detect the sensor changes, the counter must increment by one for every 50fF.

If an 8-bit counter is used, the primary capacitor's capacitance should be equal to $256\times50fF\div1.6=8pF$. The main factors in determining the amount of source current are counter frequency and the speed of the comparator. If the counter works with a frequency of 2.5MHz, in this case the counter's period is:

$$T = \frac{1}{2.5MHz} = 0.4\mu s \tag{4-7}$$

So the minimum time detectable by the counter is larger or equal to $0.2\mu s$ and is less than $0.4\mu s$. If the capacitance changes, ΔC, is equal to $5fF$ and the period, ΔT, equals 0.4 μs, then the sensor's accuracy is measured in terms of $5fFs$.

$$\Delta T = \frac{2 \times \Delta V}{I} \times \Delta C \tag{4-8}$$

If we assume $\Delta V = 2$, we have:

$$0.4\mu = \frac{2 \times 2}{I} \times 5\,fF \Rightarrow I = 50nA \tag{4-9}$$

Now if $\Delta T = 0.4\mu s$, there should be S.R[1] in the Schmitt trigger, assuming output changes size by ±2V equal or greater than $100V/\mu s$, because:

t_r or t_f <<0.4μs (4-10)

By assuming $t_r = t_f = 0.05 \times 0.4\mu s$ this can be written:

$t_r = t_f = 0.02\mu s \Rightarrow$ S.R = 2/0.02 = $100V/\mu s$ (4-11)

The results demonstrate that the values of S.R and "I" are reasonable. In addition, whenever the S.R. and counter's frequency is larger, smaller changers can be measured in the capacitors. In order to measure very small capacitances, I's magnitude should be decreased; however, "I" should be greater than the noise and leakage currents' values.

For example, if T=0.4 μs and the magnitude of the voltage scope's changes in the triangular wave, equals +2V (assuming I = 1nA), then it is possible to measure capacitance changes up to $0.1fF$. Typically, I's value ranges between 1 and 100 picoamps.

If each circuit submitted in Fig. 4-1 and Fig. 4-2 is used as single circuit, they can be used as a capacitance meter. If they are used as a mirror circuit similar to Fig. 4-3 and Fig. 4-4, they will work as a comparative detector of capacitance changes.

[1] Stochastic Resonance

4.5 Implement the block diagrams presented in circuit

4.5.1 Implement the current sources and switches

To provide the current sources, a single common current source is used then by mirroring it, creates all the current sources. To provide switching, a MOS transistor is used for each switch. Circuit schematics of Fig. 4-5 and Fig. 4-6 are implements of block diagrams of Fig. 4-1 and Fig. 4-2.

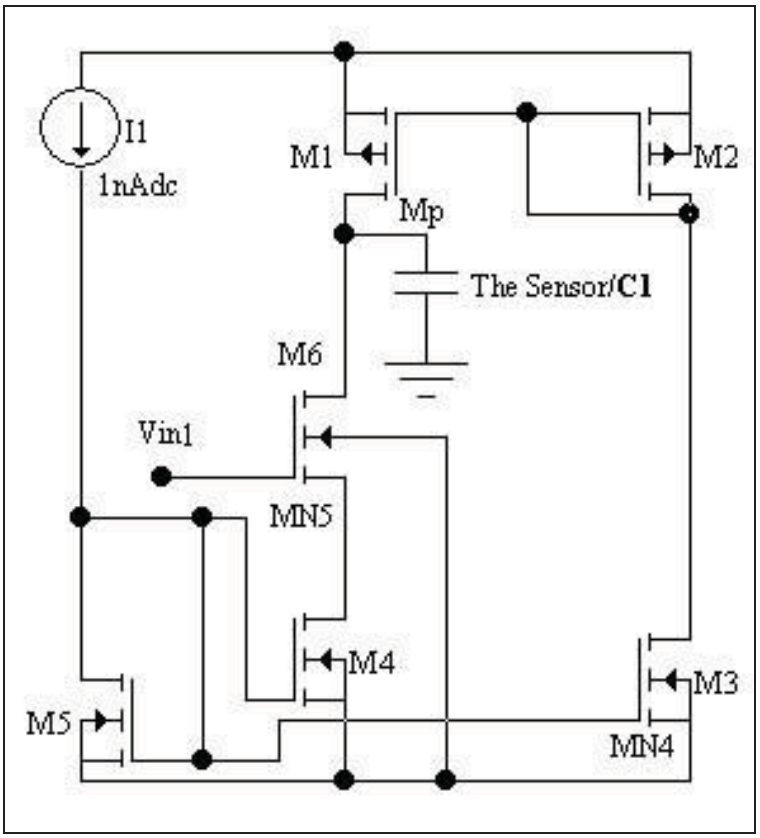

Fig. 4-5 Implements of block diagrams of Fig. 4-1

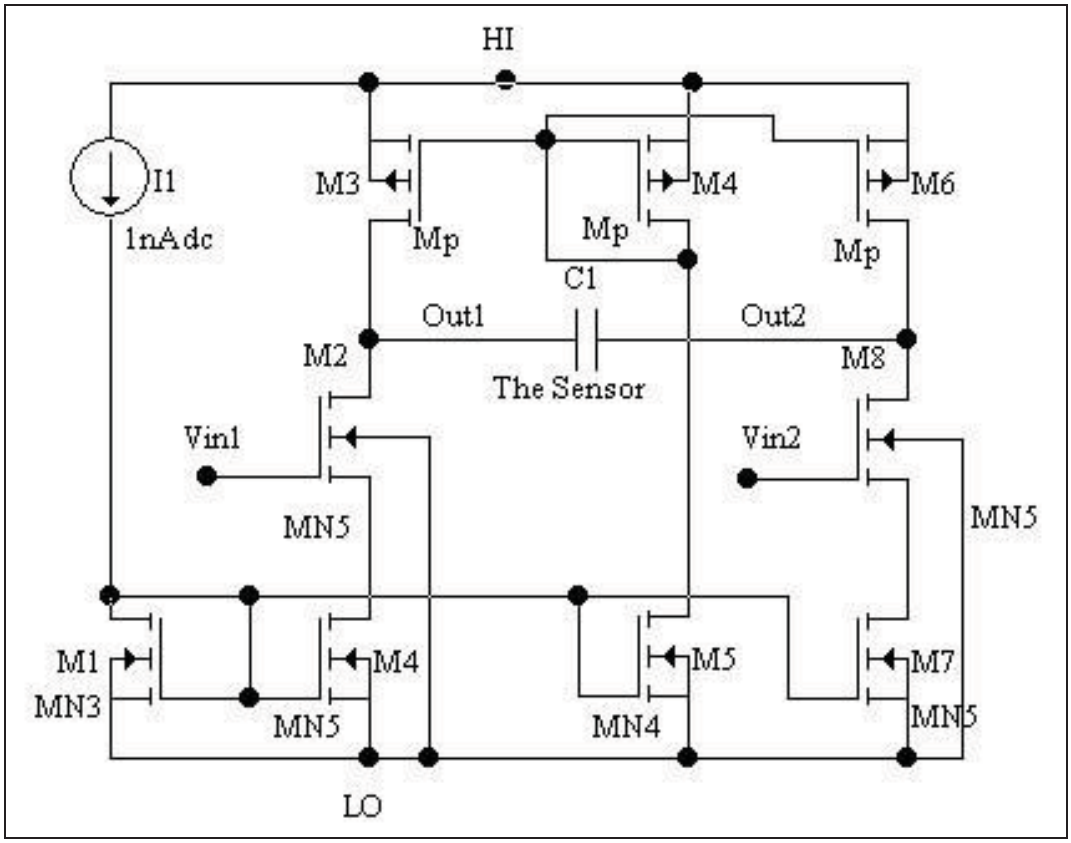

Fig. 4-6 Implements of block diagrams of Fig. 4-2

4.5.2 Schmitt Trigger Design

A comparator used in high-noise environments for disclosing signal changes around a threshold point. In this case, if the comparator is fast enough (depending on the common frequency noise) and the noise amplitude is large enough, the output will be noise. Under such circumstances, correction characteristics transition comparator is necessary, or in other words, the use of comparator hysteresis is desirable to eliminate noise output. In this project, not only because of noise, it is necessary in this research to use the comparator hysteresis. There are a few methods to create hysteresis in comparators. Supplying positive feedback in the comparator is the most important part in creating hysteresis in comparators.

For design the Schmitt trigger, a fast Op-Amp with positive feedback or standard Schmitt trigger, shown in Fig. 4-7, can be used. In high output mode, the output of the circuit is equal to the positive supply voltage. In the low output state, because the output voltage amplitude difference with the negative voltage supply is greater than the voltage needed to turn on the switches, it is unable to switch. Because of this reason this design of Schmitt trigger is not used in this project.

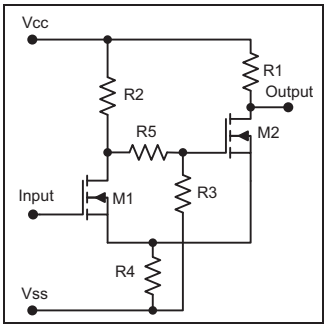

Fig. 4-7. Standard Schmitt trigger

Op-Amps are used for comparison and must be high speed and high precision with low offset. Consider the schematic of Fig. 4-8 the assumption being the ideal Op-Amp, the threshold voltages of Schmitt trigger is as follows.

$$V_H = \frac{R_2}{R_1 + R_2} V_{OMax} \qquad \text{And} \qquad V_L = \frac{R_2}{R_1 + R_2} V_{OMin} \tag{4-8}$$

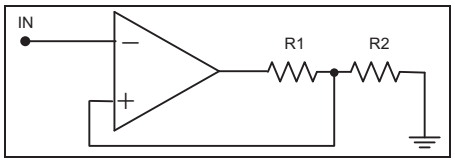

Fig. 4-8. Schmitt trigger circuit with Op-Amp

4.6 Implement an integrated Schmitt trigger using an Op-Amp

As mentioned, the most important issue in creating a Schmitt trigger is creating a positive feedback in the comparator. For designing the Schmitt circuit with Op-Amps we can use the following two methods. In both methods, positive feedback has been used.

1- Using Op-Amp circuits with external feedback resistance
2- Using Op-Amp circuits with internal feedback

4.6.1 Using Op-Amp circuits with external feedback resistance

As mentioned, the standard method for creating a Schmitt, is to use Op-Amps, like that shown in Fig. 4-8. Because this type of Schmitt trigger has an input, it can only be used for Schmitt with one side grounded capacitor. To build a Schmitt for floating capacitor mode, we can use an Op-Amp with two differential inputs and output as shown in Fig. 4-9. This schematic has two positive feedbacks. The other two inputs are used to connect the two sides of the DNA sensor. The sensor must have a floating connection as in Fig. 4-2. In capacitance meter mode by using the circuit Fig. 4-9 as Schmitt trigger, the differential performance is better than the circuit Fig. 4-8. However, for detection of capacitance changes in mirror circuit diagrams in Fig. 4-3 and Fig. 4-4, because they act as differential, we use the circuit of

Fig. 4-8 as a Schmitt trigger, as this is more suitable because it has less hardware than the circuit in Fig. 4-9. The Op-Amp in Fig. 4-9 can be designed in several ways. One method of designing this type of Op-Amp is putting together two Op-Amps like the schematic in Fig. 4-10, as the negative outputs and positive outputs can be connected to each other. If Op-Amps are designed in two levels, with positive resistance feedback, output resistance will be less. Reducing the output resistance decreases S.R and drops the amplitude output of Op-Amp. In this case, this voltage will not switch current sources. The disadvantage of reducing the output resistance can be solved by using a larger resistance in the feedback to prevent voltage drop in the output. If this greater resistance is built in to the integrated circuit, the chip surface will be high and if a larger external resistance is used, the error will increase. Another method to prevent voltage drop is to add an emitter follower or push-pull amplifier. In this case, due to increased Op-Amp level, the delay is larger. Additional delays in the Op-Amp will decrease comparator (S.R) speed. As previously mentioned, reducing the S.R, the detection of minimum capacitance changes increases. So given the results using Op-Amp circuits with external feedback for a Schmitt trigger design is not suitable for this project and a better method must be found.

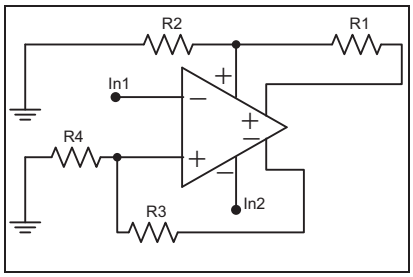

Fig. 4-9. Schmitt trigger Op-Amp with two inputs, differential inputs and output

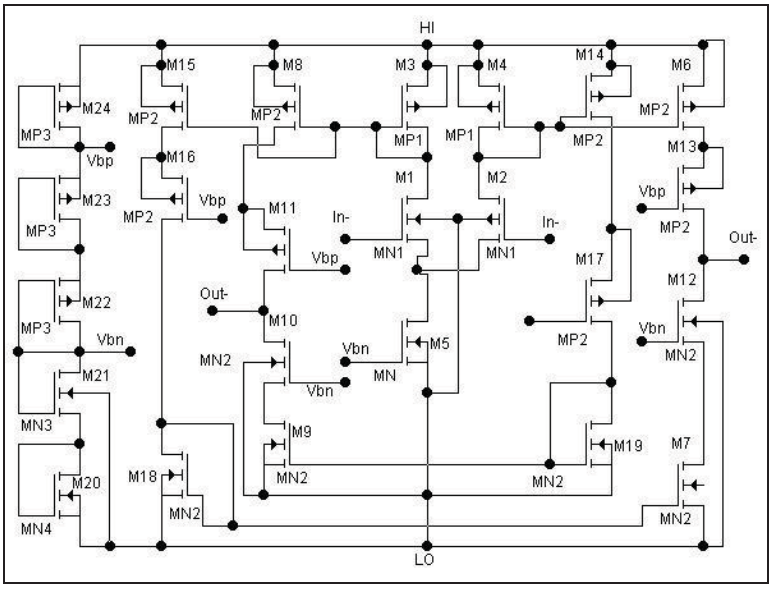

Fig. 4-10. Op-Amp differential input – differential output

4.6.2 Using Op-Amp circuits with internal feedback

All Schmitt trigger circuits use some kind of positive feedback. By adding two transistors to the input stage of the Op-Amp in Fig. 4-11, positive feedback is created. The first transistor has current feedback which is connected in series in the source loop of M_1 and M_2 transistors by M_5. This route provides negative feedback. The second route is voltage feedback which is parallel connecting to gate-drain of M_{10} and M_{11} transistors. This route provides positive feedback. If the ratio of positive feedback is less than ratio of negative feedback, the median feedback will be negative and producing no hysteresis.

If positive feedback ratio is larger than the negative feedback coefficient, hysteresis is created. The following describes hysteresis creation: comparing $\frac{\beta_{10}}{\beta_3}$ and $\frac{\beta_{11}}{\beta_4}$, if the ratios are less than one, hysteresis will not be created; if the ratios are greater than one, then hysteresis is created.

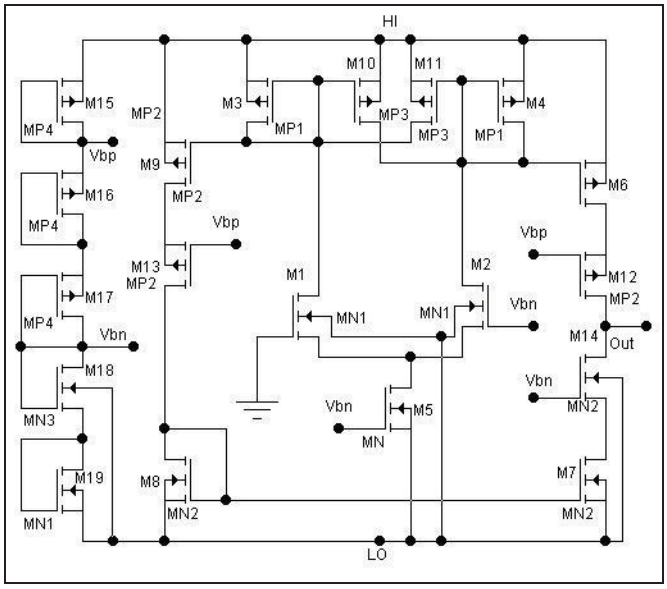

Fig. 4-11. Hysteresis comparator circuit

4.6.2.1 How the circuit works

In Fig. 4-11's schematic, if the power supply's positive and negative terminals are connected to the circuit and M_1's gate is connected to ground, M_1 receives a less than zero input and will be connected and M_2 will be cut; thus, M_3 and M_{10} will be connected and M_4 and M_{11} cut.

In this case, all current at I_5 passes from M_1 and M_3 (M_{10} is connected but it has zero current) so V_{D2} is high. In that moment M_{10} is trying to pass the following current:

$$i_{10} = \frac{(W/L)_{10}}{(W/L)_3} i_5 \tag{4-9}$$

By increasing V_{in} to the threshold point (which is not yet known), the remaining current I_5 starts to pass through the M_2. This practice is repeated up to the point where current through M_2 equals to the current of $M_{10.}$ Just after this point the comparator's mode will change. To calculate the voltage at one of the circuit points we must analyse the circuit at the point where the current is equal for i_2 and i_{10}. It is calculated as follows:

$$i_{10} = \frac{(W/L)_{10}}{(W/L)_3} = i_3 \text{ and } i_2 = i_{10} \text{ and } i_5 = i_2 + i_1 \text{ and } i_1 = i_3 \tag{4-10}$$

$$i_3 = \frac{i_5}{1 + \left[\left(\frac{W}{L}\right)_{10} \Big/ \left(\frac{W}{L}\right)_3\right]} = i_1 \text{ and } i_2 = i_5 + i_1 \tag{4-11}$$

By having currents for M_1, M_2 we can easily calculate the voltages for V_{GS}. Since the gate M_1 is connected to the ground, their deferential voltage of gate - source is a positive voltage and its value is as follows:

$$V_{GS1} = \left[\frac{2i_1}{\beta_1}\right]^{V2} + V_{TH1} \text{ and } V_{GS2} = \left[\frac{2i_2}{\beta_2}\right]^{V2} + V_{TH2} \quad (4\text{-}12)$$

$$V_{THR} = V_{GS2} - V_{GS1} \quad (4\text{-}13)$$

After reaching the threshold voltage, the comparator mode will change, where the remaining current passes through M_2 and M_4. So, M_{11} will connect (on) and M_1, M_3, M_{10} are cut. Similar previous case when the input is negative, the current for M_1 will increase until be equalled to the current of M_{11}. The input voltage at this point is V_{THR}. This voltage is obtained in the following equation same as the previous mode:

$$i_4 = \frac{i_5}{1 + \left[\left(\frac{W}{L}\right)_{11} \Big/ \left(\frac{W}{L}\right)_4\right]} = i_2 \text{ and } i_1 = i_5 - i_5 \quad (4\text{-}14)$$

Using the equation 4-12 to calculate V_{GS}, the negative voltage at this point is equal to:

$$V_{THR} = V_{GS2} - V_{GS1} \quad (4\text{-}15)$$

4.6.2.2 The method to design a comparator with hysteresis

To design the circuit of Fig. 4-11 we take the following steps.

1. Determine the output current for the desired change. To calculating the current use the equation below.

$$I = C.SR \quad (4\text{-}16)$$

C is capacitance of output load; this is the total capacitance from switches, gate and capacitors connected to drain of M_6 and M_7. Usually the gate capacitor is larger than the other capacitors. As mentioned before S.R can be measured from a minimum of ΔT. "I" is the same current as I_6 and I_7.

2. To determine minimal surface size M_6, M_7 for appropriate output voltage change. To do this used equation $V_{DS}(Sat)$:

$$V_{DS}(Sat) = \left(\frac{2I_6}{\beta}\right)^{V2} \quad (4\text{-}17)$$

The $V_{DS(Sat)}$ obtained from the difference of minimum and maximum voltage required to turn the switches on and off and the supply voltages. Minimum and maximum voltage on/off are obtained from the common mode input voltage of circuit Fig. 4-5. To ensure on/off switching it is better that to use the value of $V_{DS(Sat)}$.

3. By having the current of the second layer and the size of transistors minimal surface M_6 and M_7, we can calculate the second layer gain with the equation below:

$$A_2 = \frac{-g_{mb}}{(g_{ds6} + g_{ds7})} \quad \text{and} \quad g_m = \sqrt{2\beta I} \quad \text{and} \quad g_{ds} = \lambda I_1 \tag{4-18}$$

4. Using the comparator profile and the second layer gain, we can ascertain the first layer gain:

$$A_{V1} = \frac{A_{V1}}{V_{V2}} \tag{4-19}$$

5. To design with minimum surface and equilibrium condition, assume that $\left(\frac{W}{L}\right)_4, \left(\frac{W}{L}\right)_5$ equal to one and they are respectively a mirror M_6 and M_7. So we can obtain the current for M_4 and M_5. By Comparing I_5 with $2I_4$ then taking the larger value as I_5 and half of this value can be I_3 and I_4. Now with these currents and by mirroring M_4 with M_6 and M_5 with M_7 , we can calculate the surface sizes of M_3 and M_4:

$$\left(\frac{W}{L}\right)_4 = \left(\frac{W}{L}\right)_3 = \left(\frac{W}{L}\right)_6 \frac{I_3}{I_6} \tag{4-20}$$

Next, check the power loss profile using the following equation:

$$P_{loss}(V_{CC} - V_{SS})(I_7 + I_5) \tag{4-21}$$

V_{cc} and V_{SS} are positive and negative voltages.

6. After determining the current and gain of the first layer, by using the following equation, we can calculate the surfaces sizes of transistors M_1 and M_2:

$$A_{V1} = \frac{-g_{m1}}{(g_{ds1} + g_{ds3})} \quad \text{and} \quad \left(\frac{W}{L}\right)_1 = \left(\frac{W}{L}\right)_2 \tag{4-22}$$

7. By using the following equation, design the minimum surface size of transistor M_5 in base negative CMR[1]:

$$V_{G1}(Min) = V_{SS} + V_{DS5} + \left[\frac{I_5}{\beta_1}\right]^{V2} + V_{T1}(Max) \quad \text{and} \quad V_{DS5} = \left[\frac{2I_5}{\beta_5}\right]^{V2} \tag{4-23}$$

[1] Common mode range

But it is better that positive and negative CMR are selected by consideration of previous layers.

8. To establishing proper mirror operation between M_5 and M_7, increasing $\frac{W}{L}$ one of them the following equation is applied:

$$\left(\frac{W}{L}\right)_5 = \left(\frac{I_5}{I_7}\right)\left(\frac{W}{L}\right)_7 \tag{4-24}$$

9. For CMR positive, appropriate surfaces of M_3 and M_4 uses the following equations.

$$V_{G1}(Max) = V_{DD} - \left(\frac{I_5}{\beta_3}\right)^{V2} - \left|V_{TH3}(Max)\right| + V_{T1} \qquad \text{and} \quad \left(\frac{W}{L}\right)_3 = \left(\frac{W}{L}\right)_4 \tag{4-25}$$

10. In this step, compare the result of $\left(\frac{W}{L}\right)_3, \left(\frac{W}{L}\right)_4$ from steps 5 and 9. If the result of step 5 is larger than step 9 so for $\left(\frac{W}{L}\right)_3, \left(\frac{W}{L}\right)_4$ use the result from step 5 and then go to the next step, otherwise use the result in step 9 and increase $\left(\frac{W}{L}\right)_6$ until the current mirror equation of $\left(\frac{W}{L}\right)_3 = \left(\frac{W}{L}\right)_6 \frac{I_3}{I_6}$ be corrected and then go to next step.

11. On the positive and negative threshold voltages, the size of transistors M_{10} and M_{11}, are obtained as below.

$$V_{THR} = V_{GS2} - V_{DS1} \approx \sqrt{\frac{2}{\beta_1}\left(\sqrt{i_2} - \sqrt{i_1}\right)} \tag{4-26}$$

On the other hand, value i_5 is known and it is equal to the total currents of i_1 and i_2, so by using the two equations below we can find values of i_1 and i_2.

$$i_1 + i_2 = i_5 \qquad \text{and} \qquad V_{THR}^{+}\sqrt{\frac{\beta_1}{2}} = \sqrt{i_2 - i_1} \tag{4-27}$$

After obtaining i_1 and i_2, we can find the surface size of M_{10}.

$$i_1 = \frac{i_5}{1 + \left[\left(\frac{W}{L}\right)_{10} \Big/ \left(\frac{W}{L}\right)_3\right]} \tag{4-28}$$

To calculate the size of M_{11} using V_{THR}^{-}

$$V_{THR}^{-} = V_{GS2} - V_{GS1} = \sqrt{\frac{2}{\beta_1}\left(\sqrt{i_2 - i_1}\right)} \tag{4-29}$$

Also:

$$i_1 + i_2 = i_5 \tag{4-30}$$

By solving the two recent equations values of i_1 and i_2 are achieved then by using the equation below to obtain the surface size of M_{11}.

$$i_2 = \frac{i_5}{1 + \left[\left(\frac{W}{L}\right)_{11} \Big/ \left(\frac{W}{L}\right)_4\right]} \tag{4-31}$$

4.7 Effect of voltage supply in output period of the Schmitt Trigger

In the Schmitt trigger Fig. 4-11 threshold voltages are dependent on the current in transistor M_5. In this circuit, the Bias voltage of transistor M_5 is produced by voltage division of power supplies by transistors M_{15} to M_{19}. In this case by changes voltage of power supply, bias voltage of transistor M_5 will be changed and it causes changes in the current of the transistor M_5 or in other words it will change Schmitt trigger threshold voltages. Changes in the threshold voltages also causes change of the output period in Schmitt trigger circuit. To prevent changes in threshold voltages it is necessary to stabilise bias voltage or in other words, current in the transistor M_5. One method of stabilising the current bias of M_5 is to use the schematic shown in Fig. 4-11 with a mirror current, as shown in Fig. 4-12's schematic.

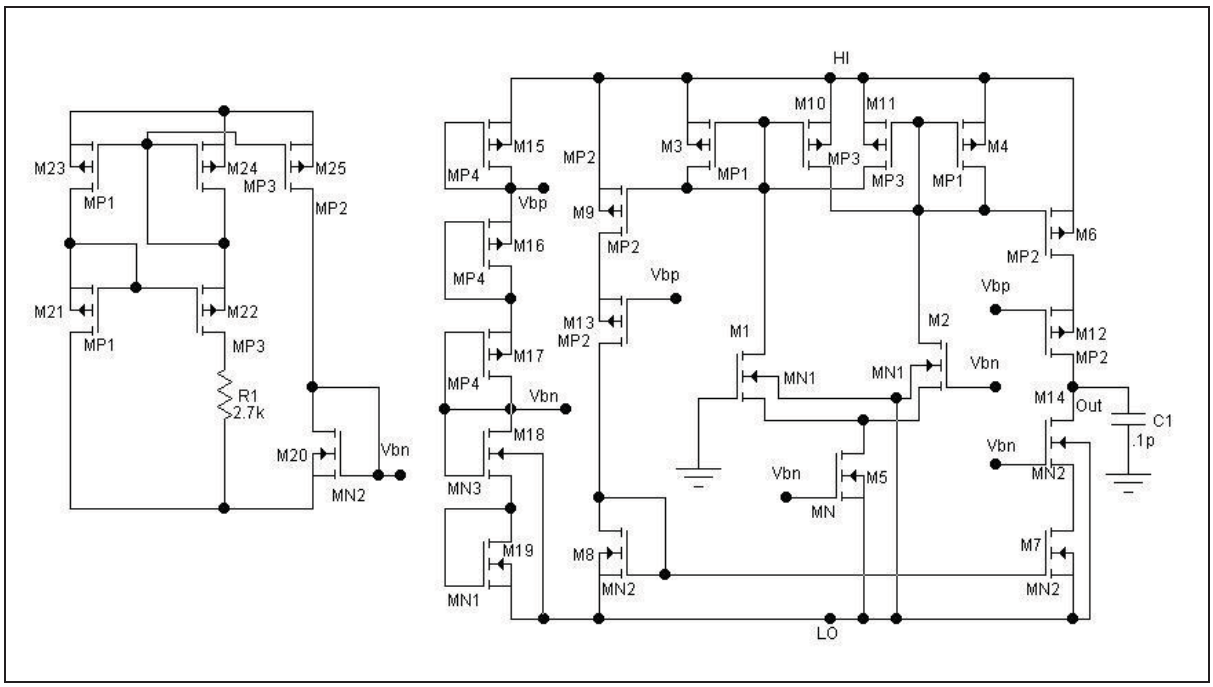

Fig. 4-12. Stabilizing current of M_5 for stabilising the threshold voltages of the Schmitt trigger

Because of errors by way of voltage drain-source in transistors M_5 and M_{20}, it is better to mirror current to stabilise bias voltage in transistor of M_5. To stabilise the bias voltage of M_5, schematic Fig. 4-13 has been used. In this schematic by assuming R_1=2.7KΩ, n=10 and

$\left(\frac{W}{L}\right)_{16}=\left(\frac{W}{L}\right)_{18}$ and $\left(\frac{W}{L}\right)_{17}=\left(\frac{W}{L}\right)_{19}=\left(\frac{W}{L}\right)_{20}$ valuation of the transistors current will be:

$$I_{M20}=I_{M19}=I_{M17}=\frac{V_T L_{nn}}{R_1}\cong 22.15\mu A \tag{4-32}$$

By having R_2=22KΩ and R_3=R_5=12KΩ value of transistors voltage bias in Fig. 4-13 can be calculated by:

$$V_{bt}=V_{SS}+V_{BE3}+R_2\frac{V_T L_{nn}}{R_1} \tag{4-32}$$

$$V_{btn}=V_{SS}+V_{BE4}+V_{BE5}+R_3\frac{V_T L_{nn}}{R_1} \tag{4-33}$$

$$V_{btp}=V_{BE8}+V_{BE9}+R_9\frac{V_T L_{nn}}{R_4} \tag{4-34}$$

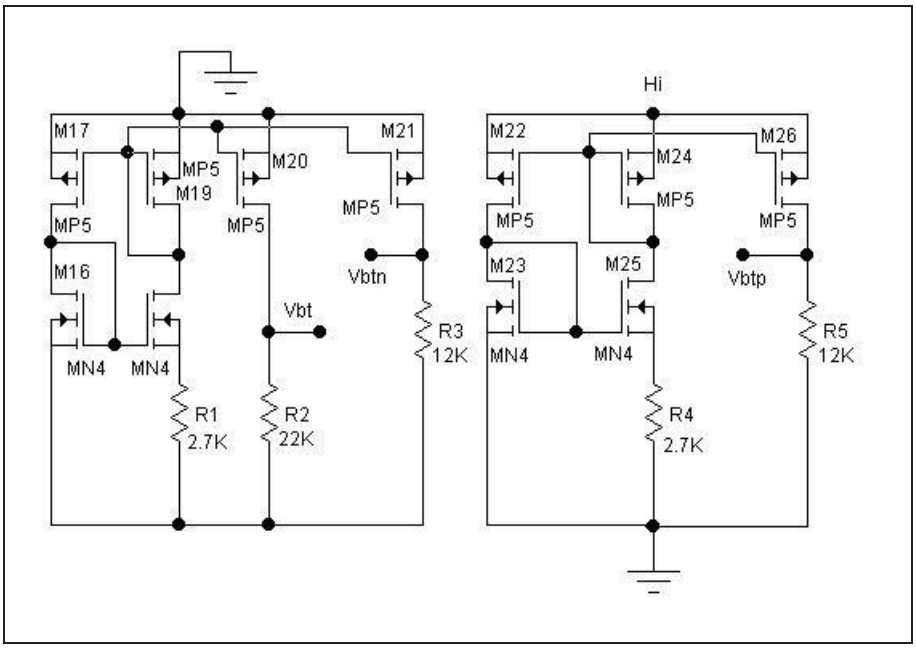

Fig. 4-13. Stabilising bias voltage in the Fig. 4-11 in order to stabilise Schmitt trigger threshold voltages.

Fig. 4-14 shows the analogue structure of the current sources and the Schmitt trigger. In addition because threshold voltages are independent of the voltages in the Schmitt trigger and dependent on power supplies values and by above equations and resistance values of the threshold voltages, it is almost independent of temperature. Also silicon surface in Fig. 4-11 has been improved. The table 4-1 shows the surfaces size of transistors in the circuit.

Transistor	**Size (W/L)**
M1–M2-M36-M37	6.5
M3-M4-M38-M39	0.5
M5-M40	9
M6-M7-M8-M9-M12-M13-M14-M15-M23-M24-M25-M26-M41-M42-M43-M44	6
M10-M11-M45-M46	10
M17-M19-M20-M21-M22	5
M30-M32	1
M29-M31-M34-M35	1.5
M16-M18	2
M27-M28-M33	3

Table 4-1 Surface sizes of the transistors in Fig. 4-14

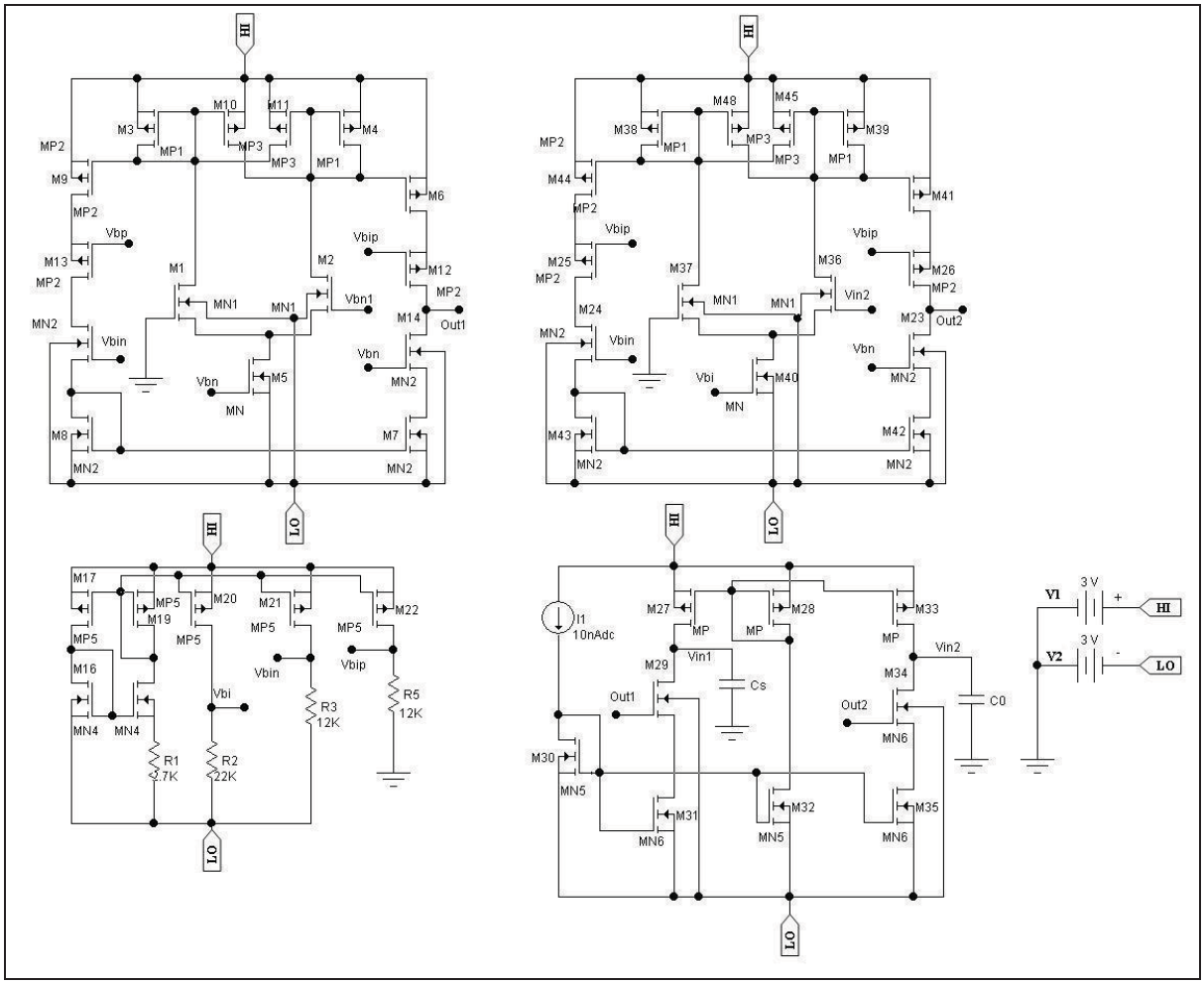

Fig. 4-14. The final analogue circuit

4.8 Effects of voltage change in the capacitance of the sensor

The amount of capacitances in integrated circuits is dependent on their voltage and temperature. Increasing the voltage may even lead to breakdown of the dielectric between the plates of capacitors. These factors cause errors in the capacitance values. Considering the structure of the capacitor sensors, such as air or liquid in the gap between the electrodes in the sensor as dielectric, it is unlike integrated circuits capacitors, voltage changes on the DNA sensor will affect very minor amounts of capacitance in the sensor. Most of this effect is due to parasitic capacitance changes which are parallel to the DNA capacitance sensor. So in other words, the changes of voltage in the DNA sensor will not affect the capacitance value.

The voltage that is created by the detector circuit in the DNA sensor must not be so great as to destroy the dielectric between the electrodes of the sensor. The maximum voltage in the designed detector circuit in this study is ±0.7V.

4.9 Effect change of temperature on capacitance in the sensor

Ambient temperature changes, in addition to changing the overall capacitance in the integrated circuit also causes changes in the internal capacitance of the sensor.

Because the mirror circuit design calculates differential performance in the DNA detector circuit, errors through the effect of changes in temperature or other environmental factors is eliminated because both sensors are subject to the same condition.

4.10 Supply voltage in the circuit

Determinants' minimum supply voltage in the analogue section of DNA detector is determined by two sections of the Schmitt trigger and currents sources. The voltage on the DNA sensor changes between ±0.7V. The positive supply voltage should be ΔV higher than 0.7V. ΔV is the difference Voltage between gate - source in transistor M_1 and the threshold voltage in the schematic Fig. 4-5. *ΔV's v*alue is proportional to the square root of current in current sources which is this amount according to current amount of current sources is smaller than 0.3V. Thus, the minimum positive voltage required to operate is almost 1V. For negative voltage, the minimum voltage corresponding to the Fig. 4-5 is almost -1.2V. Because the voltage applied to the DNA sensor will also be applied to the Schmitt trigger, the input voltage of common mode in the Schmitt trigger must be more than ±0.7V. By considering equations 4-23 and 4-25 we obtain the minimum positive and negative voltage of 0.76V and -2.1V. As mentioned above, the current sources circuit requires a minimum positive and negative voltage and the Schmitt trigger circuit also requires a minimum positive and negative so the amount of positive voltage supply must bigger than 1V and negative voltage must bigger than 2.1V

4.11 Power consumption in the circuit

Most power in the circuit is used by the Schmitt trigger. With consideration to equation 4-21, the power usage is almost 4.5mW. The results of simulation have been discussed in next chapter.

4.12 Effect of noise on wave period Schmitt Trigger Output

Noise voltage creates jitter in the output of the Schmitt trigger circuit or oscillator. Jitter causes random changes in the threshold voltage of the Schmitt trigger. Because of the use of MOSFET in current sources and switches in this circuit, effective noise is thermal noise[104]. The amount of jitter in the DNA sensor is in the range of 2pF to 20pF, and the output of

Schmitt trigger is in range of picoseconds. Because the minimum periods established are in the microsecond level, jitter does not create any appreciable error in the period.

4.13 The Digital section of the DNA detector

As mentioned before, to measure the time period of the upper pulse for the Schmitt trigger output, a counter with a certain frequency is required. The frequency counter value is dependent on the minimum and maximum upper pulse time in the output of the Schmitt trigger, the number of bits in the counter and accurate measurement.

The Frequency that selected must not overflow the counter for $T_0 + \frac{1}{2}T_0$. For example for a counter n=12bits, initial capacitance sensor C_0=2pF$_0$, the sensor charge and discharge current I=1nA, Threshold voltages V_{tH}=1V and V_{tL}=-1V so the counter frequency can be obtained by the following:

Maximum period created by the sensor capacitor is equal to:

$$T = \frac{2(V_{tH} - V_{tL})}{I} C_0 \left(1 + \frac{1}{2}\right) = 3C_0 \frac{(V_{tH} - V_{tL})}{I} \quad (4\text{-}35)$$

Value upper pulse time of Schmitt trigger output is:

$$t = \frac{T}{2} = 1.5C_0 \frac{(V_{tH} - V_{tL})}{I} \quad (4\text{-}36)$$

With values above t = 6ms. In this time counter must have a maximum count up to 2^n-1, so:

$$f = \frac{2^n}{t} = 682666.67Hz \quad (4\text{-}37)$$

In this case, measurement accuracy is constant and obtained as follows:

$$\frac{1}{f} = 2\frac{V_{tH} - V_{tL}}{I}\Delta C \Rightarrow \Delta C = \frac{1}{2}\frac{I}{f(V_{tH} - V_{tL})} \quad (4\text{-}38)$$

ΔC indicates the accuracy of measurement. With the above values, the accuracy of measurement level is 732.4aF[1]. By using 16-bit counter ΔC = 45.8aF and f=10922666.67Hz. However, if the value of ΔC is known, in this case, ΔC determines the frequency counter and the number of the counter bits. The following equations should be accurate between precision measurements, the counter frequency, the number of counter bits, and the high-signal time.

$$\Delta t = \frac{1}{f} \quad \text{and} \quad t = 2^n \Delta t \quad \text{and} \quad \Delta C = \frac{1}{2}\frac{I\Delta t}{(V_{tH} - V_{tL})} \quad (4\text{-}39)$$

Atto=10^{-18}

Control pulses of the counters should be designed so that it only counts when the pulse of the Schmitt trigger is in upper cycle. For this reason a counter that has a start and reset pin can be used. Thus, when the pulse has a rising edge, the counter is reset and starts counting on the pull-down edge. The output of the counter is recorded in a latch. Block diagrams in Fig. 4-15 and Fig. 4-16 show the block diagrams for digital part of the capacitance meter and capacitance change detector. The buffer used in the input of the latch is used to increase the accuracy. It is better that the delay of the buffer is the same or slightly larger than delay time of the counter.

This part of circuit is designed with a clock frequency 680 KHz and I=50nA. The result of the simulations is discussed in the next chapter.

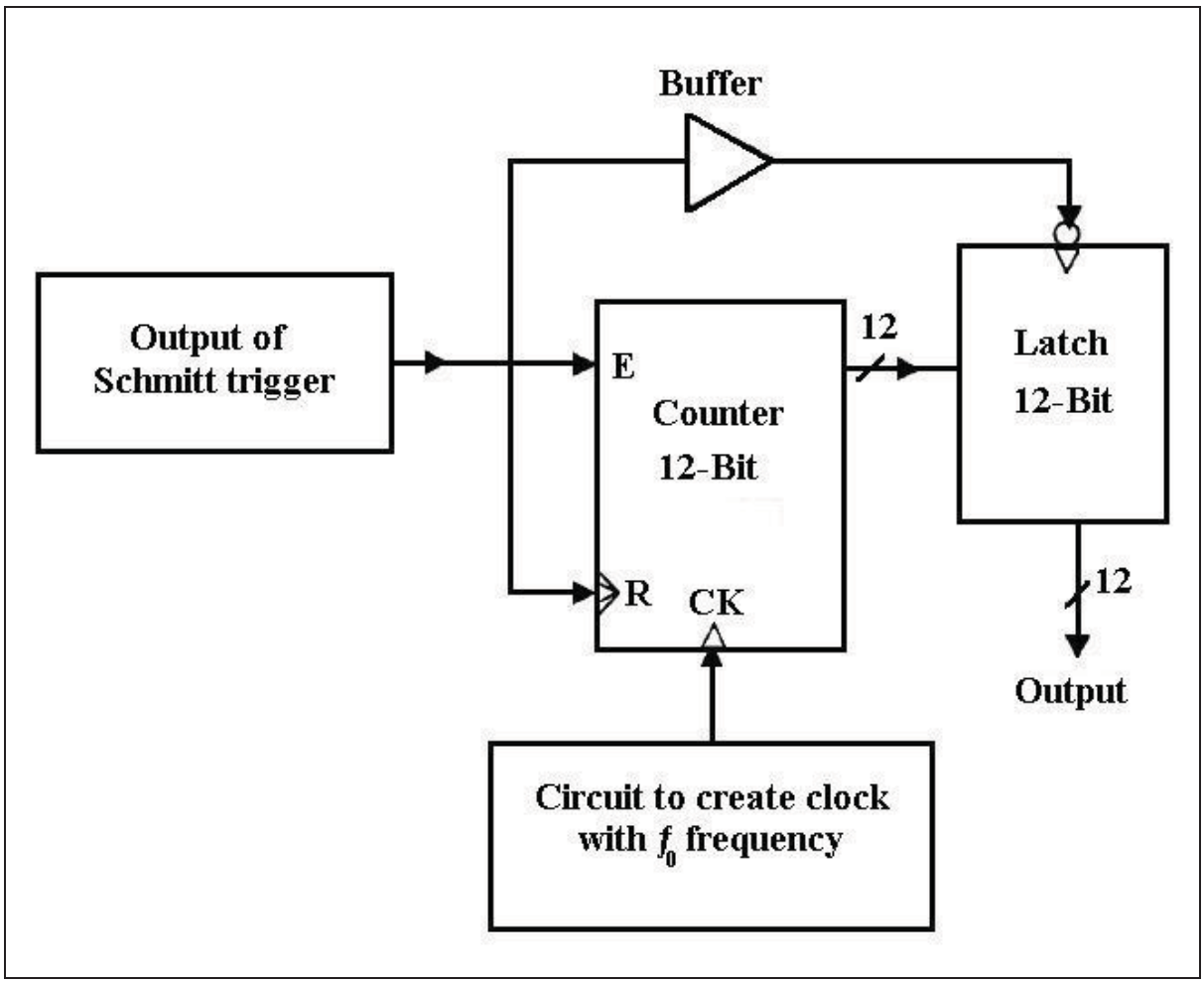

Fig. 4-15. Digital circuit for a capacitance meter option

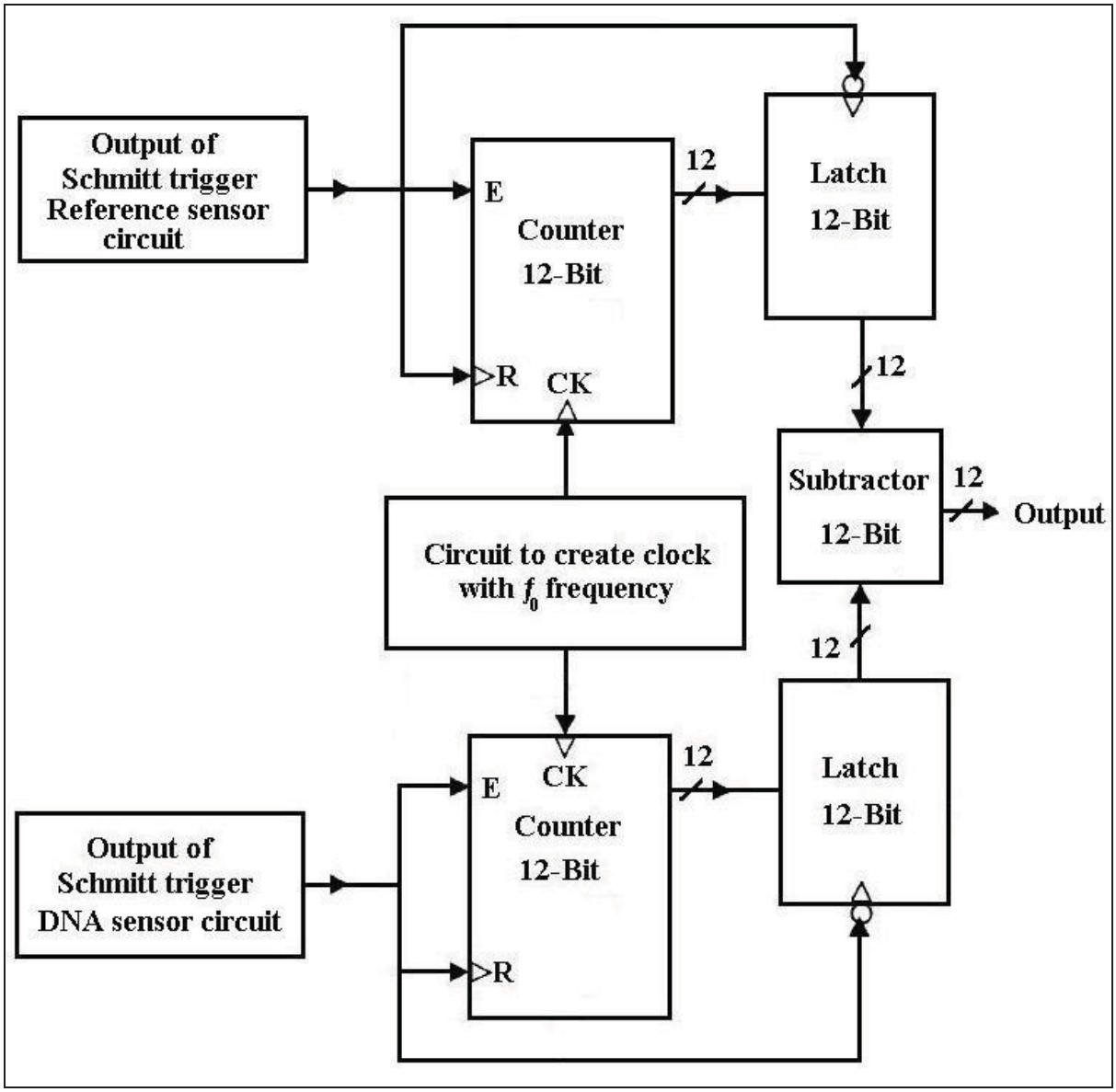

Fig. 4-16. Digital circuit for changing capacitance detector

Chapter 5: Simulation results and recommendations

5.1 The simulation results

In the previous chapter, the design of capacitance changes detector has been discussed. The analogue part has been designed using 0.25µm CMOS technology and in this chapter simulation results obtained from Tanner and HSPICE software will be displayed. First the simulation results for each designed part will be discussed and then the result of the total system will be explained. Fig. 5-1 shows the response of current sources and switches. The result is obtained by applying two symmetric pulses to the switches, rather than control signals (output of Schmitt trigger).

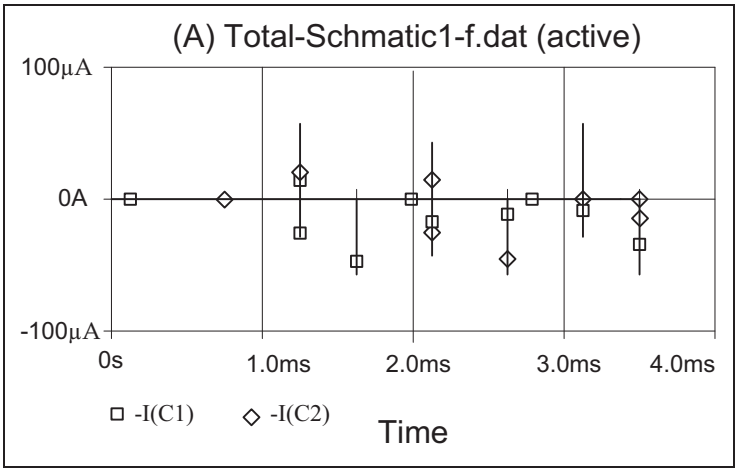

Fig. 5-1 response of current sources and switches

Fig. 5-2 shows the curve of the Schmitt trigger characteristics in Fig. 4-13. The result is obtained by applying the input triangular signal to the circuit. Fig. 5-3 shows the curve of S.R. in the Schmitt trigger.

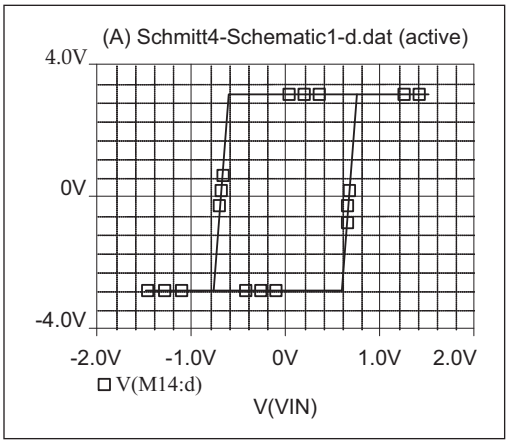

Fig. 5-2.The curve of the Schmitt trigger characteristic

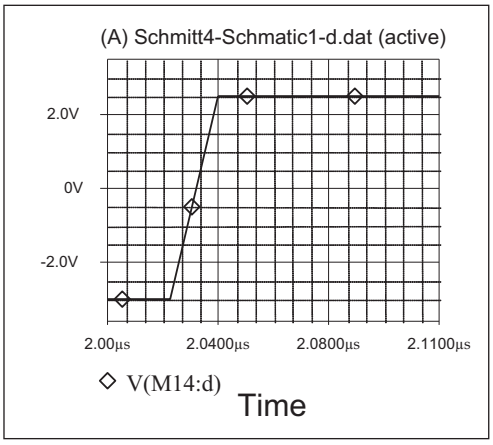

Fig. 5-3 curve of S.R. in the Schmitt trigger.

After linking the circuits of current sources and switches to the Schmitt trigger circuit, simulation results are shown with deferent capacitors and currents. Table 5-1 to table 5-6

show the results of changes in period and upper part of the period in terms of C_0 to $1.5C_0$ for currents of *I=100nA*, *I=10nA* and *I=1nA*. These tables and figures have been obtained for two different values of C_0=*2pF* and C_0=*20pF*.

C(pF)	Th(µs)	T(µs)	C(pF)	Th(µs)	T(µs)
2	52.217	79.275	2.55	66.525	100.993
2.05	53.522	81.256	2.6	67.825	102.965
2.1	54.823	83.23	2.65	69.123	104.937
2.15	56.121	85.199	2.7	70.427	106.917
2.2	57.422	87.168	2.75	71.724	108.885
2.25	58.723	89.151	2.8	73.03	110.861
2.3	60.025	91.125	2.85	74.332	112.843
2.35	61.525	93.298	2.9	75.627	114.812
2.4	62.624	95.065	2.95	76.924	116.781
2.45	63.923	97.039	3	78.229	118.757
2.5	65.225	99.022			

Table 5-1 The results for period and upper part of the period for *I=100nA*

The numbers in table 5-1 and Fig. 5-4 have demonstrate that increasing capacitance of the DNA sensor to *50fF*, the period of the Schmitt trigger output increases to *1.3µs*. Thus the time detection for *1µs* can detect capacitive changes in the sensor with an accuracy of *38.5fF*. By choosing the clock frequency f_0=*50MHz* for the digital circuit, the output counter of the circuit is producing a count of 1 for every *0.76fF* in the DNA sensor. This value indicates the accuracy of the detector circuit. The frequency of f_0 has been calculated by equations 4-35 to 4-39 for a 12bit counter.

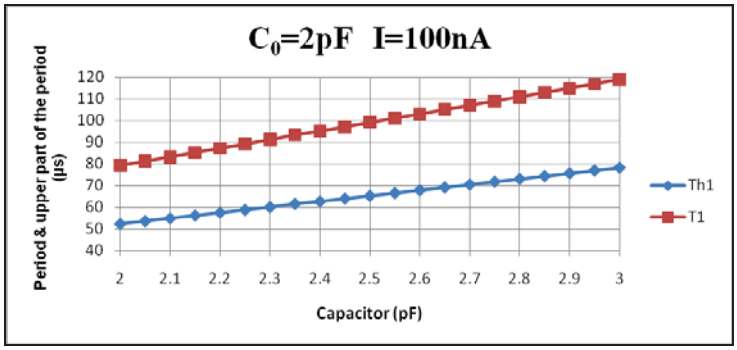

Fig. 5-4 The plot for period and upper part of the period for *I=100nA*

The numbers in table 5-2 and Fig. 5-5 have demonstrate that increasing the capacitance of the DNA sensor to *500fF*, the period of the Schmitt trigger output increases to *13μs*. Thus by time detection for *1μs*, can detect capacitive changes in the sensor with an accuracy of *33.4fF*. By choosing the clock frequency f_0=*5MHz* for the digital circuit, the output counter of the circuit is producing a count of 1 for every *7.7fF* in the DNA sensor. This value indicates the accuracy of the detector circuit.

C(pF)	Th(μs)	T(μs)	C(pF)	Th(μs)	T(μs)
20	520.4	790	25.5	663.5	1007.2
20.5	533.4	809.7	26	676.5	1026.9
21	546.5	829.5	26.5	689.4	1046.6
21.5	559.4	849.1	27	702.5	1066.3
22	572.4	869	27.5	715.4	1086
22.5	585.5	888.7	28	728.5	1105.8
23	598.4	908.4	28.5	741.5	1125.6
23.5	611.5	928.2	29	754.5	1145.3
24	624.4	947.9	29.5	767.5	1165
24.5	637.5	967.9	30	780.5	1184.8
25	650.4	987.4			

Table 5-2 The results for period and upper part of the period for *I=100nA*

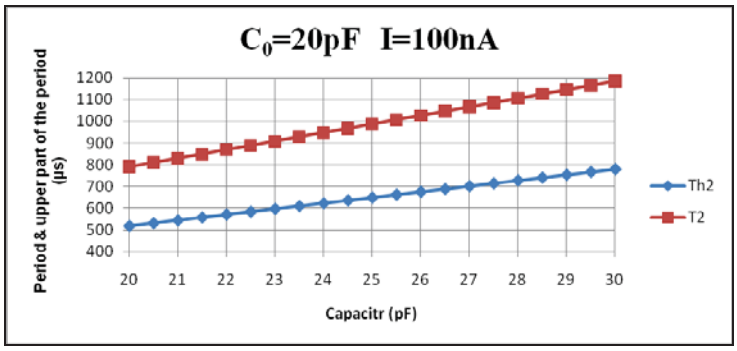

Fig. 5-5 The plot for period and upper part of the period for *I=100nA*

The numbers in table 5-3 and Fig. 5-6 have demonstrate that increasing the capacitance of the DNA sensor to *50fF*, the period of Schmitt trigger output increases to *12.1μs*. Thus by time detection for *1μs*, can detect capacitive changes in the sensor with an accuracy of *4.2fF*. By choosing the clock frequency f_0=*5.5MHz* for the digital circuit, the output counter of the circuit is producing a count of 1 for every *0.74fF* in the DNA sensor. This value indicates the accuracy of the detector circuit.

C(pF)	Th(μs)	T(μs)	C(pF)	Th(μs)	T(μs)
2	485.7	756	2.55	618.8	963.1
2.05	497.8	774.8	2.6	630.8	981.8
2.1	509.8	793.6	2.65	642.9	1000.7
2.15	522	812.5	2.7	655	1019.6
2.2	534.1	831.3	2.75	667.1	1038.4
2.25	546.2	850.1	2.8	679.2	1057.1
2.3	558.2	868.9	2.85	691.3	1076
2.35	570.4	887.8	2.9	703.4	1094.9
2.4	582.4	906.6	2.95	715.6	1113.7
2.45	594.6	925.4	3	727.6	1132.5
2.5	606.7	944.2			

Table 5-3 The results for period and upper part of the period for *I=10nA*

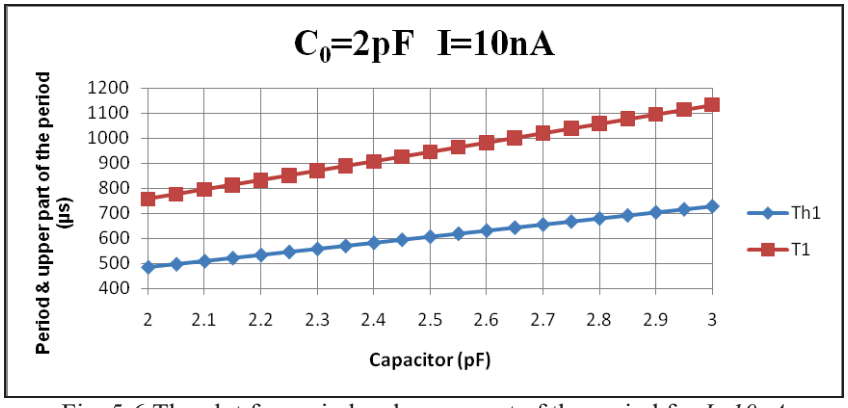

Fig. 5-6 The plot for period and upper part of the period for *I=10nA*

The numbers in table 5-4 and Fig. 5-7 have shown that increasing the capacitance of the DNA sensor to *500fF*, the period of Schmitt trigger output increases to *120μs*. Thus by time detection for *1μs*, can detect capacitive changes in the sensor with an accuracy of *4.16fF*. By choosing the clock frequency f_0=*560KHz* for the digital circuit, the output counter of the circuit is producing a count of 1 for every *7.4fF* in the DNA sensor. This value indicates the accuracy of the detector circuit.

C(pF)	Th(ms)	T(ms)	C(pF)	Th(ms)	T(ms)
20	4.841	7.534	25.5	6.172	9.605
20.5	4.963	7.723	26	6.294	9.794
21	5.083	7.91	26.5	6.414	9.981
21.5	5.204	8.099	27	6.535	10.2
22	5.325	8.288	27.5	6.656	10.359
22.5	5.446	8.475	28	6.776	10.536
23	5.567	8.664	28.5	6.898	10.745
23.5	5.689	8.859	29	7.019	10.923
24	5.81	9.041	29.5	7.14	11.112
24.5	5.93	9.229	30	7.26	11.299
25	6.051	9.417			

Table 5-4 The results for period and upper part of the period for *I=10nA*

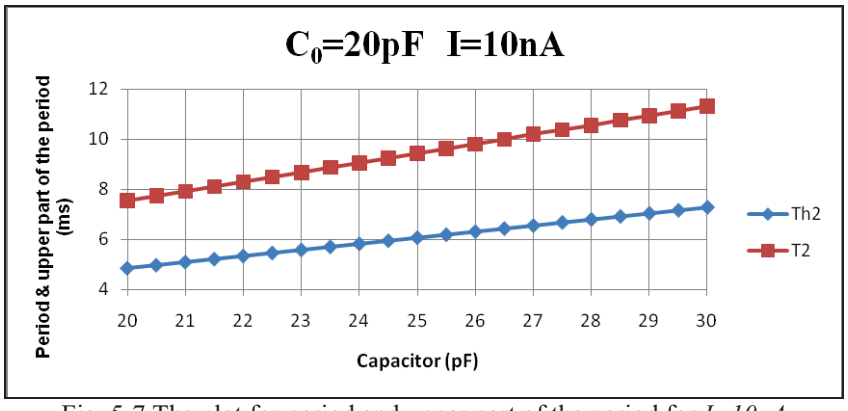

Fig. 5-7 The plot for period and upper part of the period for *I=10nA*

The numbers in table 5-5 and Fig. 5-8 have demonstrate that increasing the capacitance of the DNA sensor to *50fF*, the period of Schmitt trigger output increases to *98μs*. Thus by time detection for *1μs*, can detect capacitive changes in the sensor with an accuracy of *0.5fF*. By choosing the clock frequency f_0=*700KHz* for the digital circuit, the output counter of the circuit is producing a count of 1 for every *0.73fF* in the DNA sensor. This value indicates the accuracy of the detector circuit.

C(pF)	Th(ms)	T(ms)	C(pF)	Th(ms)	T(ms)
2	3.945	6.624	2.55	5.025	8.439
2.05	4.043	6.789	2.6	5.124	8.604
2.1	4.141	6.953	2.65	5.222	8.769
2.15	4.239	7.119	2.7	5.32	8.934
2.2	4.337	7.283	2.75	5.418	9.098
2.25	4.435	7.448	2.8	5.516	9.264
2.3	4.534	7.614	2.85	5.614	9.428
2.35	4.632	7.778	2.9	5.713	9.594
2.4	4.73	7.944	2.95	5.811	9.758
2.45	4.829	8.109	3	5.909	9.924
2.5	4.927	8.274			

Table 5-5 The results for period and upper part of the period for *I=1nA*

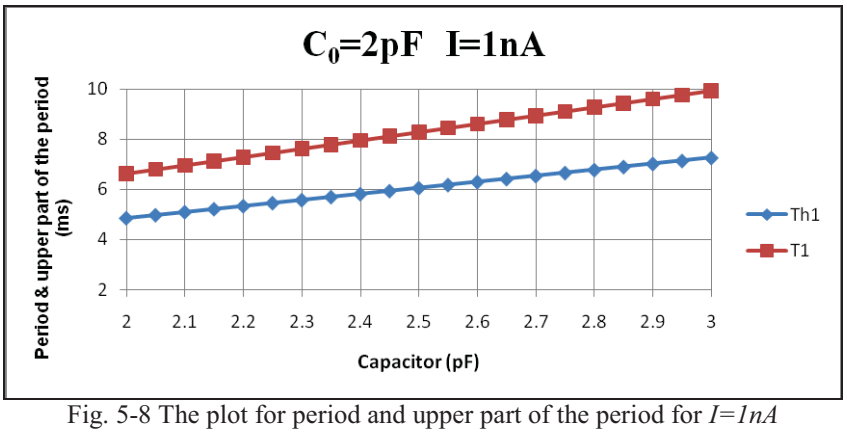

Fig. 5-8 The plot for period and upper part of the period for *I=1nA*

The numbers in table 5-16 and Fig. 5-9 have demonstrate that increasing the capacitance of the DNA sensor to *500fF*, increases the period of the Schmitt trigger to *1032μs*. Thus, the time detection for *1μs* can detect capacitive changes in the sensor, with an accuracy of *0.5fF*. By choosing the clock frequency f_0=*70KHz* for the digital circuit, the output counter of the circuit is producing a count of 1 for every *7fF* in the DNA sensor. This value indicates the accuracy of the detector circuit.

C(pF)	Th(ms)	T(ms)	C(pF)	Th(ms)	T(ms)
20	39.318	66.019	25.5	50.126	84.167
20.5	40.3	67.668	26	51.108	85.817
21	41.283	69.318	26.5	52.092	87.468
21.5	42.246	70.968	27	53.074	89.117
22	43.248	72.619	27.5	54.156	90.766
22.5	44.232	74.27	28	55.04	92.417
23	45.213	75.918	28.5	56.022	94.067
23.5	46.196	77.568	29	57.004	95.716
24	47.179	79.219	29.5	57.988	97.366
24.5	48.161	80.868	30	58.969	99.015
25	49.144	82.517			

Table 5-6 The results for period and upper part of the period for *I=1nA*

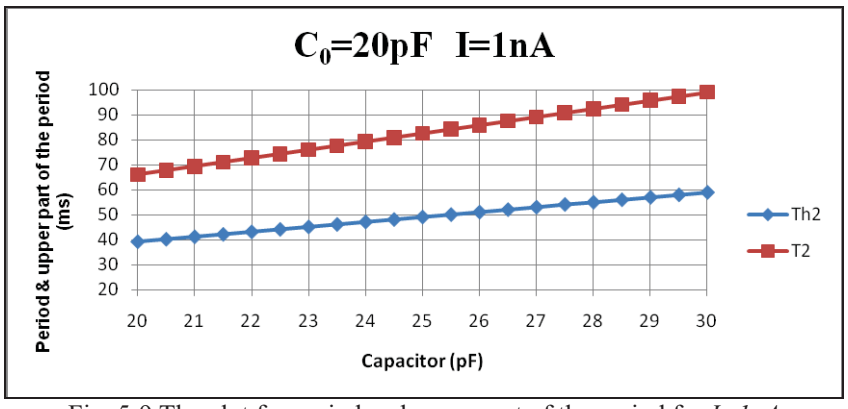

Fig. 5-9 The plot for period and upper part of the period for *I=1nA*

Tables 5-7 and 5-8 have shown the results of changes in period and upper part of the period signal in Schmitt trigger output for current changes in charge and discharge of the sensor. These figures obtained for two capacitance value of C_s=*2.5pF* and C_s=*25pF*.

I	Th(ms)	T(ms)	I	Th(µs)	T(µs)
100pA	29.075	59.921	60nA	107.63	163.95
200pA	17.89	34.015	70nA	92.554	140.83
300pA	13.172	24.093	80nA	81.199	123.446
400pA	10.519	18.768	90nA	72.329	109.878
500pA	8.793	15.423	100nA	65.225	98.523
600pA	7.573	13.116	150nA	43.762	66.291
700pA	6.664	11.426	200nA	32.949	49.85
800pA	5.957	10.131	250nA	26.428	39.951
900pA	5.391	9.106	300nA	22.066	33.335
1nA	4.927	8.274	350nA	18.943	28.603
1.5nA	3.464	5.7022	400nA	16.598	25.052
2nA	2.684	4.3653	450nA	14.77	22.285
2.5nA	2.1963	3.5427	500nA	13.304	20.068
3nA	1.8615	2.9843	550nA	12.101	18.249
3.5nA	1.6168	2.5795	600nA	11.102	16.739
4nA	1.4301	2.2728	650nA	10.255	15.458
4.5nA	1.2827	2.032	700nA	9.525	14.357
5nA	1.1633	1.8378	750nA	8.896	13.406
5.5nA	1.0646	1.6777	800nA	8.344	12.573
6nA	0.9815	1.5437	850nA	7.857	11.837
6.5nA	0.9106	1.4297	900nA	7.422	11.18
7nA	0.8495	1.3315	950nA	7.035	10.596
7.5nA	0.7967	1.2461	1µA	6.683	10.067
8nA	0.7492	1.171	2µA	3.3559	5.0479
8.5nA	0.7076	1.1047	3µA	2.2416	3.3706
9nA	0.6703	1.0854	4µA	1.6832	2.5306
9.5nA	0.6369	0.9922	5µA	1.3483	2.0266
10nA	0.6067	0.9442	6µA	1.1243	1.6897
20nA	0.3127	0.4816	7µA	0.9647	1.4497
30nA	0.2113	0.3239	8µA	0.8447	1.2692
40nA	0.1598	0.2443	9µA	0.7512	1.1287
50nA	0.1289	0.1961	10µA	0.6764	1.0162

Table 5-7 Results obtained for period and upper part of the period signal when C_s=2.5pF

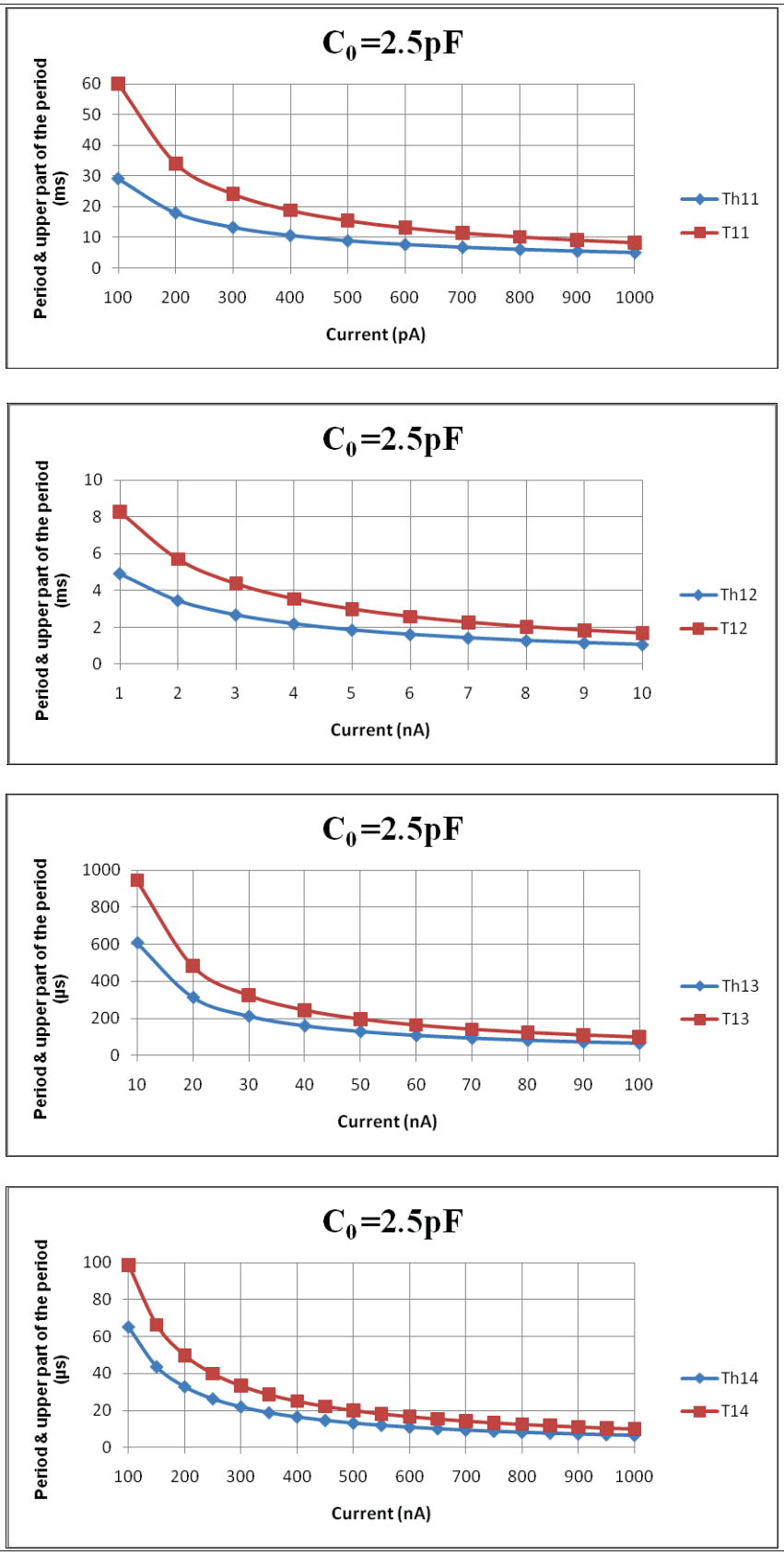

Fig. 5-10 Plots obtained for period and upper part of the period signal when C_s=2.5pF

I	Th(ms)	T(ms)	I	Th(µs)	T(µs)
100pA	290.006	597.506	60nA	1073.3	1634.8
200pA	178.451	339.26	70nA	923	1404.3
300pA	131.455	240.302	80nA	809.9	1233.1
400pA	104.926	187.194	90nA	721.4	1065.7
500pA	87.702	153.825	100nA	650.4	987.4
600pA	75.543	130.818	150nA	436.3	661
700pA	66.462	113.953	200nA	328.59	497
800pA	59.419	101.038	250nA	263.513	398.331
900pA	53.773	90.817	300nA	220.008	332.329
1nA	49.144	82.518	350nA	188.862	285.142
1.5nA	34.552	56.872	400nA	165.456	249.562
2nA	26.771	43.537	450nA	147.217	222.101
2.5nA	21.96	35.031	500nA	132.609	200.01
3nA	18.567	29.764	550nA	120.641	181.908
3.5nA	16.127	25.727	600nA	110.66	166.825
4nA	14.265	22.668	650nA	102.204	154.049
4.5nA	12.794	20.265	700nA	94.944	143.087
5nA	11.603	18.326	750nA	88.564	133.598
5.5nA	10.618	16.733	800nA	83.156	125.28
6nA	9.791	15.397	850nA	78.296	117.946
6.5nA	9.083	14.259	900nA	73.974	111.42
7nA	8.473	13.28	950nA	70.1	105.578
7.5nA	7.941	12.428	1µA	66.615	100.316
8nA	7.473	11.679	2µA	33.724	50.278
8.5nA	4.057	11.016	3µA	22.317	33.556
9nA	6.685	10.425	4µA	16.753	25.184
9.5nA	6.352	9.895	5µA	13.412	20.158
10nA	6.051	9.411	6µA	11.185	16.807
20nA	3.1194	4.7974	7µA	9.989	14.408
30nA	2.1082	3.23.9	8µA	8.394	12.611
40nA	1.5942	2.4363	9µA	7.464	11.213
50nA	1.2826	1.9964	10µA	6.719	10.092

Table 5-8 Results obtained for period and high part of period signal when C_s=25pF

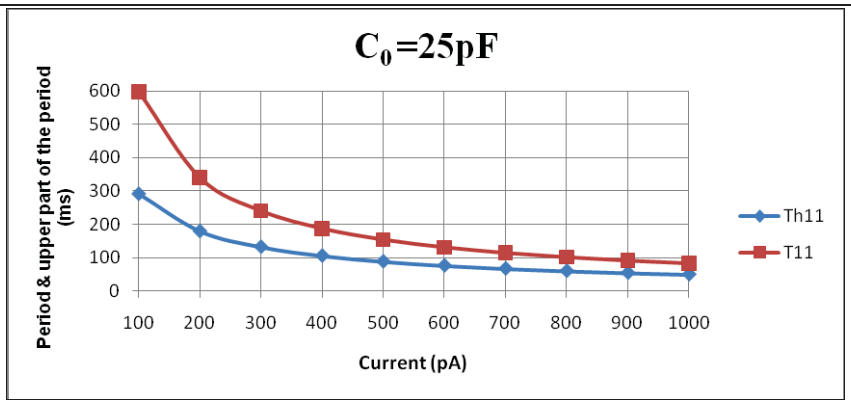

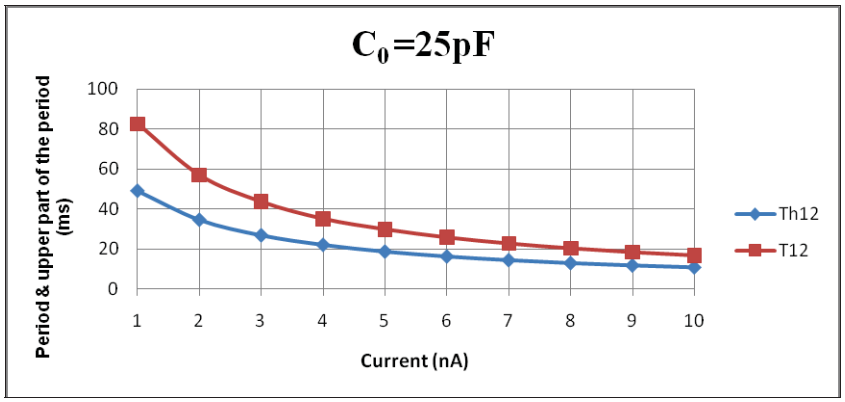

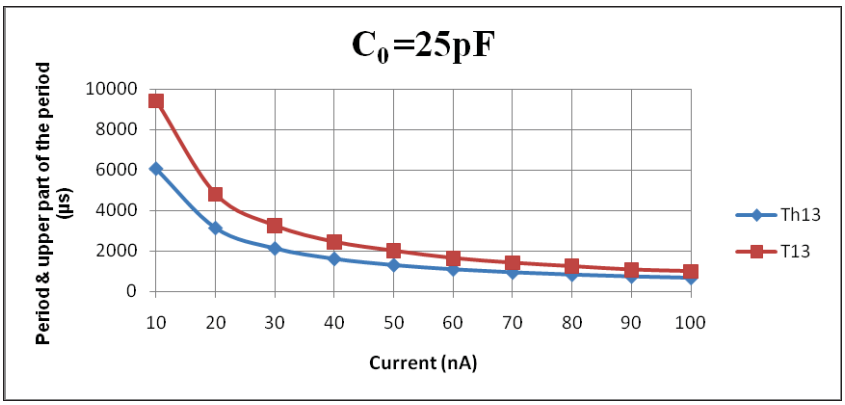

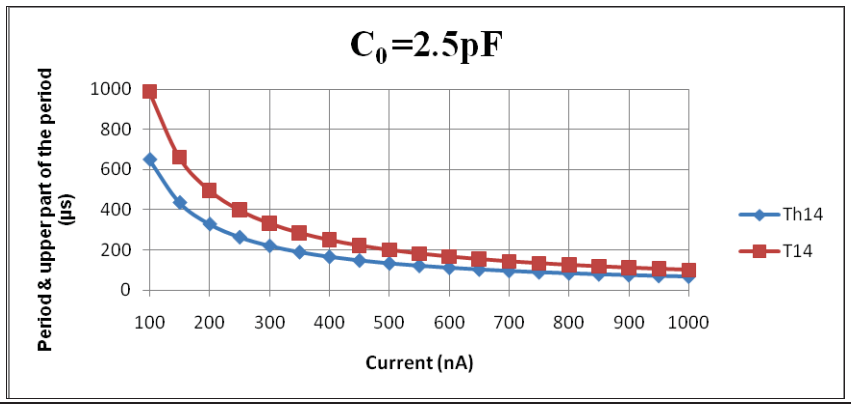

Fig. 5-11 Plots obtained for period and upper part of the period signal when C_s=25pF

The numbers in table 5-9 show output of the DNA detector circuit for *I=10nA*, *f=5.649MHz* and 12bit counter. These numbers are obtained by applying the times of the upper part of the period (Th) from table 5-3 to the digital part of DNA detector circuit and have been simulated by Modelsim software. These numbers indicate that by increasing capacitance of the capacitive sensor for every 730aF=0.73fF, the counter's value increases by one. This capacitive sensor changes provide the accuracy of the circuit.

C(pF)	Th(µs)	Output number of detector circuit	C(pF)	Th(µs)	Output number of detector circuit
2	485.7	0	2.55	618.8	752
2.05	497.8	68	2.6	630.8	820
2.1	809.8	136	2.65	642.9	888
2.15	522	206	2.7	655	957
2.2	534.1	274	2.75	667.1	1025
2.25	546.2	342	2.8	679.2	1094
2.3	558.2	409	2.85	691.3	1161
2.35	570.4	478	2.9	703.4	1230
2.4	582.4	546	2.95	715.6	1299
2.45	594.6	614	3	727.6	1365
2.5	606.7	684			

Table 5-9 output of DNA detector circuit for *I=10nA*, *f=5.649MHz*

All the above tables and charts have shown that by increasing the capacitive value, the period of the Schmitt trigger output and output number of the capacitive changes detector with constant current, increases. For constant capacitance, by increasing the current, the period of the Schmitt trigger output and output number of the capacitive sensor detector will be increased. By increasing the counter frequency and the bit number of the counter and reducing the charge and discharge current of the capacitive sensor, accuracy of measurement will be increased.

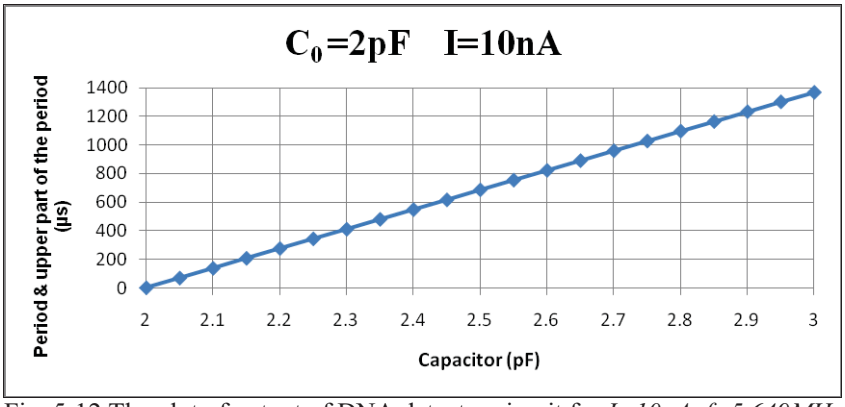

Fig. 5-12 The plot of output of DNA detector circuit for *I=10nA*, *f=5.649MHz*

5.2 The Results of change in the power supplies

Fig. 5-13 shows output period of the Schmitt trigger circuit for two different voltages $V_{cc}=V_{ss}=2.5V$ and $V_{cc}=V_{ss}=3V$ for capacitance of the sensor *2.5pF* and charge and discharge current of *10nA*. From the figure it can be concluded that by changing the voltage sources by 0.5V, period and upper part of the period in the Schmitt trigger circuit will decrease to 8µs and 54µs. This decrease in values creates an error in period of around 1.2% and in upper part of the period of around 8.9% but 0% in output number of detector circuit.

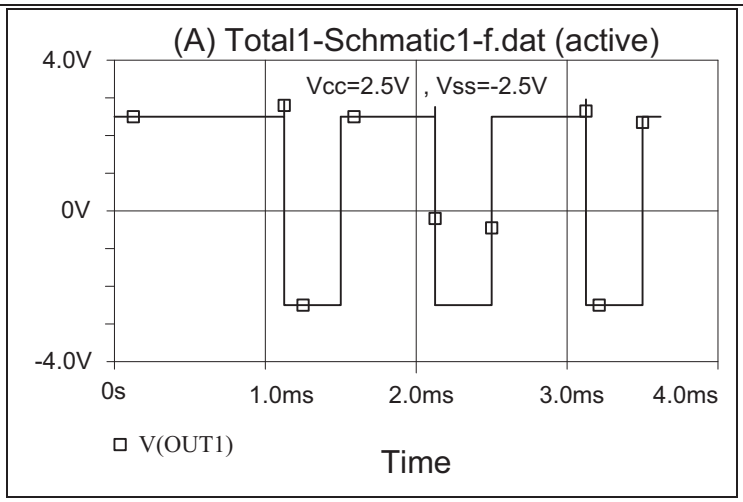

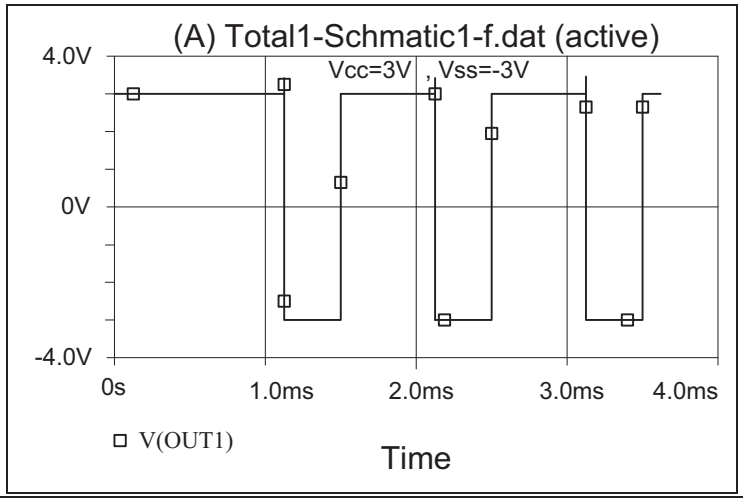

Fig. 5-13 output period of the Schmitt trigger circuit for two different voltages $V_{cc}=V_{ss}=2.5V$ and $V_{cc}=V_{ss}=3V$ with the capacitance of the sensor *2.5pF* and charge and discharge current of *10nA*

5.3 Power consumption of the analogue circuit section

The average power consumption of the DNA detector's analogue circuit, for $V_{cc}=V_{ss}=3V$, with a sensor capacitance of *2.5pF* and charge and discharge current *10nA*, is 10.386mW.

5.4 Noise in the analogue section of the DNA detector

Fig. 5-14 shows the noise in the analogue section of the DNA detector when $V_{cc}=V_{ss}=3V$, the capacitance of the sensor is *2.5pF* and charge and discharge current is *10nA*. The maximum value of the noise for the above value is *100pV*. This amount of noise voltage is less than the threshold voltage of Schmitt trigger, therefore, does not produce any error.

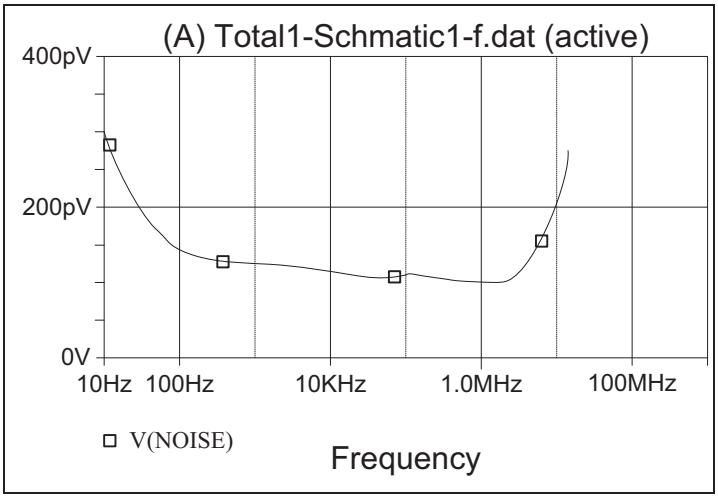

Fig. 5-14 noise in the analogue section of the DNA detector when capacitance of the sensor is *2.5pF* and charge and discharge current is *10nA*

5.4.1 GBM[1] , PM[2] , The noise referred to the input and DC gain of the designed OpAmp

Fig. 5-15 shows the frequency response of the OpAmp used, including a display of bandwidth, GBW, PM and DC gain. All of these measurements have been done in open-loop mode.

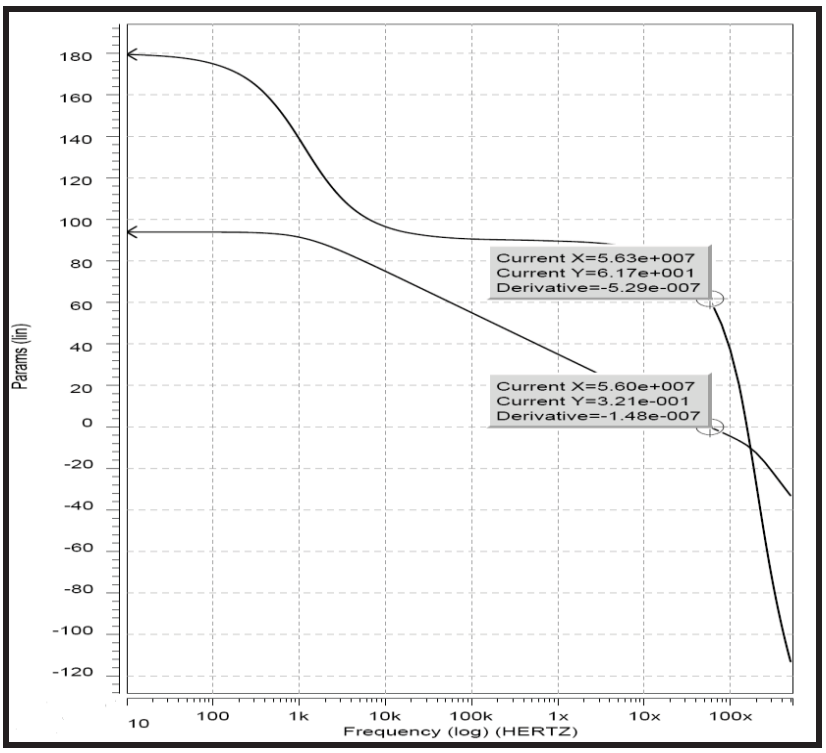

Fig. 5-15 GBW, PM and DC gain of the OpAmp

[1] Gain Bandwidth
[2] Phase-Margins

In Fig. 5-15, DC gain is equal to 94dB, GBW is equal to 56MHz and PM is equal to 62 degrees; also, the value of gain in the chopper frequency (1 MHz) is approximately 36dB. Fig. 5-16 shows the noise applied to the input of the OpAmp simulated by the software. According to this figure, thermal noise in the frequency of 1MHz (chopper frequency) is $34.6nV/\sqrt{Hz}$.

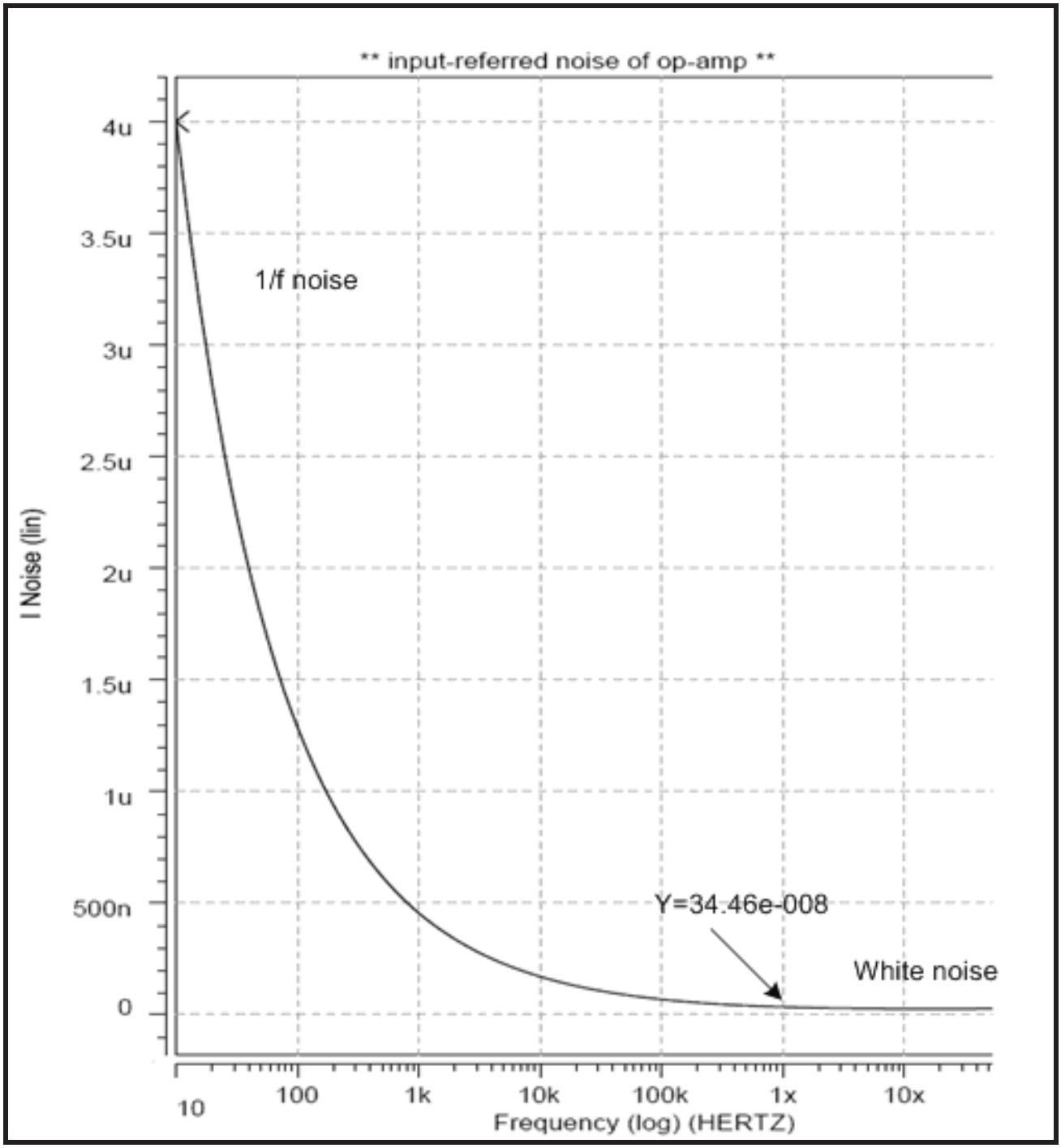

Fig. 5-16 Noise measured in the OpAmp input.

5.5 Comparison of other works

Table 5-10 shows a comparison with some other articles.

Noise	Accuracy	Sensor tech. Micromachining Bulk/Surface	Method	Parasite Capacitive C_p	ΔC_{min}	C_0	measuring method	Reference
$1.6\mu g/\sqrt{Hz}$	0.2-1.2 V/pF@ Vcc=5V	Bulk	hybrid	$C_0+C_p>80pF$	*20af*	$C_0+C_p>80pF$	CDS and CHS	[26] (2004)
$0.02aF/\sqrt{Hz}$ $50\mu g/\sqrt{Hz}$	*0.4 fF/g* @ Vcc=5V	Surface	Monolithic	*100fF*	.....	*20fF*	CHS	[105] (2004)
.....	155 mV/fF@ Vcc=3.3V	.....	Apart from the sensor system	.....	*ΔC=1fF*	*50fF*	CDS	[96] (2008)
$9.5aF/\sqrt{Hz}$	1-10 mV/fF@ Vcc=5V	Bulk	hybrid	.....	*95aF*	*700fF*	SC	[106] (2008)

Table 5-10 comparison with results of some other articles.

5.6 Recommendations for future works

This study discussed the hybridization of DNA and the methods of bonding DNA to the sensor. The analogue circuit has been designed as integrated and the digital part as discrete. With respect to future works, it is proposed that the counter, differentiator, and the counter clock be designed as integrated and be programmable; this way their layout design can be implemented on a single chip. Furthermore, in order to increase output linearly, where the output will be dependent on input, it is recommended that a search table be used; however, this will mean using memory within the circuit, memory that will contain the value of the differentiator and output's values in the memory's addresses.

To improve CHS method, further study would be pertinent on the effect of bandwidth and gain.

As mentioned previously, two methods of CDS and CHS have been combined. To improve the result of the circuit, other structures can be studied.

Detection of base pairs in DNA, creating a database for healthy DNA, and detection and measurement of other DNA base pairs in comparison with healthy DNA, could be done in the future to enhance the DNA disease detection process.

References:

[1] Clausen-Schaumann. H., Rief, M., Tolksdorf, C., Gaub, H., (2000), "Mechanical stability of single DNA molecules". Biophys J 78 (4), 1997–2007.

[2] Nagy, G. Szucs, Z., Hodossy, S., Rencz, M., Poppe, A., (2007), "Comparison of two lowpower electronic interfaces for capacitive MEMS sensors," Author manuscript, published in "DTIP 2007, Stresa, lago Maggiore : Italy"

[3] Saukoski, M., Aaltonen, L., Halonen, K., Salo, T., (2005), "Fully integrated charge sensitive amplifier for readout of micromechanical capacitive sensors," Circuits and Systems, 2005. ISCAS 2005. IEEE International Symposium on. Vol.6, May 2005, pp. 5377- 5380.

[4] Frey, A., (2003), "Design of an integrated potentiostat circuit for CMOS biosensor chips," in Proc. IEEE ISCAS, May 2003, vol. 5, pp. 9–12.

[5] Hanneborg, A; Hansen, T.E.; Ohlckers, P.A.; Carlson, E.; Dahl, B.; Holweck, O., (1986), "An integrated capacitive pressure sensors with frequency modulated output," Sensors and Actuators, vol. 9, pp. 345-351.

[6] Schoneberg, U.; Schnatz, F.V.; Brockherde, V.; Kopystynski, P.; Mehlhorn T.; Obermeier, E., (1991), "CMOS integrated capacitive pressure transducer with on chip electronics and digital calibration capability," Int. Solide-state Sensors and Actuators Conf., pp. 304-307.

[7] Patel, A., Webster, J.G., Tompking, W.j., Wertsch, J.J., (1989), "Electronic circuit for capacitive pressure sensors," J. Electro, 1989. Digest of Technical Papers.

[8] Tedder, J.M., Nechvatal, A., Murray, A.W., et al., (1972), "Amino-acids and proteins. In: Basic organic chemistry." London: John Wiley & Sons, Chapter 6:305-342.

[9] Rasmussen, S.R., Larsen, M.R., Rasmussen, S.E., (1991), "Covalent immobilization of DNA onto polystyrene microwells: The molecules are only bound at the 5' end." Anal Biochem. 198,138-142.

[10] Pericet-Camara, R., Papastavrou, G., Borkovec, M., Langmuir, (2003), 20, 3264. Leite, F. L.; Riul, A., Jr.; Herrmann, P. S. P. J. Adhes. Sci. Technol. 2003, 17, 2141.

[11] Yao, Z., Dekker, C., Avouris, P., (2001), "Electrical transport measurements on single-walled carbon nanotube." Top. Appl. Phys. 80, 147.

[12] Lazzri, M., Lopez-Quintela, M. A., (2003), "Block Copolymers as a Tool for Nanomaterial Fabrication." Adv. Mater. 15, 1583.

[13] Muskal, N., Turyan, I., Mandler, D. J., (1996) "Electroanal." Chem. 1996, 409, 131.

[14] Alberts, B., Johson, A., Lewis, J., Raff, M., Roberts, K., Walter, P., (2002), "Molecular Biology of the Cell", 4th ed.; Garland Science: London, 2002.

[15] Walczak, M. M., Chung, C., Stole, S. M., Widrig, C. A., Porter, M. D. J. Am. Chem. Soc. 1991, 113, 2370.

[16] Gaines, G. L., (1966), "Insoluble Monolayers at Liquid-Gas Interfaces"; Interscience Publishers: New York, 1966.

[17] Adamson, A. W., Gast, A. P., (1997), "Physical Chemistry of Surfaces." 6th ed.; Wiley-Interscience: New York.

[18] Love, J. C., Wolfe, D. B., Haasch, R., Chabinyc, M. L., Paul, K. E., Whitesides, G. M., Nuzzo, R. G. J. Am. Chem. Soc. 2003, 125, 2597.

[19] Poirier, G. E.; Pylant, E. D. Science (Washington, D.C.) 1996, 272, 1145.

[20] Laibinis, P. E.; Whitesides, G. M.; Allara, D. L.; Tao, Y. T.; Parikh, A. N.; Nuzzo, R. G. J. Am. Chem. Soc. 1991, 113, 7152.

[21] Carvalho, A.; Geissler, M.; Schmid, H.; Micel, B.; Delamarche, E. Langmuir 2002, 18, 2406.

[22] Li, Z.; Chang, S.-C.; Williams, R. S. Langmuir 2003, 19, 6744.

[23] Wang, Z., Li, Z., Ni, X., Mo, B., (2006), "A Low-Noise Charge Sensitive Amplifier for MEMS capacitive sensors," IEEE, 2006. Solid-State and Integrated Circuit Technology. 8th Intarnational Conference On Publication Date: 23-26 Oct. 2006 On page(s): 673-675.

[24] Love et al., Estroff, Lara A., Kriebel, Jennah K., Nuzzo, Ralph G., Whitesides, George M., (2005). "Self-Assembled Monolayers of Thiolates on Metals as a Form of Nanotechnology". Chem. Rev. 105: 1103–1170

[25] Lobur, M., Holovatyy, A., (2009), "Overview and Analysis of Readout Circuits for Capacitive Sensing in MEMS Gyroscopes (MEMS Angular Velocity Sensors),"MEMSTECH'2009, 22-24 April, 2009, Polyana-Svalyava (Zakarpattya), UKRAINE.

[26] Yazdi, N., Kulah, H., Najafi, K., (2004), "Precision readout circuits for capacitive microaccelerometers,"Proceedings of IEEE Sensors 2004, Vol.1, pp. 28-31.

[27] Yin, T., Yang1, H., Chong, Z., Wu, Q., (2008), "A Low-Noise Readout Circuit for MEMS Vibratory Gyroscope," Proceedings of the 3rd IEEE Int. Conf. On Nano/Micro Engineered and Molecular Systems, pp. 124-127, January 6-9, 2008, Sanya, China.

[28] George, B., Jagadeesh Kumar, V., (2007), "Switched Capacitor Signal Conditioning for Differential Capacitive Sensors," IEEE TRANSACTIONS ON INSTRUMENTATION AND MEASUREMENT, VOL. 56, NO. 3, pp. 913-917, JUNE 2007.

[29] Lien, W.L., Quek, B.S., Walia, R., (2003), "A displacement-to-voltage converter circuit using a switched-capacitor technique," in Proc. IEEE ISCAS, Bangkok, Thailand, May 2003, vol. 4, pp. IV-880–IV-883.

[30] Chen, J., Ni, X., Mo, B., (2007), "A Low Noise CMOS Charge Sensitive Preamplifier for MEMS Capacitive Accelerometer Readout," IEEE, pp. 490-493, 2007. 7th International Conference On.

[31] Saukoski, M., (2008), "SYSTEM AND CIRCUIT DESIGN FOR A CAPACITIVE MEMS GYROSCOPE," Doctoral Dissertation, TKK Dissertations 116, Espoo 2008.

[32] Li, X., Gerard, C.M., (1999), "A Low-Cost and Reliable Interface for Capacitive Sensors," Instrumentation and Measurement Technology Conference, 1999. IMTC/99. IEEE. VOL. 2, pp. 1256-1259.

[33] Heidary, A., Gerard C.M., (2007), "An Integrated Switched-Capacitor Front-End for Capacitive Sensors with a Wide Dynamic Range," Solid State Circuits Conference, 2007. ESSCIRC 2007. 33rd European, pages: 404-407.

[34] Meijer, Q.; Guan, G. C. M., (2005), "An integrated interface for grounded capacitive sensors," Sensors, 2005 IEEE.

[35] Jawed, S. A., (2009), "CMOS READOUT INTERFACES FOR MEMS CAPACITIVE MICROPHONES," Phd Dissertation, International Doctorate School in Information and Communication Technologies, DIT-University of Trento.

[36] Dei, M., Marchetti, E., Bruschi, P., (2007), "A Micro Power Capacitive Sensor Readout Channel Based on the Chopper Modulation Technique," Research in Microelectronics and Electronics Conference, 2007. PRIME 2007. Ph.D. in IEEE, pp. 113-116, 2-5 July 2007.

[37] Millan, K. M., Mikkelson, S. R., (1993), "Sequence-selective biosensor for DNA based on electroavtive hybridization indicators." Anal.Chem. 65, 2317-23.

[38] Millan, K. M., Saraullo, S., Mikkelson, S. R., (1994), "Voltammetric DNA Biosensor for Cystic Fibrosis based on a Modified Carbon Past Electrode." Anal.Chem. 66, 2943-8.

[39] Piunno, P. A. E., Krull, U. J., Hudson, R. H. E., Damha, M. J. Cohn, H., (1994), "Fiber optic biosensor for fluorimetric detection of DNA hybridization." Anal. Chim. Acta 288, 205-14.

[40] Minunni, M., Tombelli, S., Scielzi, R., Mannelli, J. Mascini, M., Gaudiano, C., (2003), "Detection of β-thalassemia by a DNA piezoelectric biosensor coupled with polymerase chain reaction." Anal. Chim. Acta 481 55-64.

[41] Sawata, S., Kai, E., Ikebukuro, K., Iida, T. Honda, T. Karube, I., (1999), "Application of peptide nucleic acid to the direct detection of deoxyribonucleic acid amplified by polymerase chain reaction. Biosens." Bioelectron. 14, 397-404.

[42] Kelley, S. O., Boon, E. M., Barton, J. K., Jackson, N. M., Hill, M. G., (1999), "Single-base mismatch detection based on charge transduction through DNA." Nucleic Acid Res. 27, 4830-7

[43] Fodor, S.P.A., (1997), "DNA Sequencing: Massively Parallel Genomics." Science 277, 393-403.

[44] Epstein, J. R., Biran, I., Walt, D. R., (2002), "Flurescence-based nucleic acid detection and microarrays." Anal, Chim. Acta 469, 3-36.

[45] Marshall, A., Hodgson, (1998), "DNA chip: an array of possibilities." J. Nat. Biotechnol. 16, 27-31.

[46] Epstein, J. R., Leung, A. P. K., Lee, K. H., Walt, D. R., (2003), "High-density, microsphere-based fiber optic DNA microarrays." Biosensors Bioelectron. 18, 541-546.

[47] McDonnell, J. M., (2001), "Surface Plasmon resonance: towards and understanding of the mechanisms of biological molecular recognition." Curr. Opin. Chem. Biol. 5, 572-577.

[48] Storhoff, J. J., Elghanian, R., Mucic, R. C., Mirkin, C. A. & Letsinger, R. L., (1998), "One-Pot Colorimetric Differentiation of Polynucleotides with Single Base Imperfections Using Gold Nanoparticle Probes." J. Am. Chem. Soc. 120, 1959-1964

[49] Taton, T. A., Mirkin, C. A., Letsinger, R. L., (2000), "Scanometric DNA Array Detection with Nanoparticle Probes." Science 289, 1757-1760.

[50] Wang, J., Jiang, M., Palecek, E., (1999), "Real time monitoring of enzymatic cleavage of nucleic acid using a quartz crystal microbalance Bioelectrochem." Bioenergetics 4, 477-480.

[51] Patolsky, F., Lichtenstein, A., Willner, I., (2001), "Electronic Transduction of DNA Sensing Processes on Surfaces: Amplification of DNA Detection and Analysis of Single-Base Mismatches by Tagged Liposomes." J. Am. Chem. Soc. 123, 5194-5205.

[52] Fritz, J., Baller, M. K., Lang, H. P., Rothuizen, H., Vettiger, P., Meyer, E. Güntherodt, H.-J. Gerber, Ch., Gimzewski J. K., (2000), "Translating Biomolcular Recognition into Nanomechanics." Science 288, 316-318.

[53] Mikkelsen, S.R., (1996), "Electrochemical biosensors for DNA sequence detection." Electroanalysis 8 15.

[54] Wang, J., (2002), "Electrochemical nucleic acid biosensors." Anal. Chim. Acta 469 63.

[55] Wang, J., (2002), "Portable electrochemical systems." Trends Anal. Chem. 21, 226-232.

[56] Braun, E., Eichen, Y., Sivan, U., et al., (1998), "DNA-templated assembly and electrode attachment of a conductive silver wire." Nature, 391,775–8.

[57] Vestergaard, M.; Kerman, K.; Tamiya, E., (2007), "An Overview of Label-free Electrochemical Protein Sensors." Sensors 2007, **7**, 3442-3458.

[58] Zen, J. M., Chang, M. R., Ilangovan, G., (1999), "Simultaneous determination of guanine and adenine contents in DNA,. RNA and synthetic oligonucleotides using a chemically modified electrode." Analyst 124, 679-684 (1999)

[59] Brett, O., Macedo, T.R.A., Raimundo, D., Marques, M.H., Serrano, S.H.P., (1998), "Biosens. Bioelectron." 1998, 13, 861.

[60] Erdem, A., Ozsoz, M., Turk, J. Chem. 2001, 25, 469.

[61] Brett, O., Serrano, S. H. P., Gutz, I., La Scalea, M.A., Cruz, M.L., (1997), "Electroanalysis" 1997, 9, 1132.

[62] Singhal, P., Kuhr, W.G., (1997), "Ultrasensitive voltammetric detection of underivatized oligonucleotides and DNA" Anal. Chem. 69, 4828-4832.

[63] Jelen, F., Yosypchuk, B., Korilova, A., Novotny, L. & Palecek, E., (2002), "Lable-free determination of pictogram quantities of DNA by stripping voltammetry with solid copper amalgam or mercury electrodes in the presence of copper." Anal. Chem. 74, 4788-4793.

[64] Wang, J. & Kawde, A.B., (2002), "Amplified label-free electrical detection of DNA hybridization." Analyst 127, 383-386.

[65] Souteyrand, E., Cloarec, J.P., Martin, J.R., Wilson, C., Lawrence, I., Mikkelsen, S., Lawrence, M.F., (1997), " Direct detection of the hybridization of synthetic homo-oligomer DNA sequences by field effect" J. Phys. Chem. B, vol. 101, 2980–2985.

[66] Toshiba http://www.toshiba.co.jp/about/press/2003 06/pr2001.htm.

[67] Motorola Life Sciences http://www.motorola.com/lifesciences/esensor/.

[68] Armistead, P.M.; Thorp, H.H., (2002), " Electrochemical detection of gene expression in tumor samples: overexpression of RAK nuclear tyrosine kinase." Bioconj. Chem. 13, 172-176.

[69] Gregory Drummond, T., Hill, M. G., Barton, J. K., (2003), "Electrochemical DNA sensors." Nature Biotechnology, 21(10), 1192–1199.

[70] Steel, A.B., Herne, T.M., Tarlov, M.J., (1998), "Electrochemical quantitation of DNA immobilized on gold." Anal. Chem. 70, 4670-4677.

[71] Boon, E.M., Barton, J.K., (2002), "charge transport in DNA." Curr. Opin. Struct. Biol. 12, 320-329.

[72] Myari, A., Hadjiliadis, N., Garoufis, A., Eur. J., Inorg. Chem. 2004, 142, 7–1439.

[73] Liu, C.M., Gao, S., Kou, H.Z., (2001), "Dehydrogenative coupling of phenanthroline under hydrothermal conditions: Crystal structure of a novel layered vanadate complex constructed of 4,8,10-net sheets: [(2,2-Biphen)Co]V3O8.5." Chem. Commun. 1670- 1671.

[74] Ozsoz, M., Erdem, A., Kara, P., Kerman, K. & Ozkan, D., (2003), "Electrochemical biosensor for the detection of interaction between arsenic trioxide and DNA based on guanine signal." Electroanalysis 15, 613-619.

[75] Cady, N., Stelick, S. & Batt, C.A., (2003), "Nucleic acid purification using microfabricated silicon structures." Biosensors Bioelectron.

[76] Boon, E.M., Salas, J.E., Barton, J.K., (2002), "An electrical probe of protein-DNA interactions on DNA-modified surface." Nat. Biotechnol. 20, 282-286.

[77] Grody, W.W., et al., (2001), "Laboratory standards and guidelines for population-based cystic fibrosis carrier screening." Genetics Med. 3, 149-154.

[78] Heller, A., (2003), "Plugging metal connectors into enzymes." Nat. Biotechnol. 21, 631-632.

[79] Wang, j., Xu, D.K., Kawde, A.N., Polsky, R., (2001), "Metal nanoparticle-based electrochemical stripping potentiometric detection of DNA hybridization." Anal. Chem. 73, 5576-5581.

[80] Patolsky, F., Katz, E., Willner, I., (2002), "Amplified DNA detection by electrogenerated biochemiluminescence and by the catalyzed precipitation of an insoluble product on electrodes in the presence of the doxorubicin intercalator." Angew. Chem. Int. Edn. 41, 3398-3402.

[81] Kewal, K., Jain, T., (2005), " Nanotechnology in clinical laboratory diagnostics" Clinica Chimica Acta; 358, 37–54

[82] Natalia, C. T., Zhiqiang, G., (2006), "Nanoparticles in biomolecular detection" Nanotoday ; 1 (1) , 28-37

[83] Paolo, F. , Larry, J., Saul, S., (2005), "Nanobiotechnology: the promise and reality of new approaches to molecular recognition" Trends in biotechnology ; 23 (4), 169-173

[84] Salata, O. V. (2004) "Application of nanoparticles in biology and medicine" J. Nanobiotechnology; 2 (3), 1-8

[85] Campbell, C.N., Gal, D., Cristler, N., Banditrat, C., Heller, A., (2002), "Enzyme-amplified amperometric sandwich test for RNA and DNA." Anal. Chem. 74, 158-162.

[86] Shad, C., Mirkin, C. A., (2005), "DNA-Gold-Nanoparticles Conjugates In: Nanobiotechnology: Concepts,Application and perspectives." (Niemeyer, C. M. and Mirkin, C. A.) ,WILEY-VCH. pp. 289-307

[87] Shad, T. C., Dimitra, G., Mirkin, C. A., (2005), "Gold nanoparticle probes for the detection of nucleic acid targets" Clinica Chimica Acta.

[88] Georganopoulou, D. G., Chang, L., Nam, J.M., Thaxton, C. S., Mufson, E. J., Klein, W. L., Mirkin, C. A., (2005), "Nanoparticle-Based Detection in Cerebro Spinal Fluid of a Soluble Pathogenic Biomarker for Alzheimer's Disease." Proc. Natl. Acad. Sci. U.S.A. 2005, 102, 2273–2276.

[89] Jwa, M. N. , Savka. I. S., Chad A. M., (2004), "Bio-Bar-Code-Based DNA Detection with PCR-like Sensitivity" J. Am. Chem. Soc ; 126 (19), 5932 -3

[90] Jwa, M. N. , Shad, C., Chad, C. M., (2003), "Nanoparticle-Based Bio-barcodes for the Ultrasensitive Detecetion of proteins" Science ; 301, 1884-1886

[91] Park, S. J., Chad, C. M., (2002), "Array-Based Electrical Detection of DNA with Nanoparticle probes" Science ; 295, 15031506

[92] Christian, C., Enz, Gabor, C., Temes, (1996), "Circuit Techniques for Reducing the Effects of Op-Amp Imperfections: Autozeroing, Correlated Double Sampling, and Chopper Stabilization," PROCEEDINGS OF THE IEEE, VOL 84, NO 11, pp. 1584-1614, NOVEMBER I996, Invited Paper.

[93] ___, (2000), "CMOS LOW VOLTAGE PREAMPLIFIER BASED ON 1/F NOISE CANCELLATION," University of MONTREAL, Decembre 2000.

[94] Behzad Razavi, "Design of Analog CMOS Integrated Circuits," Mc-Graw Hill, 2001.

[95] Wongkomet, N., Bernhard, E., Boser, (1998), "Correlated Double Sampling in Capacitive Position Sensing Circuits for Micromachined Applications," Circuits and Systems, 1998. IEEE APCCAS 1998. The 1998 IEEE Asia-Pacific Conference on Publication Date: 24- 27 Nov 1998, On page(s): 723-726.

[96] T. C. Lu, Y. J. Huang and H. P. Chou, (2008), "A Novel Interface Circuit for Capacitive Sensors Using Correlated Double Sampling Demodulation Technique," IEEE. The Second International Conference on Sensor Technologies and Applications.

[97] Ranganathan, S., Inerfield, M., Roy, S., Garverick, S. L., (2000), "Sub- Femtofarad Capacitive Sensing for Microfabricated Transducers Using Correlated Double Sampling and Delta Modulation," IEEE TRANSACTION ON CIRCUITS AND SYSTEMS. ANALOG AND DIGITAL SIGNAL PROCESSING, VOL. 47, NO.11, NOVEMBER 2000.

[98] Huang, M. C., Huang, Y. R., Chou, H. P., (2006), "A Low-noise CMOS Readout Circuit for Capacitive Micro-sensors," 5th IEEE International Conference On SENSORS, pp. 1135-1138 2006, EXCO, Daegu, Korea / October 22-25.

[99] Kajita, T., Moon, U., Gábor C. Temes, (2002), "A Two-Chip Interface for a MEMS Accelerometer," IEEE TRANSACTIONS ON INSTRUMENTATION AND MEASUREMENT, VOL. 51, NO. 4, pp. 853-858, AUGUST 2002.

[100] YOSHIDA, T., MASUI, Y., MASHIMO, T., SASAKI, M., IWATA, A., (2006), "A 1 V Low-Noise CMOS Amplifier Using Autozeroing and Chopper Stabilization Technique," IEICE TRANS. ELECTRON., VOL.E89-C, NO.6 JUNE 2006.

[101] ___, "High-precison CMOS amplifiers," Ph.D. dissertation, Ecole Polytechnique FtdCrale de Lausanne, 1989.

[102] Enr, C. C., Vittoz, E. A., Krummenacher, F., (1987), "A CMOS chopper amplifier," IEEE J. Solid-State Circ., vol. 22, pp. 335-342, June 1987.

[103] Enz, C., (1984), "Analysis of the low-frequency noise reduction by autozero technique," Electron. Lett. vol. 20, pp. 959-960, Nov. 1984.

[104] Spencer, R., Fleischer, M., Barth, W., Angell, B., (1988), "A Theorical study of transducer Noise In Piezoresistive and capacitive silicon pressure sensors," IEEE Transaction on Electron Divices, Vol. 35, pp. 1289-1298, August 1988.

[105] Wu, J., Fedder, G. K., Carley, L. R., (2004), "A Low-Noise Low-Offset Capacitive Sensing Amplifier for a 50μ g / Hz Monolithic CMOS MEMS Accelerometer," IEEE JOURNAL OF SOLID-STATE CIRCUITS, VOL. 39, NO. 5, pp. 722-730, MAY 2004.

[106] Yin, T.; Yang1, H., Zhang, C., Wu, Q., (2008), "A Low-Noise Readout Circuit for MEMS Vibratory Gyroscope," Proceedings of the 3rd IEEE Int. Conf. On Nano/Micro Engineered and Molecular Systems, pp. 124-127, January 6-9, 2008, Sanya, China.